Monitoring fungal infection in maize with high resolution X-ray micro computed tomography

by
Irene Nyangoge Orina

Dissertation presented for the degree of
Doctor of Philosophy
(Food Science)
at
Stellenbosch University
Department of Food Science, Faculty of AgriSciences

UNIVERSITEIT
iYUNIVESITHI
STELLENBOSCH
UNIVERSITY

The financial assistance of the National Research Foundation (NRF) towards this research is hereby acknowledged. Opinions expressed, and conclusions arrived at are those of the author and are not necessarily to be attributed to the NRF.

Supervisor: Dr Paul J. Williams

Co-supervisor: Prof Marena Manley

Co-supervisor: Prof Glaston M. Kenji

March 2018

Declaration

By submitting this thesis electronically, I declare that the entirety of the work contained therein is my own, original work, that I am the sole author thereof (save to the extent explicitly otherwise stated), that reproduction and publication thereof by Stellenbosch University will not infringe any third party rights and that I have not previously in its entirety or in part submitted it for obtaining any qualification.

Irene Orina
March 2018

Abstract

Maize (*Zea mays* L.) is an important cereal crop used for human food as well as animal feed. Maize is however vulnerable to contamination by fungi that produce harmful mycotoxins. *Fusarium verticillioides* is among the most frequently isolated fungus from maize and maize-based products worldwide. Conventional methods for evaluation of fungal infection are destructive in nature and involve tedious sample preparation procedures. X-ray micro computed tomography (X-ray micro CT) was used as a non-destructive technique to monitor the effect of fungal damage on the internal structure of maize kernels infected with *F. verticillioides*.

X-ray images of control and infected kernels were acquired post inoculation using high resolution X-ray micro CT over time. After image acquisition, consecutive two-dimensional (2D) cross sectional images were reconstructed into three dimensional (3D) volumes of the maize kernels. Qualitative results were presented as 2D projection images, and 3D volumes which enable visualisation in different views (top, front and side view). More voids were observed especially in the germ and floury endosperm regions of both the control and infected kernels over time. Quantitative parameters including total volume, mean grey value and total volume of voids were calculated. Total volume and mean grey value increased, while total volume decreased over time in both the control and infected kernels. No significant difference ($P \geq 0.05$) was reported between the control and infected for the first four days scanned.

Algorithms were developed to extract image textural features from selected 2D images of both the control and infected kernels. First order statistics (mean, standard deviation, kurtosis and skewness) and grey level co-occurrence matrix (GLCM) features were extracted from the side, front and top view of each kernel for the days scanned. The outputs from calculation of these textural features were used as inputs for calculating principal component analysis (PCA) and developing classification models using partial least square discriminant analysis (PLS-DA). Clear separation of the control from the infected was seen on day 8 post inoculation using the first order statistical features. Classification accuracies of 97.22% for control and 55.56% for infected kernels was achieved using the developed PLS-DA model. The GLCM extracted features gave a better classification accuracy of 79.16% for infected kernels with less infected kernels classified as controls compared to first order statistics features.

This study demonstrated that, although X-ray micro CT cannot be used as a rapid technique for detection of fungal infection especially during early stages of infection, it allows monitoring of structural changes in the kernel over time, and therefore offer a better understanding of the effect of fungal damage on the microstructure of maize kernel at high resolution.

Opsomming

Mielies (*Zea mays* L.) is ‘n belangrike graangewas wat gebruik word vir menslike voeding sowel as vir dierevoeding. Mielies is egter kwesbaar vir kontaminasie deur fungi wat skadelike mikotoksiene produseer. *Fusarium verticillioides* is een van die fungi wat wêreldwyd die gereeldste in mielies en mielie-gebasseerde produkte voorkom. Konvensionele metodes vir die evaluering van swaminfeksiesies is vernietigend van aard en sluit tydrowende monstervoorbereidingsprosedures in. X-straal mikro-berekende tomografie (X-straal mikro CT) is gebruik as ‘n nie-vernietigende tegniek om die effek van swamskade op die interne strukture van mieliepitte wat met *F. verticillioides* geïnfekteer is, te monitor.

X-straal beelde van kontrole en geïnfekteerde pitte is na inokulasie verkry deur hoë resolusie X-straal mikro CT oor tyd. Na die beelde verkry is, is agtereenvolgende twee-dimensionele (2D) deursnee-beelde herbou in drie-dimensionele (3D) volumes van die mieliepitte. Kwalitatiewe resultate is aangebied as 2D projeksie beelde, en 3D volumes wat visualisering in verskeie aansigte (bo-, voor-, en syaansig) moontlik maak. Meer ruimtes is waargeneem in veral die kiem en melerige endosperm van beide die kontrole en geïnfekteerde pitte oor tyd. Kwantitatiewe parameters insluitende totale volume, gemiddelde gryswaarde en totale volume leemtes is bereken. Totale volume en gemiddelde gryswaarde het oor tyd toegeneem in beide die kontrole en geïnfekteerde pitte. Geen beduidende verskil ($P \geq 0.05$) is gerapporteer vir die kontrole en geïnfekteerde pitte vir die eerste vier dae waarop geskandeer is nie.

Algoritmes is ontwikkel om beeld-tekstuur kenmerke van geselekteerde 2D beelde van beide kontrole en geïnfekteerde pitte te onttrek. Eerste-orde statistiek (gemiddeld, standaardafwyking, kurtoses en skeefheid) en grysvlak mede-voorkoms matriks (GLCM) kenmerke is onttrek uit die sy, voor- en bo-aansig van elke pit vir die dae waarop geskandeer is. Die uitsette van die berekening van hierdie tekstuur kenmerke is gebruik as insette vir die berekening van hoofkomponent analise (PCA) en vir die ontwikkeling van klassifikasie modelle deur die gebruik van parsiële kleinste kwadrate diskriminantanalise (PLS-DA). Duidelike skeiding tussen die kontrole en die geïnfekteerde pitte is gesien op dag 8 na inokulasie met die gebruik van eerste orde statistiese kenmerke. Klassifikasie akkuraatheid van 97% vir kontrole en 55% vir geïnfekteerde pitte is verkry met die ontwikkelde PLS-DA model. Die GLCM onttrekte kenmerke het ‘n beter klassifikasie akkuraatheid van 79% vir geïnfekteerde pitte, met minder geïnfekteerde pitte wat as kontrole geklassifiseer is in vergelyking met eerste orde statistiese kenmerke.

Hierdie studie het gedemonstreer dat, al kan X-straal mikro CT nie as ‘n vinnige tegniek vir die opsporing van ‘n swaminfeksie - veral in die vroeë stadia van infeksie - gebruik word nie, sal dit

die monitering van strukturele veranderinge in die mieliepit oor tyd toelaat, en sal dus ‘n beter begrip van die effek van swambeskadiging op die mikrostruktuur van die mieliepit teen hoë resolusie bied.

"For Thou wilt light my candle; the Lord my God will enlighten my darkness.
For by thee I have run through a troop; and by my God have I leaped over a wall".
(Psalms 18:28-29)

Acknowledgements

First and foremost, I would like to express my gratitude to the Almighty God for granting me wisdom, good health and strength that enable me to come thus far.

I would like to thank my supervisors, Dr Paul J. Williams and Professor Marena Manley, for their excellent team work, professional supervision, guidance, patience, motivation and mentorship. I could never find enough words to truly express my appreciation.

My co-supervisor, Prof Glaston Kenji (Department of Food Science and Technology, Jomo Kenyatta University of Agriculture and Technology, Nairobi, Kenya), for his guidance, motivation, mentorship and support.

A special thanks to my husband Nixon; his support, encouragement and prayers throughout this journey was extraordinary. And my son Jayden, whose presence cheered and motivated me.

I would like to express my sincere gratitude to the following people and institution for their contribution to the successful completion of my study:

Agri- Hope project at Stellenbosch University for financial support;

Schlumberger foundation, Faculty for the future fellowship to women in STEM for financial grant;

National Research Foundation Unique Grant No. 94031 for research grant;

Doctor Lindy Rose (Department of Plant Pathology, Stellenbosch University) for supplying fungal cultures and assisting in spore preparation;

Professor Sergey Kucheryavskiy from Department of Chemistry and Biosciences, Aalborg University, Esbjerg, Denmark for his assistance in image texture analysis in MATLAB.

Jomo Kenyatta University of Agriculture and Technology (JKUAT) for granting me study leave to future my studies;

Petro Du Buisson for translating my Abstract to Afrikaans.

Postgraduate office, Stellenbosch University for their very informative workshops;

My parents, sisters, brother and friends, for their endless WhatsApp chats that keep me going and relieved my homesick, their prayers, encouragement and motivation. Thank you, guys.

And finally, to the entire staff and postgraduate students at the Department of Food Science, Stellenbosch University for their support, encouragement and motivation.

Preface

This dissertation is presented as a compilation of manuscripts where each chapter is introduced separately and some repetition between chapter has, therefore been unavoidable. The language, style and referencing format used are in accordance with the requirements of the International Journal of Food Science and Technology. This dissertation includes two original papers published in peer reviewed journals and two unpublished papers.

TABLE OF CONTENTS

List of Figures

List of Tables

List of Abbreviations

%	percentage
µA	microamperes
ºC	degree Celsius
2D	two dimensional
3D	three dimensional
C	control
cm	centimetres
CT	computed tomography
e.g.	*exempli gratia* (for example)
et al	*et alibi* (and elsewhere)
Fig.	figure
g	gram
GLCM	grey level co-occurrence matrix
h	hour
I	infected
i.e.	*id est* (that is)
KNO_3	potassium nitrate
kV	kilovolt
L	litres
mA	milliampere
min	minutes
mL	millilitre
mm^3	cubic millimetres
MRC	medical research council
ms	milliseconds
n	number of samples

NIR	near infrared
PC	principal component
PCA	principal component analysis
PDA	potato dextrose agar
PLS	partial least squares
PLS-DA	partial least squares discriminant analysis
ppb	parts per billions
ppm	parts per million
rpm	revolutions per minute
s	seconds
SEM	scanning electron microscopy

Chapter 1
General Introduction

Maize (*Zea mays* L.) is one of the most important cereal grains worldwide. It is used as a source of food for both humans and animals. The use of maize for human consumption is very diverse, ranging from specialised foods in developed countries to staple food in developing countries (Nuss & Tanumihardjo, 2010). In the field as well as during storage, depending on the environmental conditions, maize is vulnerable to infection by fungi belonging to *Fusarium* species (Fandohan *et al.*, 2003). Among the several phytopathogenic species of *Fusarium*, *F. verticillioides* is considered the predominant species isolated worldwide from diseased maize (Munkvold & Desjardins, 1997). Fungal infection causes undesirable effects in maize kernels including discolouration, loss in nutritional value, off-odour production and loss in germination ability (Magan *et al.*, 2004). However, of major concern is production of mycotoxins which are harmful to humans and animals. Acute or chronic exposure to mycotoxins, including fumonisins produced by *F. verticillioides*, has shown to have carcinogenic, mutagenic, teratogenic, nephrotoxic, hepatoxic, neurotoxic and/or immunosuppressive effects (Wagacha & Muthomi, 2008; Pereira *et al.*, 2014). Therefore, detection of these fungi, with subsequent removal of infected grains, is essential in ensuring food safety, storage longevity and seed quality.

Conventional methods for detection of fungal infection in maize and other cereal grains include culture and colony based methods (Gourama & Bullerman, 1995), immunology-based methods (Notermans & Kamphuis, 1992), polymerase chain reaction methods (Dolezal *et al.*, 2013), microscopic techniques such as light microscopy (Bacon & Hinton, 1996), scanning electron microscopy (SEM) (Bacon *et al.*, 1992) and confocal laser scanning microscopy (Duncan & Howard, 2010b). These methods, though reliable, are time consuming, labour intensive (involving tedious sample preparation) and destructive in nature as they require cutting of the sample to access regions of interest. The microscopic techniques are limited to two dimensional (2D) images and sectioning of the sample is likely to disrupt the structure causing imaging artefacts (Salvo *et al.*, 2010). The limitations of these techniques have led to increasing interest in non-destructive techniques for detection of fungal infection in cereal grains.

Non-destructive techniques such as colour imaging (Singh *et al.*, 2012), Fourier transform photoacoustic infrared spectroscopy (Gordon *et al.*, 1997), near infrared (NIR) spectroscopy (Berardo *et al.*, 2005), electronic nose (Eifler *et al.*, 2011), thermal imaging (Chelladurai *et al.*, 2010), NIR hyperspectral imaging (Williams *et al.*, 2012) and neutron imaging (Cleveland *et al.*, 2008) have been

explored for detection of fungal damage in cereal grains. Although these techniques are effective, they offer limited information on internal structural changes that occur during fungal damage.

X-ray micro computed tomography (X- ray micro CT) is an emerging technique in the field of food science for non-destructive visualisation and characterisation of the internal microstructure of food products at high resolution (Schoeman *et al.*, 2016b). This technique allows one to investigate the interior of an object, without sacrificing it, and thus enables monitoring of structural changes over time (Cnudde & Boone, 2013). X-ray micro CT is based on the contrast in X-ray images resulting from differences in X-ray attenuation that arises mainly from differences in density within a sample (Landis & Keane, 2010). X-rays are passed through a rotating sample (usually 180º or 360º), creating a series of 2D projection images. The denser regions within the sample will appear brighter on the 2D image as they correspond to areas of higher X-ray attenuation and vice versa (Schoeman *et al.*, 2016b). The consecutive 2D images can be rendered into a 3D volume allowing for not only multidirectional examination of the sample, but also permits quantitative measurements (Herremans *et al.*, 2013).

X-ray micro CT enables qualitative (visualisation) and quantitative analysis of the internal structure using two-dimensional (2D) projection images and three-dimensional (3D) rendered volume of a sample (Landis & Keane, 2010). This technique has found wide application in food science, for example to observe foam microstructure by measuring cell size and shape, void space and spatial distribution (Lim & Barigou, 2004), to study ice crystals within frozen foods (Mousavi *et al.*, 2005) and to assess intramuscular fat levels and distribution in beef muscles (Frisullo *et al.*, 2009; Frisullo *et al.*, 2010). It has also been used for 3D quantitative analysis of bread crumbs (Falcone *et al.*, 2005), to evaluate the role of sugar and fat in sugar-snap cookies (Pareyt *et al.*, 2009) and microstructural characterisation of fruits e.g. apples (Mendoza *et al.*, 2007; Herremans *et al.*, 2013b), commercial kiwifruit (Cantre *et al.*, 2014) and pomegranate fruit (Magwaza & Opara, 2014).

In cereal grains studies, Schoeman *et al.* (2016a) used X-ray micro CT to evaluate the effect of conventional oven and forced convection continuous tumble (FCCT) roasting on the microstructure of whole wheat kernels. Considerable structural changes were observed after roasting the kernels, especially in the oven roasted wheat kernels which had large cavities resulting in more open porous and expanded structure compared to the FCCT-roasted kernels. Quantitative measurements including volume, porosity, expansion ratio and relative density were calculated from the rendered 3D volumes. Roasting caused an increase in volume, porosity, expansion ratio and a decrease in relative density. These measurements were higher in oven roasting compared to FCCT roasting, implying FCCT roasting had minimal structural damage (Schoeman *et al.*, 2016a). Gustin *et al.* (2013) and Guelpa *et al.* (2015) demonstrated the potential of X-ray micro CT to determine

maize kernel volume and density. Using this technique, the different components within the maize kernel could be distinguished based on their differences in density. The embryo and scutellum were more dense as they appeared brighter (higher grey value) on the 2D cross-sectional images of the kernels (Gustin *et al.*, 2013). Large cavities were observed in the floury endosperm, especially in the soft maize kernels (Guelpa *et al.*, 2015). X-ray micro CT enabled estimation of maize hardness using a density calibration, and quantification of porosity and cavities within the endosperm (Guelpa *et al.*, 2015).

Limited studies have explored the potential of X-ray micro CT to evaluate the effect of fungal infection on maize kernel internal structure. Pearson and Wicklow (2006) analysed the potential of traditional X-ray imaging to detect fungal infection in maize kernels. Kernels were radiographed using a cabinet X-ray system (43855A, Faxitron Corp. Wheeling. I11) and X-ray films were digitally scanned for further analysis. The authors reported a significantly lower mean X-ray intensity in fungal infected kernels than in undamaged kernels at a 95% confidence level. This indicated lower density in the fungal infected kernels as they absorbed less X-ray energy. Classification accuracy of 100% for undamaged kernels and 82% for fungal damaged kernels were obtained using Stepwise Discriminant analysis with selected X-ray image features (mean, standard deviation and maximum pixel intensity).

In another study, Narvankar *et al.* (2009) used X-ray imaging to detect fungal infection in wheat. The wheat kernels infected with common storage fungi, namely *Aspergillus niger, A. glaucus* group and *Penicillium* species, as well as healthy kernels were scanned using an X-ray imaging system (Lixi fluoroscope, LX-85708, Lixi Inc., Downer Grove, IL). Image features were extracted from single images of fungal infected and healthy wheat kernels. The image features were then given as input to statistical discriminant classifiers (linear, quadratic and Mahalanobis) and back-propagation neural network (BPNN) classifier. Accuracies of 92.2 to 98.9% were achieved using a two-class Mahalanobis discriminant classifier in distinguishing fungal infected wheat kernels from healthy kernels. A major drawback in traditional X-ray imaging is the loss of depth information, i.e. only one projection image (X-ray transmission through the sample) is acquired per sample.

Image texture analysis is an essential tool for evaluation of images, that seeks to find a relationship between different image features extracted and characteristics of the food product under investigation (Zheng *et al.*, 2006a). Image texture can be defined as the spatial arrangement of grey levels of pixels on digitised images (Du & Sun, 2004). The meaning of the term texture in image analysis is completely different from the usual meaning in food science. Food texture described as hardness, cohesiveness, viscosity, elasticity, adhesiveness, brittleness, chewiness and gumminess, normally referred to the manner in which human senses responses to food (Bourne, 2002). Image

texture analysis on the other hand entails extracting meaningful information from images which results in quantitative measurements useful for characterising a sample (Gunasekaran, 1996). Four categories are usually defined for extracting textural features including statistical texture, structural texture, model-based texture and transform-based texture (Bharati *et al.*, 2004). Among them, statistical texture is the most widely used in the food industry due to its high accuracy and less computation time (Zheng *et al.*, 2006b).

Statistical texture methods characterise the texture of an image region using statistical measures. The simplest set of features are those based on the pixel intensity distribution histogram of an image region, also known as first order statistics (Patel *et al.*, 2012). The most common ones are the position features such as mean and median, and those associated with statistical central moments such as variance, skewness and kurtosis. They, however, do not provide any information about the relative position of pixels and the correlation of their intensities (Prats-Montalbán *et al.*, 2011). Second order statistics of the statistical texture methods are based on spatial arrangement and interrelation of grey levels of the pixels in a region of an image (Bharati *et al.*, 2004). The most widely used second-order statistic in the field of image analysis is that related to the grey level co-occurrence matrices (GLCM) (Haralick & Shanmugam, 1973). The GLCM of an image is a square matrix whose elements correspond to the relative frequency of occurrence $p(i, j)$ of two pixels (one with intensity of i and other with intensity j), separated by a certain distance d in a given direction Θ (Zheng *et al.*, 2006a). Haralick and Shanmugam (1973) proposed 14 textural features extracted from GLCM, however the most common are energy, entropy, correlation, contrast, homogeneity and variance.

The computed image textural features can be subjected to multivariate analysis tools such as principal component analysis (PCA), partial least square discriminant analysis (PLS-DA), linear discriminant analysis (LDA) and artificial neutral networks (ANN) to aid in classification and even prediction. Image texture analysis have been used in classification and dockage identification of cereal grains (Majumdar & Jayas, 2000), to study dehydration of apple discs (Fernandez *et al.*, 2005), to evaluate image texture as an indicator of beef tenderness (Li *et al.*, 1999) and to discriminate crumb grain visual appearance of organic and non-organic bread loaves (Gonzales-Barron & Butler, 2008).

The aim of this study was to evaluate the feasibility of high resolution X-ray micro CT as a non-destructive technique for visualisation and quantification of internal structural changes in fungal infected maize kernels. Specific objectives were to:

- monitor internal structural changes in maize kernels infected with *Fusarium verticillioides* over time using high resolution X-ray micro CT;

- apply image texture analysis to X-ray images of uninfected and infected maize kernels to quantify the effect of fungal damage;
- discriminate infected from uninfected maize kernels using image textural features extracted from X-ray images and applied to multivariate analysis.

Reference

Bacon, C., Bennett, R., Hinton, D. & Voss, K. (1992). Scanning electron microscopy of *Fusarium moniliforme* within asymptomatic corn kernels and kernels associated with equine leukoencephalomalacia. *Plant Disease*, **76**, 144-148.

Bacon, C. & Hinton, D. (1996). Symptomless endophytic colonization of maize by *Fusarium moniliforme*. *Canadian Journal of Botany*, **74**, 1195-1202.

Berardo, N., Pisacane, V., Battilani, P., Scandolara, A., Pietri, A. & Marocco, A. (2005). Rapid detection of kernel rots and mycotoxins in maize by near-infrared reflectance spectroscopy. *Journal of Agricultural and Food Chemistry*, **53**, 8128-8134.

Bharati, M.H., Liu, J.J. & MacGregor, J.F. (2004). Image texture analysis: methods and comparisons. *Chemometrics and Intelligent Laboratory Systems*, **72**, 57-71.

Bourne, M. (2002). *Food texture and viscosity: concept and measurement.* Academic press. 2nd edition, Cornell University, Geneva, New York.

Cantre, D., East, A., Verboven, P., Araya, X.T., Herremans, E., Nicolaï, B.M., Pranamornkith, T., Loh, M., Mowat, A. & Heyes, J. (2014). Microstructural characterisation of commercial kiwifruit cultivars using X-ray micro computed tomography. *Postharvest Biology and Technology*, **92**, 79-86.

Chelladurai, V., Jayas, D. & White, N. (2010). Thermal imaging for detecting fungal infection in stored wheat. *Journal of Stored Products Research*, **46**, 174-179.

Cleveland, T., Hussey, D., Chen, Z.-Y., Jacobson, D., Brown, R., Carter-Wientjes, C. & Arif, M. (2008). The use of neutron tomography for the structural analysis of corn kernels. *Journal of Cereal Science*, **48**, 517-525.

Cnudde, V. & Boone, M.N. (2013). High-resolution X-ray computed tomography in geosciences: A review of the current technology and applications. *Earth-Science Reviews*, **123**, 1-17.

Dolezal, A.L., Obrian, G.R., Nielsen, D.M., Woloshuk, C.P., Boston, R.S. & Payne, G.A. (2013). Localization, morphology and transcriptional profile of *Aspergillus flavus* during seed colonization. *Molecular Plant Pathology*, **14**, 898-909.

Du, C.J. & Sun, D.W. (2004). Recent developments in the applications of image processing techniques for food quality evaluation. *Trends in Food Science & Technology*, **15**, 230-249.

Duncan, K.E. & Howard, R.J. (2010). Biology of maize kernel infection by *Fusarium verticillioides*. *Molecular Plant-Microbe Interactions*, **23**, 6-16.

Eifler, J., Martinelli, E., Santonico, M., Capuano, R., Schild, D. & Di Natale, C. (2011). Differential detection of potentially hazardous *Fusarium* species in wheat grains by an electronic nose. *PloS One*, **6**, e21026.

Falcone, P.M., Baiano, A., Mancini, L., Tromba, G., Zanini, F., Dreossi, D., Montanari, F., Scuor, N. & Del Nobile, M.A. (2005). Three dimensional quantitative analyss of bread crumb by X-ray microtomography. *Journal of Food Science*, **70**, E38-E43.

Fandohan, P., Hell, K., Marasas, W. & Wingfield, M. (2003). Infection of maize by *Fusarium* species and contamination with fumonisin in Africa. *African Journal of Biotechnology*, **2**, 570-579.

Fernandez, L., Castillero, C. & Aguilera, J. (2005). An application of image analysis to dehydration of apple discs. *Journal of Food Engineering*, **67**, 185-193.

Frisullo, P., Laverse, F., Marino, R. & Nobile, M.A.D. (2009). X-ray computed tomography to study processed meat microstructure. *Journal of Food Engineering*, **94**, 283-289.

Frisullo, P., Marino, R., Laverse, J., Albenzio, M. & Del Nobile, M. (2010). Assessment of intramuscular fat level and distribution in beef muscles using X-ray microcomputed tomography. *Meat Science*, **85**, 250-255.

Gonzales-Barron, U. & Butler, F. (2008). Discrimination of crumb grain visual appearance of organic and non-organic bread loaves by image texture analysis. *Journal of Food Engineering*, **84**, 480-488.

Gordon, S., Schudy, R., Wheeler, B., Wicklow, D. & Greene, R. (1997). Identification of fourier transform infrared photoacoustic spectral features for detection of *Aspergillus flavus* infection in corn. *International Journal of Food Microbiology*, **35**, 179-186.

Gourama, H. & Bullerman, L.B. (1995). Detection of molds in foods and feeds: potential rapid and selective methods. *Journal of Food Protection*, **58**, 1389-1394.

Guelpa, A., Plessis, A.d., Kidd, M. & Manley, M. (2015). Non-destructive estimation of maize kernel hardness by means of an X-ray micro-computed tomography density calibration. *Food Bioprocess Technology*, **8**, 1419-1429.

Gunasekaran, S. (1996). Computer vision technology for food quality assurance. *Trends in Food Science & Technology*, **7**, 245-256.

Gustin, J., Jackson, S., Williams, C., Patel, A., Armstrong, P., Peter, G.F. & Settles, M.A. (2013). Analysis of maize (*Zea mays*) kernel density and volume using microcomputed tomography and single kernel near-infrared spectroscopy. *Journal of Agriculture and Food Chemistry*, **61**, 10872-10880.

Haralick, R.M. & Shanmugam, K. (1973). Textural features for image classification. *IEEE Transactions on Systems, Man, and Cybernetics*, **3**, 610-621.

Herremans, E., Verboven, P., Bongaers, E., Estrade, P., Verlinden, B.E., Wevers, M., Hertog, M.L.A.T.M. & Nicolai, B.M. (2013). Characterisation of 'Braeburn' browning disorder by means of X-ray micro-CT. *Postharvest Biology and Technology*, **75**, 114-124.

Landis, E.N. & Keane, D.T. (2010). X-ray microtomography. *Materials Characterization*, **61**, 1305-1316.

Li, J., Tan, J., Martz, F. & Heymann, H. (1999). Image texture features as indicators of beef tenderness. *Meat Science*, **53**, 17-22.

Lim, K.S. & Barigou, M. (2004). X-ray micro-computed tomography of cellular food products. *Food Research International*, **37**, 1001-1012.

Magan, N., Sanchis, V. & Aldred, D. (2004). Role of spoilage fungi in seed deterioration. Fungal biotechnology in agricultural, food and environmental applications, Marcel Dekker Inc., New York, USA, pp. 311-323.

Magwaza, L.S. & Opara, U.L. (2014). Investigating non-destructive quantification and characterization of pomegranate fruit internal structure using X-ray computed tomography. *Postharvest Biology and Technology*, **95**, 1-6.

Majumdar, S. & Jayas, D. (2000). Classification of cereal grains using machine vision: III. Texture models. *Transactions of the ASAE*, **43**, 1681-1687.

Mendoza, F., Verboven, P., Mebastsion, H.K., Kerckhofs, G., Wevers, M. & Nicolai, B.M. (2007). Three dimensional pore space quantification of apple tissue using X-ray computed microtomography *Planta*, **226**, 559-570.

Mousavi, R., Miri, T., Cox, P. & Fryer, P.J. (2005). A novel technique for ice crystal visualization in frozen solids using X-Ray micro-computed tomography. *Journal of Food Science*, **70**, e437-e442.

Munkvold, G.P. & Desjardins, A.E. (1997). Fumonisins in maize: can we reduce their occurrence? *Plant Disease*, **81**, 556-565.

Narvankar, D., Singh, C., Jayas, D. & White, N. (2009). Assessment of soft X-ray imaging for detection of fungal infection in wheat. *Biosystems Engineering*, **103**, 49-56.

Notermans, S. & Kamphuis, H. (1992). Detection of fungi in foods by latex agglutination: a collaborative study. In: Modern methods of food mycology. pp. 205-212. New York, USA.

Nuss, E.T. & Tanumihardjo, S.A. (2010). Maize: a paramount staple crop in the context of global nutrition. *Comprehensive Reviews in Food Science and Food Safety*, **9**, 417-436.

Pareyt, B., Talhaoui, F., Kerckhofs, G., Brijs, K., Goesaert, H., Wevers, M. & Delcour, J.A. (2009). The role of sugar and fat in sugar-snap cookies: structural and textural properties. *Journal of Food Engineering*, **90**, 400-408.

Patel, K.K., Kar, A., Jha, S. & Khan, M. (2012). Machine vision system: a tool for quality inspection of food and agricultural products. *Journal of Food Science and Technology*, **49**, 123-141.

Pearson, T. & Wicklow, D. (2006). Detection of corn kernels infected by fungi. *Transactions of the ASABE*, **49**, 1235-1245.

Pereira, V., Fernandes, J. & Cunha, S. (2014). Mycotoxins in cereals and related foodstuffs: A review on occurrence and recent methods of analysis. *Trends in Food Science & Technology*, **36**, 96-136.

Prats-Montalbán, J., De Juan, A. & Ferrer, A. (2011). Multivariate image analysis: a review with applications. *Chemometrics and Intelligent Laboratory Systems*, **107**, 1-23.

Salvo, L., Suéry, M., Marmottant, A., Limodin, N. & Bernard, D. (2010). 3D imaging in material science: Application of X-ray tomography. *Comptes Rendus Physique*, **11**, 641-649.

Schoeman, L., du Plessis, A. & Manley, M. (2016a). Non-destructive characterisation and quantification of the effect of conventional oven and forced convection continuous tumble (FCCT) roasting on the three-dimensional microstructure of whole wheat kernels using X-ray micro-computed tomography (µCT). *Journal of Food Engineering*, **187**, 1-13.

Schoeman, L., Williams, P., du Plessis, A. & Manley, M. (2016b). X-ray micro-computed tomography (µCT) for non-destructive characterisation of food microstructure. *Trends in Food Science & Technology*, **47**, 10-24.

Singh, C.B., Jayas, D.S., Paliwal, J. & White, N.D. (2012). Fungal damage detection in wheat using short-wave near-infrared hyperspectral and digital colour imaging. *International Journal of Food Properties*, **15**, 11-24.

Wagacha, J. & Muthomi, J. (2008). Mycotoxin problem in Africa: current status, implications to food safety and health and possible management strategies. *International Journal of Food Microbiology*, **124**, 1-12.

Williams, P.J., Geladi, P., Britz, T.J. & Manley, M. (2012). Investigation of fungal development in maize kernels using NIR hyperspectral imaging and multivariate data analysis. *Journal of Cereal Science*, **55**, 272-278.

Zheng, C., Sun, D.-W. & Zheng, L. (2006a). Recent applications of image texture for evaluation of food qualities—a review. *Trends in Food Science & Technology*, **17**, 113-128.

Zheng, C., Sun, D.-W. & Zheng, L. (2006b). Recent developments and applications of image features for food quality evaluation and inspection–a review. *Trends in Food Science & Technology*, **17**, 642-655.

Declaration by student

With regard to Chapter 2 (pp 10- 51) the nature and scope of my contribution were as follows:

Nature of contribution	Extent of contribution (%)
Literature search and writing of chapter	70%

The following co-authors have contributed to Chapter 2:

Name	e-mail address	Nature of contribution	Extent of contribution (%)
Dr Paul J. Williams	pauljw@sun.ac.za	Research inputs, editorial suggestions and proofreading	15%
Prof Marena Manley	mman@sun.ac.za	Research inputs, editorial suggestions and proof reading	15%

Signature of student: I. Orina

Date: 13/12/2017

The undersigned hereby confirm that:

1. the declaration above accurately reflects the nature and extent of the contributions of the candidate and the co-authors to Chapter 2 (pp 10- 51),
2. no other authors contributed to Chapter 2 (pp 10- 51) besides those specified above, and
3. potential conflicts of interest have been revealed to all interested parties and that the necessary arrangements have been made to use the material in Chapter 2 (pp 10-51) of this dissertation.

Signature	Institutional affiliation	Date
Dr Paul J. Williams	Department of Food Science, Stellenbosch University	13/12/2017
Prof Marena Manley	Department of Food Science, Stellenbosch University	13/12/2017

Chapter 2

Literature review

Non-destructive techniques for the detection of fungal infection in cereal grains*

Abstract

Infection of cereal grains by fungi is a serious problem worldwide. Depending on the environmental conditions, cereal grains may be colonized by different species of fungi. These fungi cause reduction in yield, quality and nutritional value of the grain; and of major concern is their production of mycotoxins which are harmful to both humans and animals. Early detection of fungal contamination is an essential control measure for ensuring storage longevity and food safety. Conventional methods for detection of fungal infection, such as culture and colony techniques or immunological methods are either slow, labour intensive or difficult to automate. In recent years, there has been an increasing need to develop simple, rapid, non-destructive methods for early detection of fungal infection and mycotoxins contamination in cereal grains. Methods such as near infrared (NIR) spectroscopy, NIR hyperspectral imaging, and electronic nose were evaluated for these purposes. This chapter reviews the different non-destructive techniques that have been considered thus far for detection of fungal infection and mycotoxins in cereal grains, including their principles, application and limitations.

Keywords: Cereal grains; Fungal detection; mycotoxins contamination; non-invasive techniques.

*Published as: Irene Orina, Marena Manley & Paul J. Williams (2017). Non-destructive techniques for the detection of fungal infection in cereal grains. *Food Research International*, **100,**74-86.

Introduction

Cereal grains constitute major sources of dietary energy and protein for humans and livestock. Maize, wheat, rice and barley represent the key staple cereal grains worldwide (Haard, 1999). Other cereal grains such as sorghum, oats, rye and millet are also relatively important. A chronic problem with cereal grains worldwide is the infection by fungi, belonging to the genera *Aspergillus*, *Penicillium*, *Fusarium* and *Alternaria* (Wagacha & Muthomi, 2008). The growth of fungi in the grains results in discolouration; contributes to heating and losses in dry matter through utilisation of carbohydrates as energy sources; degrades lipids and proteins or alter their digestibility; produces volatile metabolites giving off-odours; causes loss of germinability, hence affect their use as seed; and loss of baking and malting quality (Christensen, 1973). Of major concern, however, is the production of toxic fungal secondary metabolites, mycotoxins, which pose health hazards to humans and animals (Hussein & Brasel, 2001; Naresh *et al.*, 2004). The major mycotoxins that occur in cereal grains include aflatoxins produced by *Aspergillus*; ochratoxins produced by *Penicillium* and *Aspergillus*; and fumonisins, deoxynivalenol, trichothecenes and zearalenone produced by *Fusarium* (Pascale, 2009; Pereira *et al.*, 2014). Although these toxins are typically present in levels as low as parts per million (ppm) or parts per billion (ppb), acute or chronic exposure to mycotoxins has been associated with immuno-suppression (Wagacha & Muthomi, 2008), impaired growth in children (Gong *et al.*, 2004), malnutrition (Ramjee *et al.*, 1992), liver cancer (Williams *et al.*, 2004) and death in some incidences (Lewis *et al.*, 2005). Early detection and, if possible, removal of fungal contaminated grains is an important control measure in ensuring storage longevity, seed quality and food safety (Pasikatan & Dowell, 2001).

Traditional methods used to detect fungal infection and/or mycotoxin contamination include: culture and colony techniques (Gourama & Bullerman, 1995a); chemical analyses (Lin & Cousin, 1985); enzyme linked immunosorbent assay (ELISA) (Meirelles *et al.*, 2006); adenosine triphosphate (ATP) bioluminescence, the polymerase chain reaction (PCR) method (Boutigny *et al.*, 2012), chromatographic techniques (Pereira *et al.*, 2014) and biosensors (van der Gaag *et al.*, 2003). Although reliable, specific and sensitive; these methods are time-consuming and labour-intensive; they involve tedious sample preparation which lead to destruction of the sample. Hence, efforts have been made to develop simple, rapid, accurate and non-destructive methods for detection of fungal contamination in cereal grains. Non-destructive techniques for fungal detection and mycotoxins contamination have thus become a major area of interest recently.

The emergence of modern imaging acquisition techniques, in conjunction with image processing methods has offered many potential avenues for non-destructive evaluation of agricultural products (Chen & Sun, 1991). Techniques such as colour imaging (Tallada *et al.*, 2011), Fourier

transform infrared photoacoustic spectroscopy (FTIR-PAS) (Greene *et al.*, 1992), electronic nose (Paolesse *et al.*, 2006), near infrared (NIR) spectroscopy (Berardo *et al.*, 2005), hyperspectral imaging (Siripatrawan & Makino, 2015), thermal imaging (Chelladurai *et al.*, 2010), neutron tomography (Cleveland *et al.*, 2008) and X-ray imaging (Narvankar *et al.*, 2009) have been investigated for their application of fungal and/or mycotoxins detection in grains. The present chapter provides a review of the non-destructive techniques that have been utilised to determine fungal infection and mycotoxin contamination (where applicable) in cereal grains along with their limitations.

Colour imaging

Colour is a vital visual attribute of cereal grains used in grain inspection and grading. Characterisation of different grains and their varieties is based on kernel colour and discolouration due to grain damage (Luo *et al.*, 1999). Colour images are described either using the primary colours red, green and blue (RGB system) or by converting the RGB component value of the object image to the main factors of human colour sensation namely hue, saturation and intensity (HSI system) (Gunasekaran, 1996; Majumdar, 1998). A colour imaging system essentially consists of a sample holding platform, digital camera for capturing the image, image capture board (frame grabber or digitiser) for digitising the image, light source for proper illumination, and computer hardware and software to process the images (Fig. 2.1) (Vithu & Moses, 2016). A digital image is acquired by incident light in the visible spectrum falling on a partially reflective surface of the sample. The scattered photons are gathered up in the camera lens and then converted to electrical signals by either a vacuum tube or charge-coupled device (CCD), and saved on a hard disk for further image display and image analysis (Wu & Sun, 2013).

A system consisting of a high-pixel resolution CCD chip and associated hardware is the commonly used method for generating digital images (Patel *et al.*, 2012). The acquired digital images of the object are then pre-processed for the purpose of enhancing the image quality or for removing irrelevant sources of variation (Vithu & Moses, 2016). Image acquisition and image analysis are the two vital steps for the application of colour imaging. A high-quality image can help to reduce the time and complexity of the subsequent image processing steps. The colour features of an object are extracted by examining every pixel within the object boundaries (Du & Sun 2004). Colour image features including the mean, histograms of the red, green and blue colour, intensity, range of hue, saturation and textural features derived from grey level co-occurrence matrices (GLCM) are extracted using appropriate image processing algorithms (Gunasekaran, 1996). These features are then used as input to statistical discriminant classifiers to differentiate the grains. The advantage of colour imaging is the possibility of analysing each pixel of the entire surface of the grain and quantifying surface characteristics and defects (Brosnan & Sun, 2004; Du & Sun, 2004).

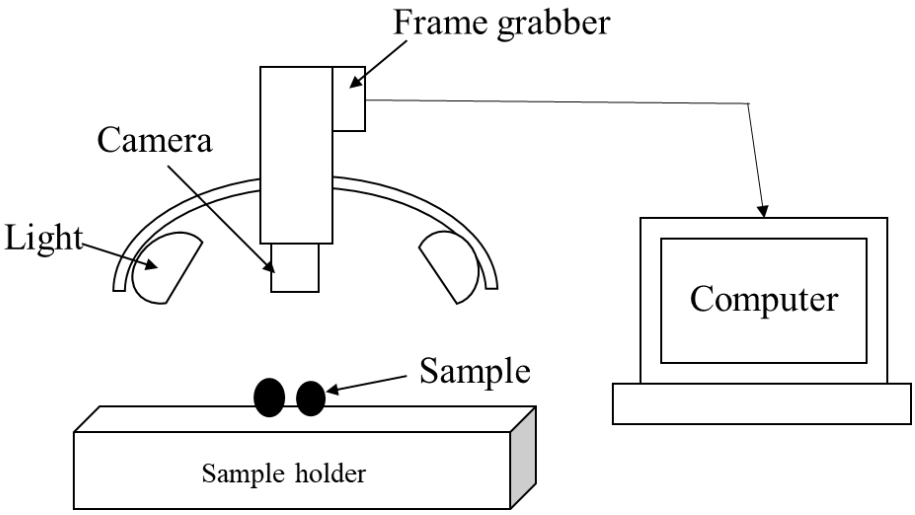

Figure 2.1. Schematic diagram of a typical colour imaging system, adapted from Vithu and Moses (2016). Digital images of the sample are acquired using the camera and processed further in the computer to extract useful information.

Fungal damage of cereal grains is usually associated with discolouration and fissures on the seed coats, and the degree of discolouration varies with the type of fungi (Wang *et al.*, 2004). Colour imaging has been used to detect fungal infection in wheat (Singh *et al.*, 2012; Jirsa & Polišenská, 2014) and maize (Tallada *et al.*, 2011). A summary of the different non-destructive techniques that have been used in the study of fungal infection in cereal grains is given in Table 2.1. Singh *et al.* (2012) extracted a total of 179 features (colour and textural) from the colour images of fungal infected and healthy wheat kernels. Two-way classification algorithms were developed using the top ten selected features of the 179 colour and textural features. The top ten features were selected due to their high discrimination capability using the STEPDISC (step-wise discrimination analysis) procedure in SAS (Version 9.1, SAS Institute Inc., Cary, NC, USA). Healthy kernels were correctly classified with 94.3, 90.3, and 89.3% accuracy by linear discriminant analysis (LDA), quadratic discriminant analysis (QDA) and Mahalanobis discriminant classifiers, respectively (Singh *et al.*, 2012).

The performance of colour imaging to discriminate maize kernels infected by eight fungal species at different levels of infection was evaluated by Tallada *et al.* (2011). Colour images were used to develop linear and nonlinear prediction models using LDA and multi-layer perceptron (MLP) neural networks. Higher levels of infection had better classification accuracies of 81 to 89%. Colour imaging was not able to classify mould species well. The use of principal component analysis (PCA) on image data did not improve the classification results. The LDA models performed as well as the MLP models, with or without the use of PCA (Tallada *et al.*, 2011). One likely constraint in the use of colour imaging is the limited electromagnetic range in which optical data can be obtained, and

physical discolouration in the kernels is the only source of variation. Therefore, this technique could possibly work well at a rather advanced stage of infection (Tallada *et al.*, 2011).

Fourier transform infrared photoacoustic spectroscopy (FTIR-PAS)

Photoacoustic spectroscopy (PAS) is a non-destructive technique that directly measures energy absorbed by the sample rather than what is transmitted or reflected (Ryczkowski, 2010). PAS operating in a Fourier transform mid-infrared (FTIR) system, is based on the photoacoustic effect caused when a modulated infrared beam from the spectrophotometer impinges on a sample surface in a sealed cell purged with inert helium (Sivakesava & Irudayaraj, 2000; Ryczkowski, 2010). Helium is commonly used because of its superior thermoacoustic coupling properties (Jiang & Palmer, 1997). The infrared (IR) light absorbed by the sample heats it and the heat migrates to the gas/sample interface and produces a pressure wave in proportion to the absorbance by the sample. The resultant pressure signal is then detected by a sensitive microphone and converted into a wavenumber versus absorbance intensity spectrum (Anderson *et al.*, 2013). A schematic diagram of a PAS cell is shown in Fig. 2.2. The shape of the photoacoustic spectrum is independent of the morphology of the sample under investigation (Ryczkowski, 2010). Among the key advantages of FTIR-PAS is the depth profiling capability for non-destructive evaluation of successive layers below the sample surface (Sivakesava & Irudayaraj, 2000). FTIR-PAS in food related research is limited, it has found application in food characterisation (Irudayaraj *et al.*, 2001), microorganism detection (Irudayaraj *et al.*, 2002), classification of rapeseed varieties (Lu *et al.*, 2014), analysis of potato chips (Sivakesava & Irudayaraj, 2000), pea seeds (Letzelter *et al.*, 1995) and coffee (Gordillo-Delgado *et al.*, 2012).

FTIR-PAS was used to detect fungal infection in maize (Table 2.1) (Greene *et al.*, 1992; Gordon *et al.*, 1997). Gordon *et al.* (1997) selected 10 major photoacoustic spectral features by visual inspection of the photoacoustic spectrum of *Aspergillus flavus* cultured on potato dextrose agar against the photoacoustic spectrum of an uninfected maize kernel. These top 10 spectral features were selected based on the theoretical comparison of the relative chemical composition of the fungi and maize. They then manually categorised the kernels into classes based on spectral differences. They also performed a 'blind' study on the FTIR-PAS using 10 maize kernels showing bright greenish yellow fluorescence (BGYF) and 10 BGYF negative kernels. FTIR-PAS was able to correctly classify the infected and non-infected maize kernels (Gordon *et al.*, 1997). The FTIR-PAS technique, with its multifactor classification scheme, was able to detect several major chemical changes in the infected maize kernels and is thus considerably more reliable than the single-factor BGYF test for detecting infection in maize (Gordon *et al.*, 1997).

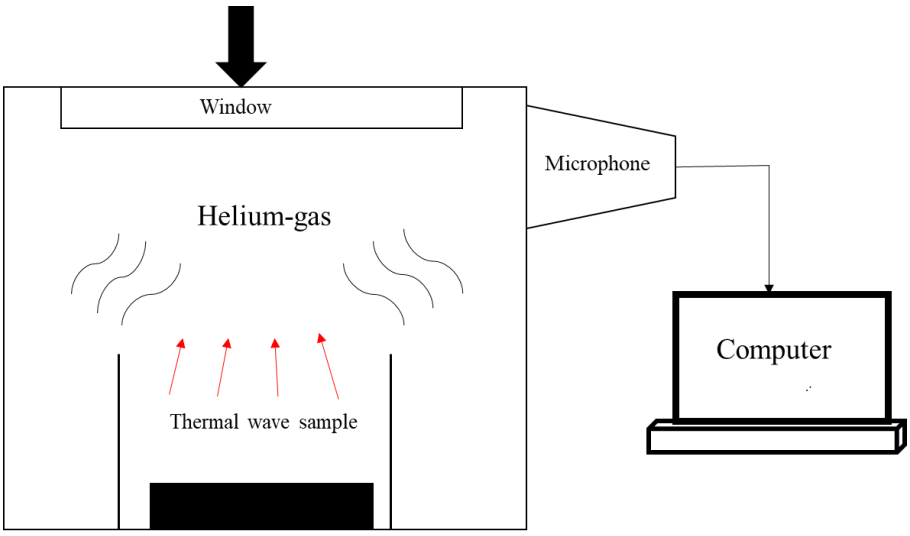

Figure 2.2. Illustration of a typical photoacoustic spectroscopy cell, adapted from Dole *et al.* (2011). Pressure waves generated by the sample are detected by a sensitive microphone which sends a signal to the computer to generate an infrared (IR) spectrum.

Greene *et al.* (1992) demonstrated the potential of using FTIR in conjunction with PAS to detect maize infected with *Fusarium moniliforme*. The spectrum of an intact maize kernel infected with *F. moniliforme* was dramatically different from the one recorded from uninfected maize. A difference spectrum was generated by subtracting the spectrum of the uninfected from the spectrum of the infected maize. Strong amide I (1650 cm^{-1}) and amide II (1550 cm^{-1}) absorbance in conjunction with a downfield shift of the broad peak between 3000 and 3600 cm^{-1} were observed in the difference spectrum, suggesting an increase in protein or acetylated amino sugar content due to subsequent fungal infection. The various absorption bands evident in the difference spectrum were indicative of specific biochemical changes that occur when *F. moniliforme* attack the maize (Greene *et al.*, 1992). The FTIR-PAS technique is however limited by the design of commercially available photoacoustic detectors which allows analysis of a single maize kernel in a small sealed sample cell. Hence, the technique could be adequate for plant pathologists and breeders seeking to study individual seeds (Gordon *et al.*, 1999).

Electronic nose

The electronic nose aims to mimic the mammalian sense of smell by producing a composite response unique to each odour (Casalinuovo *et al.*, 2006). The system consists of an array of electronic chemical gas sensors with different selectivity, a signal collection unit which converts the sensor signal to a readable format and software analysis of the data to produce characteristic output related to the odour encountered (Fig. 2.3) (Schaller *et al.*, 1998; Liu *et al.*, 2012). The electronic nose is therefore based on non-selective sensors that interact with volatile compounds present in the headspace of a sample. A signal is then sent to a computer which makes a classification based on

calibration and training processes, leading to pattern recognition (Baldwin *et al.*, 2011). The interpretation of the signal is accomplished using multivariate techniques such as pattern recognition algorithms, discriminant functions, cluster analysis and artificial neural networks (Schaller *et al.*, 1998; Magan & Evans, 2000). Metal oxide semiconductors (MOS), conducting polymer and surface acoustic waves (transducers) are the most common electronic nose sensors (Deisingh *et al.*, 2004). Electronic nose techniques for detection of fungal infection is based on identification of specific volatile compounds associated with the growth of several microorganisms on cereal grains (Magan & Evans, 2000).

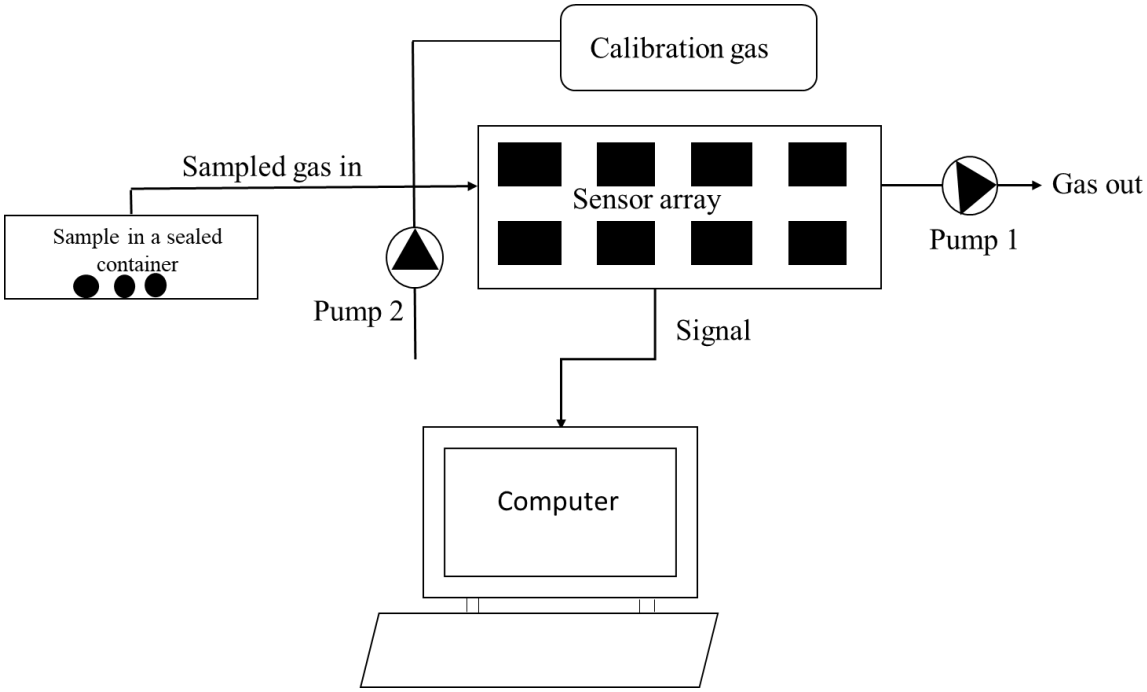

Figure 2.3. Display of basic components of an electronic nose system, adapted from Gómez *et al.* (2006). The headspace of the sample is pumped into the sensor array to obtain a signal which is interpreted on the computer.

The electronic nose has been used for quality classification of wheat (Stetter *et al.*, 1993), to group grain samples (wheat, barley, oats) based on their smell and to predict degree of mouldy/musty odours (Börjesson *et al.*, 1996) and microbial grading of grains (Jonsson *et al.*, 1997; Magan & Evans, 2000). Paolesse *et al.* (2006) studied the application of the electronic nose for detection of fungal infection in soft wheat seeds (50 g) stored in sealed bottles with inlet and outlet. The volatile components in the grain headspace were introduced into a stainless-steel measurement chamber using a micro-pump. They developed a partial least square discriminant analysis (PLS-DA) model with a classification accuracy of 85.3%. The PLS-DA model showed some overlapping between classes with the same water activity and the same species of fungi, reducing the classification accuracy.

Complex chemical patterns of volatile components prevented a complete characterisation of the different volatile organic compounds present in the grain headspace (Paolesse *et al.*, 2006).

Electronic nose data combined with artificial neural network (ANN) was used for microbial quality classification of oats, rye, barley and wheat (Jonsson *et al.*, 1997). These cereals were heated in a chamber and the released gas was led over the sensory array. The ANN model predicted the odour of good, mouldy, weakly and strongly musty oats with a high degree of accuracy. The ANN model also indicated the percentage of mouldy barley or rye grains in mixtures with fresh grains. A high correlation was observed in wheat between the ANN predictions and measured ergosterol, fungal and bacterial colony forming units (Jonsson *et al.*, 1997). Börjesson *et al.* (1996) classified wheat, barley and oat samples using the electronic nose based on their odour. The sample classification was divided into either four classes i.e. mouldy/musty, acid/sour, burnt or normal, or the two classes good and bad per the inspector description. The sensor signal from the headspace of the heated samples were evaluated with a pattern recognition software program based on ANN. The electronic nose correctly classified approximately 75% of the samples when using the four-class system and approximately 90% when using the two-class system. The drawbacks of the electronic nose include its inability to identify specific volatile compounds, and the training procedures can be lengthy and laborious (Concina *et al.*, 2009).

Table 2.1. A summary of non-destructive techniques that have been used for the detection of fungal infection in cereal grains

Technique	Principle	Features	Classifier	Cereal	Fungi	References
Colour imaging	Colour variation (red, green, blue)	Hue, saturation, intensity, RGB histograms, chromaticity coordinates, textural features	LDA	Wheat	*Fusarium* spp.	Jirsa and Polišenská (2014)
			LDA and MLP neutron networks	Maize	*Aspergillus flavus, Bipolaris zeicola, Diplodia maydis, Fusarium oxysporum, Penicillium oxalicum, P. funiculosum, Trichoderma harzianum*	Tallada *et al.* (2011)
			LDA, QDA and Mahalanobis	Wheat	*Penicillium* spp., *Aspergillus glaucus, A. niger*	Singh *et al.* (2012)
			Stepwise-DA	Maize	*Aspergillus flavus, A. niger, Diplodia maydis, Fusarium graminearum, F. verticillioides, Trichoderma viride*	Pearson and Wicklow (2006)

			QDA and k-nearest neighbour	Wheat	Mould damage	Luo *et al.* (1999)
			Neural networks	Wheat	*Fusarium* spp.	Ruan *et al.* (1998)
				Maize	Mould damage	Steenoek *et al.* (2001)
				Maize	Mould damage	Ng *et al.* (1998)
				Triticale	*Fusarium* spp.	Wiwart *et al.* (2001)
				Popcorn	*Penicillium* spp.	Yorulmaz *et al.* (2012)
Fourier transform photo-acoustic infrared spectroscopy	Infrared spectroscopy with photo acoustic detector	Spectral features	Manual classification using spectral features	Maize	*Fusarium moniliforme*	Greene *et al.* (1992)
				Maize	*Aspergillus flavus*	Gordon *et al.* (1997)
				Maize	*Aspergillus flavus*	Gordon *et al.* (1999)
Electronic nose	Headspace sampling to generate signal pattern used to characterise odours	Volatiles in grain headspace	PCA	Wheat and triticale	*Fusarium culmorum*	Perkowski *et al.* (2008)
			PLS-DA	Wheat	*Fusarium* spp.	Eifler *et al.* (2011)
			PCA, PLS-R, PLS-DA, SIMCA	Barley	Mould damage	Olsson *et al.* (2000)
			PLS-R	Wheat	*Penicillium roqueforti*	Schnürer *et al.* (1999)

			PCA, PLS-DA	Wheat	*Penicillium aurantiogriseum, Penicillium vulpinum, Penicillium verrucosum, Fusarium culmorum, Aspergillus niger, A. flavus*	de Lacy Costello *et al.* (2003)
					Penicillium chrysogenum, Fusarium verticillioides	Paolesse *et al.* (2006)
			ANN, PLS	Wheat, barley, oats	Mould damage	Börjesson *et al.* (1996)
			ANN	Oats, rye, barley, wheat	Mould damage	Jonsson *et al.* (1997)
NIR spectroscopy	Spectral differences	Spectral features	PLS-R	Rice	*Aspergillus* spp.	Dachoupakan Sirisomboon *et al.* (2013)
				Maize	*Fusarium verticillioides*	Berardo *et al.* (2005)

	Wheat	*Fusarium* spp.	Dowell *et al.* (2002)
	Wheat	*Fusarium* spp.	Peiris *et al.* (2010)
LDA	Wheat	*Fusarium* spp.	Delwiche (2003)
LDA and non-parametric (k-nearest neighbour)	Wheat	*Fusarium* spp.	Delwiche and Hareland (2004)
PLS-R	Wheat	*Fusarium*	Wegulo and Dowell (2008)
SIMCA and neural network	maize	*Fusarium*	Draganova *et al.* (2010)
PLS-R	Wheat	*Mildew damage*	Shahin *et al.* (2014)
LDA and MLP neural networks	Maize	*Aspergillus flavus, Bipolaris zeicola, Diplodia maydis, Fusarium oxysporum, Penicillium oxalicum, P. funiculosum, Trichoderma harzianum*	Tallada *et al.* (2011)
Stepwise-DA	Maize	*Aspergillus flavus, A. niger, Diplodia maydis,*	Pearson and Wicklow (2006)

					Fusarium graminearum, *F. verticillioides*, *Trichoderma viride*	
NIR hyperspectral imaging	Spectral and spatial differences	Spectral features and image pixels	PCA	Maize	*Aspergillus parasiticus*, *A. flavus*, *A. niger*, *Fusarium graminearum*, *F. verticilliodes*	Del Fiore *et al.* (2010)
				Wheat	*Fusarium* spp.	Bauriegel *et al.* (2011)
				Wheat	*Fusarium* spp.	Shahin and Symons (2011)
			PCA, LDA, QDA, Mahalanobis	Wheat	*Penicillium* spp., *Aspergillus glaucus*, *A. niger*	Singh *et al.* (2007)
					Aspergillus glaucus, *Penicillium* spp.	Senthilkumar *et al.*, (2016b)
			SOM, PLS-R	Rice	*Aspergillus oryzae*	Siripatrawan and Makino (2015)
			PLS-R	Wheat	*Fusarium*	Polder *et al.* (2005)
			PCA, LDA, QDA, Mahalanobis	Barley	*Aspergillus glaucus*, *Penicillium* spp.	Senthilkumar *et al.* (2016a)

			PLS-R	Maize	*Fusarium verticillioides*	Williams *et al.* (2012)
			PLS-DA	Maize	*Fusarium verticillioides*	Williams *et al.* (2009)
				Wheat	*Fusarium* spp.	Shahin and Symons (2012)
			LDA, QDA, Mahalanobis	Wheat	*Penicillium* spp., *Aspergillus glaucus*, *A. niger*	Singh *et al.* (2012)
			PLS-R	Oats	*Fusarium*	Tekle *et al.* (2015)
			PCA, PLS-DA, interval PLS-DA	Wheat	*Fusarium* spp.	Serranti *et al.* (2013)
			LDA	Wheat	*Fusarium* spp.	Delwiche *et al.* (2011)
Thermal imaging	Temperature and heat flow measurements	Thermal images	LDA and QDA	Wheat	*Aspergillus glaucus, A. niger, Penicillium* spp.	Chelladurai *et al.* (2010)
Neutron imaging	Absorption and scattering of neutron beams	Neutron attenuation coefficient		Maize	*Aspergillus flavus*	Cleveland *et al.* (2008)
X-ray imaging		Mean grey value, grey level histogram,	Stepwise-DA	Maize	*Aspergillus flavus, A. niger, Diplodia maydis, Fusarium graminearum,*	Pearson and Wicklow (2006)

Absorption and scattering of X-ray beams	porosity, textural features			*F. verticillioides*, *Trichoderma viride*	
		-		*Fusarium verticillioides*	Orina, Manley and Williams (2017)
		LDA, QDA, Mahalanobis, BPNN	Wheat	*Aspergillus glaucus*, *A. niger*, *Penicillium* spp.	Narvankar *et al.* (2009)

Mould damage: fungus studied was not specified; LDA: linear discriminant analysis; MLP: multi-layer perceptron; QDA: quadratic discriminant analysis; DA: discriminant analysis; PCA: principal component analysis; PLS-DA: partial least square discriminant analysis; PLS-R: partial least square regression; SIMCA: soft independent modelling of class analogy; ANN: artificial neural networks; SOM: sample organizing map; BPNN: back propagation neural network.

Several researchers have demonstrated the potential of the electronic nose to detect mycotoxins in various cereal grains (Table 2.2). The production of mycotoxins by particular mould strains is generally associated with production of volatile substances such as alcohols, aldehydes, ketones and esters (Magan & Evans, 2000). Patterns of these volatiles and their accumulation can be used as indicators of fungal activity, as well as taxonomic markers for differentiating between fungal strains that produce toxins and those that do not (Magan & Evans, 2000; Yao *et al.*, 2015). Cheli *et al.* (2009) used the electronic nose to detect aflatoxins in maize. The authors differentiated contaminated and non-contaminated maize samples using an electronic nose equipped with 10 MOS (metal oxide semiconductors). Using principal component analysis (PCA), a clear difference in the volatile profiles of maize in the presence and absence of aflatoxins was observed. A classification accuracy of 100% for maize contaminated with aflatoxins was achieved using linear discriminant analysis (LDA) (Cheli *et al.*, 2009). In another study, Olsson *et al.* (2002) found a positive correlation between the concentration of five compounds (pentane, methylpyrazine, 3-pentanone, 3-octene-2-ol and isooctyl acetate) and the level of deoxynivalenol in naturally contaminated barley grains. The results also showed that it was possible to classify ochratoxin A levels in the barley grains as below, or above the maximum limit of 5 µg/kg as established by the Swedish National Food Administration. The major drawback of this technique is the limited information available regarding its capability to quantify mycotoxin concentration in cereal grains (Cheli *et al.*, 2012).

Near infrared (NIR) spectroscopy

The potential use of NIR spectroscopy for the detection of fungal infection in cereal grains has been an area of focus by many researchers (Pearson & Wicklow, 2006; Peiris *et al.*, 2010; Tallada *et al.*, 2011). NIR spectroscopy utilises the electromagnetic spectrum in the range of 780 to 2500 nm (12500 to 4000 cm^{-1}) (Cen & He, 2007). The NIR technique is based on the measurement of bond vibrations between the atoms of organic molecules involving mainly C-H, C-O, O-H and N-H. These bonds are subject to vibrational energy changes when irradiated by NIR frequencies. Stretch and bend vibration patterns exist in these bonds (Cen & He, 2007). NIR absorption occurs when the vibrations at a given frequency coincide with those of a molecular bond in the material being scanned (Manley, 2014). An NIR instrument consists of: (1) a source of radiant energy, (2) a device for wavelength selection, (3) a means of presenting the sample, (4) a detector to convert energy to an electrical signal and (5) a signal processor and readout (Givens *et al.*, 1997). The sample is irradiated with NIR radiation, the incident radiation may be reflected, absorbed or transmitted, and the relative contribution of each phenomenon depends on the chemical constitution and physical parameters of the sample. Advanced multivariate techniques are then used to extract useful information from the NIR spectrum (Nicolaï *et al.*, 2007). The NIR technique uses the spectral difference between healthy

and infected cereal grains caused by differences in the chemical composition of the sound and damaged grains to achieve discrimination (Shah & Khan, 2014).

NIR spectroscopy has been applied to detect mycotoxins and mycotoxigenic fungal contamination in cereal grains (Table 2.1), including rapid detection of kernel rots and mycotoxins in maize (Berardo *et al.*, 2005); determination of deoxynivalenol (DON) in wheat kernels (Pettersson & Åberg, 2003); aflatoxigenic fungal contamination in rice (Dachoupakan Sirisomboon *et al.*, 2013); and detecting fumonisins in single maize kernels infected with *Fusarium verticillioides* (Dowell *et al.*, 2002). Tallada *et al.* (2011) evaluated the performance of single kernel NIR spectroscopy to discriminate maize kernels infected by eight fungal species at different levels of infection. NIR spectra (904 to 1685 nm) were used to develop linear and non-linear prediction models using linear discriminant analysis (LDA) and multi-layer perceptron (MLP) neural networks. The method could discriminate between infected and healthy maize kernels. At advanced levels of infection, the LDA classified the uninfected kernels better than infected ones (96 vs. 74%) while MLP had almost similar classification rates of 92 and 91% for uninfected and infected kernels, respectively (Tallada *et al.*, 2011).

NIR spectroscopy with a wavelength range of between 950 and 1650 nm was used to determine the percentage of fungal infection found in rice samples (Dachoupakan Sirisomboon *et al.*, 2013). Calibration models for the total fungal infection were developed using original and pre-processed absorbance spectra in conjunction with partial least square regression (PLS-R). The statistical model developed from the untreated spectra provided the greatest accuracy in prediction, with a correlation coefficient (r) of 0.668, a standard error of prediction (SEP) of 28.87%, and a bias of -0.10% (Dachoupakan Sirisomboon *et al.*, 2013). In yet another study, NIR spectroscopy was able to accurately predict the incidence of maize kernels infected by *Fusarium verticillioides* (Berardo *et al.*, 2005). The best predictive ability for the percentage of global fungal infection and *F. verticillioides* was obtained using a calibration model utilising whole kernels (R^2 = 0.75 and SECV = 7.43%). This predictive performance was confirmed by the scatter plot of measured *F. verticillioides* infection verses NIR predicted values in maize kernel samples (R^2 = 0.80) (Berardo *et al.*, 2005). NIR spectrophotometers are unable to capture internal constituent gradients within food products, this may result in differences between predicted and measured composition (Gowen *et al.*, 2007). The extraction of only useful information from the large data sets and the complexity of the spectra is a challenge with this technique (Manley, 2014).

Table 2.2. A summary of non-destructive techniques that have been used for the detection of mycotoxins in cereal grains

Technique	Classifier	Cereal	Mycotoxin	Range tested	Reference
Electronic nose	PCA, PLS	Maize	Fumonisins	< 1.6 ppm – > 1000 ppm	Gobbi *et al.* (2011)
	DFA	Wheat	DON	1000 – 2500 ppb	Lippolis *et al.* (2014)
	PCA, LDA	Maize	Aflatoxins	< 4 – 100 ppb	Cheli *et al.* (2009)
	PCA, CART	Wheat	DON	< 1750 ppb or > 1750 ppb	Campagnoli *et al.* (2011)
	PCA	Wheat	DON	< 0.001 – 2.130 ppm	Tognon *et al.* (2005)
	PCA and PLS	Barley	Ochratoxin A	0 – 934 ppb	Olsson *et al.* (2002)
			DON	0 – 857 ppb	
NIR spectroscopy	PLS	Maize and barley	Aflatoxin B_1	Positive > 20 ppb; Negative < 20 ppb	Fernández-Ibañez *et al.* (2009)
	PCA and PLS-R	Wheat	DON	1600 ppb – 13 700 ppb	Pettersson and Åberg (2003)
	PLS-R	Wheat	DON	> 5 ppm	Dowell *et al.* (1999)
	NIR spectra	Wheat	DON	0.5 – 2000 ppm	Peiris *et al.* (2009)
	PLS-R	Wheat	DON	< 60 ppm & > 60 ppm	Peiris *et al.* (2010)
	PLS-R and DA	Maize	Aflatoxins	< 10 ppb or > 100 ppb	Pearson *et al.* (2001)
	DA	Maize	Aflatoxins	> 100 ppb	Pearson *et al.* (2004)
	PLS-DA	Maize	Fumonisins	< 10 ppm or > 100 ppm	Dowell *et al.* (2002)

	PCA and PLS-R	Wheat	DON	< 0.1 – 100.75 ppm	Beyer *et al.* (2010)
	PLS	Maize	Fumonisins	0.357 – 11.845 ppm	Della Riccia Giacomo (2013)
	PCA and QDA	maize	Fumonisins	< or > 4000 ppb	Levasseur-Garcia *et al.* (2015)
	PLS	Wheat	DON	0 – 32 ppm	Czechlowski and Laskowska (2013)
	Modified partial least squares	maize	DON and fumonisins	DON 1.04 – 8.68 ppm; Fumonisins 0.14 – 6.43 ppm	Bolduan *et al.* (2009)
	Neural networks and NIR spectra	Barley	DON	0.3 – 50.8 ppm	Ruan *et al.* (2002)
	PLS-DA	Wheat	DON	0 – 90 ppm	Dvořáček *et al.* (2012)
	PLS-R	Rice	Aflatoxin B_1	6.90 – 54.82 ppb	Qiang *et al.* (2014)
NIR hyperspectral imaging	PCA-stepwise FDA	Maize	Aflatoxin B_1	10, 20, 100, 500 ppb	Wang *et al.* (2014)
	PCA	Maize	Aflatoxins	1 – 3500 ppb	Wang *et al.* (2015b)
	PCA-FDA	Maize	Aflatoxins	10, 20, 100, 500 ppb	Wang *et al.* (2015a)
	PLS	Maize	Aflatoxins	10, 100, 500, 1000 ppb	Kandpal *et al.* (2015)
	PCA	maize	Aflatoxin B_1	< 10 ppb or ≥ 100 ppb	Wang *et al.* (2015c)

PCA, QDA, LDA, Mahalanobis	Wheat	Ochratoxin A	72, 100, 382, 430,600 ppb	Senthilkumar *et al.* (2016b)
PCA, LDA, QDA, Mahalanobis	Barley	Ochratoxin A	140, 251, 536, 620, 814 ppb	Senthilkumar *et al.* (2016a)
PLS-R	Oats	DON	1.8, 0.52, 355.8, 209.1 ppm	Tekle *et al.* (2015)

DON: deoxynivalenol; DA: discriminant analysis; PCA: principal component analysis; PLS: partial least squares; PLS-DA: partial least square discriminant analysis; PLS-R: partial least square regression; DFA: discriminant function analysis; LDA: linear discriminant analysis; CART: classification and regression tree; QDA: quadratic discriminant analysis; FDA: factorial discriminant analysis; ppb: parts per billion; ppm: parts per million.

The use of NIR spectroscopy for the determination of mycotoxins in cereal grains has been investigated since the late 1990s (Table 2.2). Peiris *et al.* (2009) studied the spectral characteristics of pure deoxynivalenol (DON), serially diluted with acetonitrile from 2000 to 0.5 ppm, as well as sound and *Fusarium* damaged wheat kernels. They reported that DON had distinct bands in the NIR region (*ca.* 1408 nm, 1904 nm and 1919 nm). They also found differences in absorption between the sound and *Fusarium* damaged kernels and concluded that it may arise, in part, due to the differences in the DON levels in the grains. In a follow-up study, the same authors developed an NIR method for identification of *Fusarium* head blight and prediction of DON in single wheat kernels (Peiris *et al.*, 2010). They reported that it was possible to estimate DON levels in kernels having more than 60 ppm DON and could thus sort kernels accordingly. NIR spectroscopy (reflectance and transmittance) was also applied to detect fumonisins in single maize kernels infected with *Fusarium verticillioides* (Dowell *et al.*, 2002). Maize kernels with fumonisins levels greater than 100 ppm were classed as positive, whereas kernels with less than 10 ppm were classed as fumonisins negative. Furthermore, models based on reflectance spectra had higher correct classification than models based on transmission spectra. Fernández-Ibañez *et al.* (2009) used NIR spectroscopy for the detection of aflatoxin B_1 in maize and barley. The discriminant models they developed gave satisfactory results and highlighted the potential of NIR spectroscopy as a rapid method for screening grains contaminated with aflatoxins.

Beyer *et al.* (2010) estimated DON content of wheat samples containing different levels of *Fusarium* damaged kernels (0, 20, 40, 60, 80 and 100%) by diffuse reflectance spectroscopy (350-2500 nm). The authors concluded that they were capable of distinguishing DON levels of damaged kernels ranging from 0.21 ± 0.03 µg/kg to 2.39 ± 0.12 µg/kg irrespective, if the grain sample contained 20 or 100% of *Fusarium* damaged kernels. The slope of the linear regression equation, relating estimated DON content to measured DON content, indicated that approximations matched average measurements very well. However, the coefficient of determination (0.84) as well as the large standard error (3.61 mg/kg DON) clearly indicated that the precision of the procedure was not sufficient for reliable separation of samples below legal limits (1.25 mg/kg in the European Union). It is important to note that the detection limit of the various mycotoxins using NIR spectroscopy has not been clearly identified. Furthermore, care should be taken when developing calibration or classification models to quantify or detect contaminants at the ppm level as numerous factors contribute to the method's sensitivity and accuracy (Norris, 2009).

NIR hyperspectral imaging

Conventional NIR spectroscopy provides one spectrum of the target sample without giving information about the spatial distribution of the chemical constituents of the sample; hyperspectral imaging on the other hand provides spectral information in a spatially resolved manner (Gowen *et al.*, 2007). NIR hyperspectral imaging is an imaging technique that combines spectral and spatial information of an object. The collected data is arranged into a three-way data cube, commonly called a hypercube, which are made up of hundreds of contiguous wavebands for each spatial position of a sample under study (Chen *et al.*, 2013; Manley, 2014). The two commonly used means of generating hyperspectral images from a sample include, the 'staring imager' configuration and the 'push-broom' or line scan system (Gowen *et al.*, 2007). In the 'staring imager' configuration, the image field of view is kept fixed and the images are obtained one wavelength after another. With the push-broom system, all the spectral information is acquired simultaneously from a series of adjacent spatial positions as the sample moves relative to the instrument (Manley, 2014). Fig. 2.4 shows an illustration of typical components of a push-broom hyperspectral imaging system which consists of an objective lens, spectrograph, camera, acquisition system, moving stage, illumination source and computer. NIR hyperspectral images are acquired at the wavelengths in the NIR region (ElMasry *et al.*, 2012).

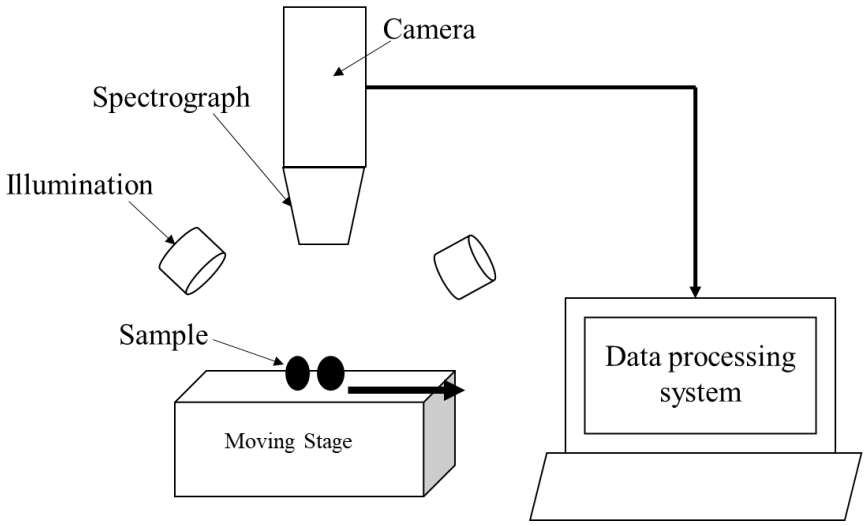

Figure 2.4. Components of a push-broom hyperspectral imaging system, adapted from Gowen *et al.* (2007). Hyperspectral images containing spectral and spatial information of the sample are acquired as the sample moves.

The basis of hyperspectral imaging is that all biological materials reflect, scatter, absorb and emit electromagnetic energy in a distinctive pattern at specific wavelengths. This is due to differences in their chemical composition and inherent physical structure (ElMasry *et al.*, 2012). This pattern is called a spectrum/spectral signature/spectral fingerprint and is a unique characteristic of an object. Therefore, the spectral signature can be used to uniquely characterise, identify and discriminate

between classes/types of a given material (ElMasry *et al.*, 2012). The data obtained by hyperspectral imaging are initially mathematically pre-processed to extract analytical information from the spectra and remove non-chemical biases such as scattering effects caused by surface heterogeneities. The data is then subjected to chemometric analysis through the application of sophisticated multivariate analysis tools (e.g. principal component analysis, partial least squares, multi-linear regression, linear discriminant analysis, Fischer discriminant analysis and artificial neutral networks) to highlight possible differences between analysed samples (Del Fiore *et al.*, 2010).

NIR hyperspectral imaging has found wide application in detection, identification and discrimination of fungal infection in cereals (Table 2.1) (Hamid Muhammed & Larsolle, 2003; Singh *et al.*, 2007; Delwiche *et al.*, 2011; Shahin & Symons, 2012; Yang *et al.*, 2012; Zhang *et al.*, 2012; Karuppiah *et al.*, 2016). Williams *et al.* (2012) used NIR hyperspectral to track changes in whole maize kernels infected with *F. verticillioides*. Hyperspectral images of healthy and infected kernels with a spectral range of 1000 to 2489 nm were acquired at predetermined time intervals after infection. Prominent peaks at approximately 1900 nm (associated with starch) and 2136 nm (associated with protein) confirmed that the differences in the time intervals was due to changes in starch and protein, most likely the depletion thereof as the fungus grows and more spores germinate. The authors were also able to establish partial least squares regression (PLS-R) models that could predict degree of infection (Williams *et al.*, 2012). In a similar study, Del Fiore *et al.* (2010) were able to detect fungal contamination in maize 48 h post inoculation using NIR hyperspectral imaging. They discriminated the contaminated from the uncontaminated maize samples based on the changes produced by the fungus in the spectral profile of the maize kernels.

Healthy and fungal damaged wheat kernels infected by storage fungi namely *Penicillium* spp., *Aspergillus glaucus* and *A. niger* were scanned using a short wave infrared (SWIR) hyperspectral imaging system in the 700-1100 nm wavelength range (Singh *et al.*, 2012). Wavelength 870 nm was important due to the highest factor loading of the first principal component (PC). Thirteen features (six statistical and seven histogram features) from the 870-nm waveband image were used as input to statistical discriminant classifiers (linear, quadratic, and Mahalanobis) to distinguish fungal infected wheat kernels from healthy kernels. The three classifiers gave a high accuracy in classifying fungal infected kernels. Both LDA and QDA classified 95.7-98.0% and 96.0-98.3% fungal infected kernels, respectively while Mahalanobis classifier classified 94.0-96.7% fungal infected kernels (Singh *et al.*, 2012). The main limiting factors of the use of NIR hyperspectral imaging include: the high cost and the lengthy time needed for pre-processing of the data and classification. Depending on the sample size and image resolution, acquisition time can range from few a seconds to 4 min, while pre-

processing and classification time are largely dependent on computer hardware and software capabilities (Gowen *et al.*, 2007).

More recently, NIR hyperspectral imaging has also found application in the detection of mycotoxins in cereal grains (Table 2.2). A SWIR hyperspectral imaging system was used to evaluate the potential to detect aflatoxin B_1 contamination on the surface of maize kernels (Wang *et al.*, 2014). Four aflatoxin B_1 solutions of different concentrations (10, 20, 100 and 500 ppb) were prepared and deposited onto kernel surfaces while control samples were inoculated with methanol. The results indicated that it was possible to discriminate between the control and contaminated kernels and between the various concentrations of aflatoxin. The authors also claimed that they could distinguish the kernels inoculated with 10 ppb of aflatoxin from the rest. However, the authors concluded that at lower concentrations the wavelengths corresponding to aflatoxin B_1 were not significantly strong when compared to those associated with the kernels' nutritional composition. Senthilkumar *et al.* (2016b) used NIR hyperspectral imaging to distinguish healthy from fungal infected wheat kernels and to detect ochratoxin A contamination. Principal component analysis revealed that 1300, 1350 and 1480 nm were significant wavelengths, based on the highest factor loadings, for the ochratoxin contaminated samples. They could distinguish contaminated samples from healthy ones with a classification accuracy of more than 98% at levels as low as 72 ppb.

In another study, a SWIR hyperspectral imaging system was utilized to detect aflatoxin contamination on maize kernels (Kandpal *et al.*, 2015). Maize samples were inoculated with four different aflatoxin B_1 concentrations (10, 100, 500, and 1000 ppb) and it was noted that as the aflatoxin B_1 concentrations increased, spectral deviations were observed between the control and inoculated samples. A partial least squares discriminant analysis (PLS-DA) model was developed to categorize the control and contaminated kernels and the highest overall classification accuracy yielded was 96.9%. Misclassifications were observed when the aflatoxin concentration level was low (10 ppb), influencing the classification accuracy of the PLS-DA model.

In the aforementioned studies, concentrations at the ppb level were investigated. At these low concentrations, it is highly unlikely that the contaminant was detected/sensed (Norris, 2009). Its presence, however, may have influenced the absorption profile of major constituents such as starch and protein, permitting detection and thus discrimination. Although many authors have investigated the use of NIR hyperspectral imaging for mycotoxin detection, its quantification has not been reported on to date.

Thermal imaging

Thermal imaging is based on the fact that all materials emit infrared irradiation, hence the technique utilises the radiation to produce a pseudo image of the thermal distribution of the body surface (Vadivambal & Jayas, 2011; Chen *et al.*, 2013). The amount of radiation emitted by an object is dependent on its temperature and emissivity. Emissivity is defined as the ratio of energy emitted from an object to that emitted from a black body at the same temperature, it varies from 0 (perfect white body) to 1 (perfect black body) (Gowen *et al.*, 2010). Infrared thermal imaging systems typically comprises the following components: camera, an optical system (e.g., focussing lens, collimating lenses, and filters), detector array (e.g. microbolometers), signal processing, and an image processing system (Chen *et al.*, 2013). The infrared energy emitted from the objects is converted into an electrical signal via IR detectors in the cameras of the thermal imaging system and displayed as colour or monochrome thermal images.

Thermal images can be obtained using passive or active thermal imaging systems (Fig. 2.5). Passive thermography does not require application of any external energy to the object because the features of interest are naturally at a higher or lower temperature than the background. On the other hand, active thermography requires application of thermal energy to produce a thermal contrast between the features of interest and the background (Chen *et al.*, 2013). Several point temperatures are measured over an area and processed into a thermal map or thermogram of the target surface. The thermogram can be further analysed using a wide range of image processing techniques (Gowen *et al.*, 2010). Image processing is performed on the thermal images to improve the contrast, hence highlighting regions of interest. Statistical and textural features are extracted to aid in classification. Various supervised and unsupervised data mining techniques, commonly used in imaging techniques, are also applicable in thermal image processing (Gowen *et al.*, 2010).

Chelladurai *et al.* (2010) studied the potential of an infrared thermal imaging system to identify fungal infection in stored wheat. An un-cooled focal planar array type infrared thermal camera was used to obtain thermal images of bulk wheat grains infected with *Aspergillus glaucus* group, *A. niger* and *Penicillium* spp. A total of twelve temperature features were derived from heating the grains for 180 seconds at 90ºC, maintained at this temperature and finally cooled for 30 seconds in ambient air. The differences in thermal properties between the healthy and damaged samples was the basis for their discrimination. The rate of heating and cooling of fungal infected grains was slightly higher than that of healthy kernels, this was due to the biochemical changes induced by fungal growth in the wheat kernels. Pair-wise LDA and QDA classification models gave a maximum accuracy of 100% for healthy samples and more than 97% and 96% respectively, for infected samples. Differentiation of fungal species was not possible because of similar changes in the chemical

composition of kernels (Chelladurai *et al.*, 2010). Some of the limitations of thermal imaging include: heating and cooling process may alter heat sensitive products in an undesirable way; the variation in the heat distribution may add unwanted variability to the thermogram.

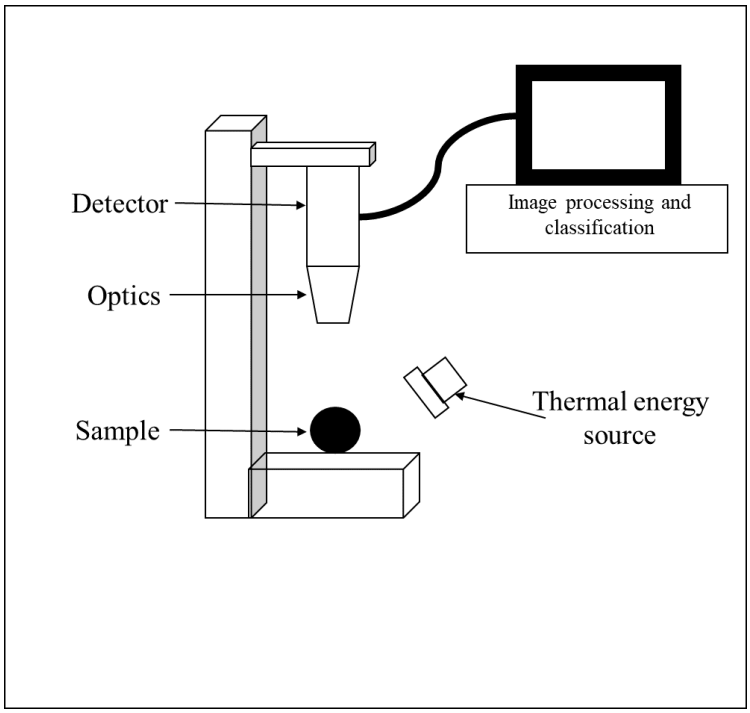

Figure 2.5. Schematic display of an active thermal imaging system, adapted from Gowen *et al.* (2010). The sample is heated to a set temperature before acquiring thermal images using a thermal camera which are further processed.

Neutron tomography

Neutron tomography was used to study structural changes in maize kernels infected with *Aspergillus flavus* (Cleveland *et al.*, 2008). This technique is based on the absorption and scattering of a neutron beam as it passes through a sample. With this technique, inner macroscopic structure and material composition of the sample can be visualised (Vontobel *et al.*, 2006). The neutrons interact with the nucleus of the atom rather than its electron cloud. The tomographic system consists of a neutron source, an object turntable, a scintillator, a mirror, a cooled CCD camera and computer support (Gibbons *et al.*, 1996). The object under investigation is rotated in angular steps either 180º or 360º in the illuminating neutron field. The resulting two-dimensional (2-D) image is a map of the neutrons attenuated within the sample under investigation (Strobl *et al.*, 2009; Perfect *et al.*, 2014). Neutron tomography, like other tomographic techniques, provides a three dimensional (3-D) volume from a series of two dimensional images which display the attenuation coefficient distribution in the sample volume (Strobl *et al.*, 2009). Neutrons have high sensitivity to hydrogen detection; hence,

most biological studies have used the technique to examine water movement through the sample (de Jesus *et al.*, 2002; Okuni *et al.*, 2002; Lehmann *et al.*, 2005).

Using neutron tomography, Cleveland *et al.* (2008) was able to clearly distinguish the well-known anatomical features of the maize kernel in the reconstructed slices. Using histograms of neutron attenuation coefficients, differences were detected between susceptible kernels that had been inoculated with *Aspergillus flavus* and those that had not. Infected kernels had lower neutron attenuation in the scutellum and embryo regions. This was attributed to released hydrogen, bound as water (e.g., by metabolising starch) during fungal degradation and thus decreasing the material's hydrogen density (Cleveland *et al.*, 2008). The drawbacks of using neutron imaging include the limited quantitative information that can be obtained from the images, limited accessibility to reactor facilities which produce neutrons and its lower spatial resolution (~10-50 µm) (Lehmann *et al.*, 2004; Defraeye *et al.*, 2013).

X-ray imaging and computed tomography

X-rays are electromagnetic radiation with a wavelength ranging from about 0.01-10 nm. X-rays can traverse through matter and the image produced can directly reflect internal defect or contamination, and internal structural changes (Chen *et al.*, 2013). Electromagnetic waves with wavelengths ranging from 0.1 to 10 nm with corresponding energies of 0.12 to 12 keV are called soft X-rays. Due to their low penetrating power and ability to reveal internal density changes, they are more suitable to be used for agricultural products (Kotwaliwale *et al.*, 2014). X-ray imaging is rapid and takes few seconds (3-5 s) to produce an X-ray radiograph (Neethirajan *et al.*, 2007). Radiographs, also known as projection images, displays a 3-D object on a 2-D detector plane, leading to loss of depth information (Cnudde & Boone, 2013). Developments in the X-ray imaging technique that allows 3-D images is computed tomography (CT). The basic principle behind CT imaging is that a 3-D volume/image of an object can be reconstructed using dedicated computer algorithms from multiple projections of the object from different directions (Landis & Keane, 2010). This allows an in-depth analysis of the internal structure of an object. The CT scans produces images of superior quality compared to traditional X-ray imaging systems, however, they are costly and involve lengthy scanning and data processing times (Haff & Toyofuku, 2008).

X-ray imaging and computed tomography is based on the differences in X-ray attenuation arising, principally from differences in density within the sample under investigation (Curry *et al.*, 1990). The difference in X-ray attenuation creates a contrast to differentiate low density and high density regions within the sample (Zwiggelaar *et al.*, 1996). A typical X-ray imaging setup consists of an X-ray source, a sample manipulator and a detector (Kotwaliwale *et al.*, 2014). In X-ray

computed tomography, the object under investigation is the one that rotates while the X-ray source and detector remain stationary (Cnudde & Boone, 2013). During scanning, the sample is illuminated with X-rays. The X-rays pass through the sample in many different directions and along different pathways to yield an image which exhibits variation in density at numerous points in a 2-D slice (Lim & Barigou, 2004). A series of 2-D radiographs are collected at fixed angular increments while the sample is rotated (Fig. 2.6). The total angle of rotation is determined by the geometry of the sample and the beam, but generally is either 180º when nearly parallel beams are used (normally at a synchrotron) or 360º when cone-beam geometry is used (normally in laboratory apparatus) (Baker *et al.*, 2012).

The numerous 2-D projections, covering the entire sample, can be reconstructed into a 3-D volume that can be presented as a whole or as virtual slices of the sample at different depths and in different directions (Frisullo *et al.*, 2009). X-ray micro-CT enables both 2-D and 3-D visualisation of the internal structure of an object as well as quantitative characterization of the data volumes. A number of microstructural parameters as well as mass density information can be extracted from the X-ray images using dedicated software packages (Cnudde & Boone, 2013). Quantitative results from the 3-D analysis can include sample volume, density, porosity, pore size and distribution, object surface to volume ratio, morphology (shape, sphericity, roundness), surface texture and many more (Schoeman *et al.*, 2016b). The quantitative parameters aid in discrimination of the different classes.

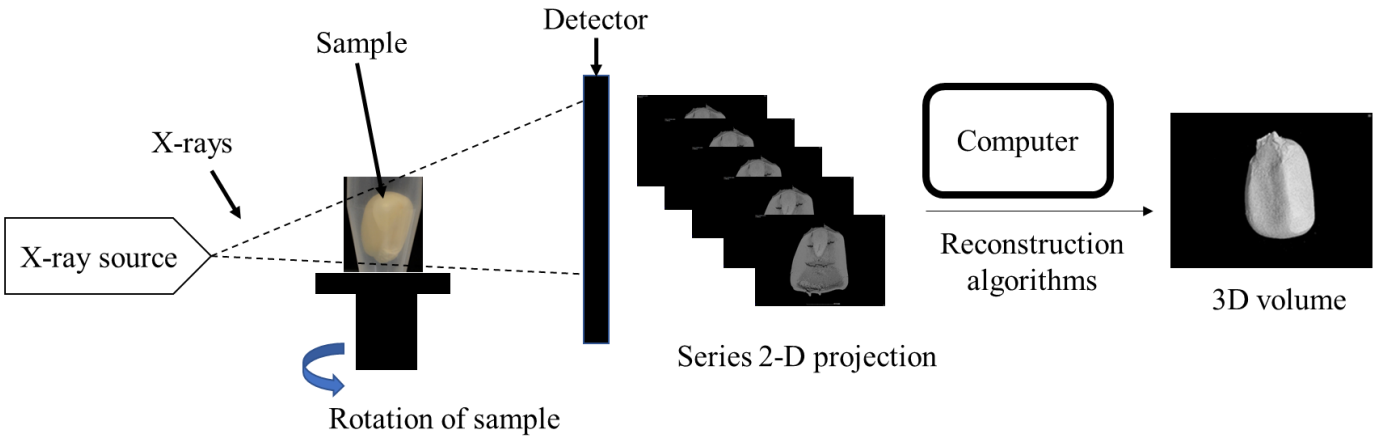

Figure 2.6. Illustration of an X-ray computed tomography setup. Acquisition of 2-D projection images of the sample which are then reconstructed into a 3-D volume.

The ability of X-ray imaging to detect fungal damage is attributed to changes in grain density caused by fungal infection. This density change can be detected by comparing the features extracted from the X-ray images of healthy and infected kernels (Narvankar *et al.*, 2009). Pearson and Wicklow (2006) used a cabinet X-ray system (18 kV, 3mA) to detect fungal infection in maize kernels. The X-ray films were digitally scanned at 800 pixels/inch and the images saved for further analysis. The

mean X-ray intensity of the fungal infected kernels was significantly lower than that of the undamaged kernels at 95% confidence level. This indicated lower density, as the fungal infected kernels absorbed less X-ray energy. Classification was performed by stepwise discriminant analysis using selected X-ray image features (i.e. mean, standard deviation and maximum pixel intensity). A classification accuracy of 82% was achieved (Pearson & Wicklow, 2006).

In a similar study, soft X-ray imaging (13.6 kV,184 µA) was used to detect fungal infection in wheat kernels infected with common storage fungi namely *Aspergillus niger*, *A. glaucus* group and *Penicillium* spp. (Narvankar *et al.*, 2009). A total of 34 image features (maximum, minimum, mean, median, standard deviation, variance of grey levels, and 28 grey-level co-occurrence matrix (GLCM) features) were selected and extracted from X-ray images of healthy and infected wheat kernels using algorithms developed in MATLAB (Mathworks Inc. Natick, MA). The image features were given as input to statistical discriminant classifiers: linear, quadratic and Mahalanobis and back propagation neural network (BPNN) classifier. Two-class Mahalanobis discriminant classifier classified 92.2-98-9% fungal infected wheat kernels. Linear discriminant classifier gave better results than quadratic, Mahalanobis and BPNN classifiers in identifying healthy kernels with more than 82% classification accuracy. BPNN classifier did not improve the classification accuracy and in some cases gave higher false positive errors compared to statistical classifiers (Narvankar *et al.*, 2009).

High resolution X-ray micro-CT (50 kV, 250 µA) was used to study the internal structural change in maize kernels infected with *Fusarium verticillioides* (Orina *et al.*, 2017). Details of the structural changes in the infected and control maize kernels could be visualised in the 2-D and 3-D images, and quantified in terms of total kernel volume, total volume of void space and mean grey value. There was a decrease in total volume and mean grey value and increase in the total volume of voids of the kernels with time, and the authors attributed these observed changes to breakdown of the maize reserves. Compared with other imaging techniques, X-ray imaging has a distinct advantage as it allows non-destructive imaging of the interior features of a sample to detect hidden defects or contaminants. The limitation of X-ray micro computed tomography include it being costly and requires lengthy image analysis procedures (Schoeman *et al.*, 2016b).

Conclusion and future trends

Non-destructive techniques can provide rapid, consistent and objective assessment of the samples under investigation. In conjunction with appropriate multivariate data or image analysis techniques, they could be effective tools for the detection of fungal infection and mycotoxins contamination of cereal grains. The methods reviewed have the potential for automation, thus eliminating tedious and time consuming traditional methods. However, the major barrier preventing commercial

implementation of these non-destructive techniques is the high cost of equipment, production of large data sets, lengthy image processing procedures and interpretation. Furthermore, selecting an efficient though practical classification algorithm could pose a challenge. The operation of these equipment also requires scientific knowledge and the effectiveness to determine fungal infection and presence of mycotoxins in grains could largely depend on the virulence of the fungus, the extent of damage it caused and level of mycotoxins, if any, present.

Recognition and quantification of mycotoxins have been considered using the respective non-destructive techniques. The detection limits of these instruments have, however, not been thoroughly studied and determined. Caution should thus be exercised when employing these methods for qualitative and, especially, quantitative purposes. Although limits of detection have been mentioned in a number of studies using NIR spectroscopy and NIR hyperspectral imaging, these were determined indirectly by discrimination of mycotoxin contaminated vs. healthy grains. The very low concentration levels (ppm or ppb) of mycotoxin contamination in cereal grains is the limiting factor for its effective detection and quantification. At such low levels, it is highly unlikely that the mycotoxins, themselves, are detected. However, their presence in the cereal grains may influence the composition of the major constituents, thus allowing detection.

Future trends for fungal detection are towards developing high-performance, low-cost non-destructive equipment. Combining results of different non-destructive techniques, e.g. hyperspectral imaging with X-ray micro-CT or an imaging method combined with a non-imaging method such as the electronic nose could provide a more complete description of the sample under investigation. Reduction of image size and processing speed are areas of consideration if these techniques are to be used in real time applications.

References

Anderson, T.J., Ai, Y., Jones, R.W., Houk, R.S., Jane, J.-L., Zhao, Y., Birt, D.F. & Mcclelland, J.F. (2013). Analysis of resistant starches in rat cecal contents using fourier transform infrared photoacoustic spectroscopy. *Journal of Agricultural and Food Chemistry*, **61**, 1818-1822.

Baker, D.R., Mancini, L., Polacci, M., Higgins, M.D., Gualda, G.a.R., Hill, R.J. & Rivers, M.L. (2012). An introduction to the application of X-ray microtomography to the three-dimensional study of igneous rocks. *Lithos*, **148**, 262-276.

Baldwin, E.A., Bai, J., Plotto, A. & Dea, S. (2011). Electronic noses and tongues: Applications for the food and pharmaceutical industries. *Sensors*, **11**, 4744-4766.

Bauriegel, E., Giebel, A., Geyer, M., Schmidt, U. & Herppich, W. (2011). Early detection of *Fusarium* infection in wheat using hyper-spectral imaging. *Computers and Electronics in Agriculture,* **75**, 304-312.

Berardo, N., Pisacane, V., Battilani, P., Scandolara, A., Pietri, A. & Marocco, A. (2005). Rapid detection of kernel rots and mycotoxins in maize by near-infrared reflectance spectroscopy. *Journal of Agricultural and Food Chemistry,* **53**, 8128-8134.

Beyer, M., Pogoda, F., Ronellenfitsch, F.K., Hoffmann, L. & Udelhoven, T. (2010). Estimating deoxynivalenol contents of wheat samples containing different levels of *Fusarium*-damaged kernels by diffuse reflectance spectrometry and partial least square regression. *International Journal of Food Microbiology,* **142**, 370-374.

Bolduan, C., Montes, J., Dhillon, B., Mirdita, V. & Melchinger, A. (2009). Determination of mycotoxin concentration by Elisa and near-infrared spectroscopy in *Fusarium*-inoculated maize. *Cereal Research Communications,* **37**, 521-529.

Börjesson, T., Eklöv, T., Jonsson, A., Sundgren, H. & Schnürer, J. (1996). Electronic nose for odor classification of grains. *Cereal Chemistry,* **73**, 457-461.

Boutigny, A.L., Beukes, I., Small, I., Zühlke, S., Spiteller, M., Van Rensburg, B.J., Flett, B. & Viljoen, A. (2012). Quantitative detection of *Fusarium* pathogens and their mycotoxins in South African maize. *Plant Pathology,* **61**, 522-531.

Brosnan, T. & Sun, D.-W. (2004). Improving quality inspection of food products by computer vision––a review. *Journal of Food Engineering,* **61**, 3-16.

Campagnoli, A., Cheli, F., Polidori, C., Zaninelli, M., Zecca, O., Savoini, G., Pinotti, L. & Dell'orto, V. (2011). Use of the electronic nose as a screening tool for the recognition of durum wheat naturally contaminated by deoxynivalenol: A preliminary approach. *Sensors,* **11**, 4899-4916.

Casalinuovo, I.A., Di Pierro, D., Coletta, M. & Di Francesco, P. (2006). Application of electronic noses for disease diagnosis and food spoilage detection. *Sensors,* **6**, 1428-1439.

Cen, H. & He, Y. (2007). Theory and application of near infrared reflectance spectroscopy in determination of food quality. *Trends in Food Science & Technology*, **18**, 72-83.

Cheli, F., Campagnoli, A., Pinotti, L. & Dell'orto, V. (2012). Rapid methods as analytical tools for food and feed contaminant evaluation: Methodological implications for mycotoxin analysis in cereals. In: Food production-approaches, challenges and tasks. InTech, Rijeka, Croatia, Chapter 11. DOI: http://dx.doi.org/10.5772/33254.

Cheli, F., Campagnoli, A., Pinotti, L., Savoini, G. & Dell'orto, V. (2009). Electronic nose for determination of aflatoxins in maize. *Biotechnologie, Agronomie, Société et Environnement,* **13**, 39-43.

Chelladurai, V., Jayas, D. & White, N. (2010). Thermal imaging for detecting fungal infection in stored wheat. *Journal of Stored Products Research,* **46**, 174-179.

Chen, P. & Sun, Z. (1991). A review of non-destructive methods for quality evaluation and sorting of agricultural products. *Journal of Agricultural Engineering Research,* **49**, 85-98.

Chen, Q., Zhang, C., Zhao, J. & Ouyang, Q. (2013). Recent advances in emerging imaging techniques for non-destructive detection of food quality and safety. *Trends in Analytical Chemistry,* **52**, 261-274.

Christensen, C. (1973). Loss of viability in storage: Microflora. *Seed Science and Technology,* **1**, 547-562.

Cleveland, T., Hussey, D., Chen, Z.-Y., Jacobson, D., Brown, R., Carter-Wientjes, C. & Arif, M. (2008). The use of neutron tomography for the structural analysis of corn kernels. *Journal of Cereal Science,* **48**, 517-525.

Cnudde, V. & Boone, M. (2013). High-resolution X-ray computed tomography in geosciences: A review of the current technology and applications. *Earth-Science Reviews,* **123**, 1-17.

Concina, I., Falasconi, M., Gobbi, E., Bianchi, F., Musci, M., Mattarozzi, M., Pardo, M., Mangia, A., Careri, M. & Sberveglieri, G. (2009). Early detection of microbial contamination in processed tomatoes by electronic nose. *Food Control,* **20**, 873-880.

Curry, T.S., Dowdey, J.E. & Murry, R.C. (1990). Christensen's physics of diagnostic radiology. 4th edition, Lippincott Williams & Wilkins.

Czechlowski, M. & Laskowska, M. (2013). The development and validation of the calibration model for the vis-NIR spectrometer used for the evaluation of deoxynivalenol content in wheat grain directly during combine harvest. *Journal of Research and Applications in Agricultural Engineering*, **58**, 27-30.

Dachoupakan Sirisomboon, C., Putthang, R. & Sirisomboon, P. (2013). Application of near infrared spectroscopy to detect aflatoxigenic fungal contamination in rice. *Food Control*, **33**, 207-214.

De Jesus, S.P., Crispim, V.R. & Brandão, L. (2002). The use of neutron radiography in agriculture to improve the food quality. *Cellular and Molecular Biology (Noisy-le-Grand, France),* **48**, 819-821.

De Lacy Costello, B., Ewen, R., Gunson, H., Ratcliffe, N.M., Sivanand, P. & Spencer-Phillips, P.T. (2003). A prototype sensor system for the early detection of microbially linked spoilage in stored wheat grain. *Measurement Science and Technology,* **14**, 397-409.

Defraeye, T., Aregawi, W., Saneinejad, S., Vontobel, P., Lehmann, E., Carmeliet, J., Verboven, P., Derome, D. & Nicolaï, B. (2013). Novel application of neutron radiography to forced convective drying of fruit tissue. *Food and Bioprocess Technology*, **6**, 3353-3367.

Deisingh, A.K., Stone, D.C. & Thompson, M. (2004). Applications of electronic noses and tongues in food analysis. *International Journal of Food Science & Technology*, **39**, 587-604.

Del Fiore, A., Reverberi, M., Ricelli, A., Pinzari, F., Serranti, S., Fabbri, A., Bonifazi, G. & Fanelli, C. (2010). Early detection of toxigenic fungi on maize by hyperspectral imaging analysis. *International Journal of Food Microbiology*, **144**, 64-71.

Della Riccia Giacomo, D.Z.S. (2013). A multivariate regression model for detection of fumonisins content in maize from near infrared spectra. *Food Chemistry*, **141**, 4289-4294.

Delwiche, S. (2003). Classification of scab–and other mold–damaged wheat kernels by near–infrared reflectance spectroscopy. *Transactions of the ASAE*, **46**, 731-738.

Delwiche, S.R. & Hareland, G.A. (2004). Detection of scab-damaged hard red spring wheat kernels by near-infrared reflectance. *Cereal Chemistry*, **81**, 643-649.

Delwiche, S.R., Kim, M.S. & Dong, Y. (2011). *Fusarium* damage assessment in wheat kernels by vis/NIR hyperspectral imaging. *Sensing and Instrumentation for Food Quality and Safety*, **5**, 63-71.

Dole, M.N., Patel, P.A., Sawant, S.D. & Shedpure, P.S. (2011). Advance applications of fourier transform infrared spectroscopy. *International Journal of Pharmaceutical Science Review and Research*, **7**, 159-166.

Dowell, F., Ram, M. & Seitz, L. (1999). Predicting scab, vomitoxin, and ergosterol in single wheat kernels using near-infrared spectroscopy. *Cereal Chemistry*, **76**, 573-576.

Dowell, F.E., Pearson, T.C., Maghirang, E.B., Xie, F. & Wicklow, D.T. (2002). Reflectance and transmittance spectroscopy applied to detecting fumonisin in single corn kernels infected with *Fusarium verticillioides*. *Cereal Chemistry*, **79**, 222-226.

Draganova, T., Daskalov, P. & Tsonev, R. (2010). An approach for identifying of *Fusarium* infected maize grains by spectral analysis in the visible and near infrared region, SIMCA models, parametric and neural classifiers. *International Journal of Bioautomation*, **14**, 119-128.

Du, C.-J. & Sun, D.-W. (2004). Recent developments in the applications of image processing techniques for food quality evaluation. *Trends in Food Science & Technology*, **15**, 230-249.

Dvořáček, V., Prohasková, A., Chrpová, J. & Štočková, L. (2012). Near infrared spectroscopy for deoxynivalenol content estimation in intact wheat grain. *Plant Soil Environment*, **58**, 196-203.

Eifler, J., Martinelli, E., Santonico, M., Capuano, R., Schild, D. & Di Natale, C. (2011). Differential detection of potentially hazardous *Fusarium* species in wheat grains by an electronic nose. *PloS One*, **6**, e21026.

Elmasry, G., Kamruzzaman, M., Sun, D.-W. & Allen, P. (2012). Principles and applications of hyperspectral imaging in quality evaluation of agro-food products: A review. *Critical Reviews in Food Science and Nutrition*, **52**, 999-1023.

Fernández-Ibañez, V., Soldado, A., Martínez-Fernández, A. & De La Roza-Delgado, B. (2009). Application of near infrared spectroscopy for rapid detection of aflatoxin B1 in maize and barley as analytical quality assessment. *Food Chemistry*, **113**, 629-634.

Frisullo, P., Laverse, F., Marino, R. & Nobile, M.a.D. (2009). X-ray computed tomography to study processed meat microstructure. *Journal of Food Engineering,* **94**, 283-289.

Gibbons, M.R., Richards, W.J. & Shields, K.C. (1996). Detection of hydrogen in titanium aircraft components using neutron tomography. In: Nondestructive evaluation techniques for aging aircrafts, airports and aerospace hardware. pp. 104-115. SPIE proceeding 2945.

Givens, D.I., De Boever, J. & Deaville, E. (1997). The principles, practices and some future applications of near infrared spectroscopy for predicting the nutritive value of foods for animals and humans. *Nutrition Research Reviews,* **10**, 83-114.

Gobbi, E., Falasconi, M., Torelli, E. & Sberveglieri, G. (2011). Electronic nose predicts high and low fumonisin contamination in maize cultures. *Food Research International,* **44**, 992-999.

Gómez, A.H., Hu, G., Wang, J. & Pereira, A.G. (2006). Evaluation of tomato maturity by electronic nose. *Computers and Electronics in Agriculture,* **54**, 44-52.

Gong, Y., Hounsa, A., Egal, S., Turner, P.C., Sutcliffe, A.E., Hall, A.J., Cardwell, K. & Wild, C.P. (2004). Postweaning exposure to aflatoxin results in impaired child growth: A longitudinal study in benin, West Africa. *Environmental Health Perspectives***, 112**, 1334-1338.

Gordillo-Delgado, F., Marín, E., Cortés-Hernández, D.M., Mejía-Morales, C. & García-Salcedo, A.J. (2012). Discrimination of organic coffee via fourier transform infrared–photoacoustic spectroscopy. *Journal of the Science of Food and Agriculture*, **92**, 2316-2319.

Gordon, S., Jones, R., Mcclelland, J., Wicklow, D. & Greene, R. (1999). Transient infrared spectroscopy for detection of toxigenic fungi in corn: Potential for on-line evaluation. *Journal of Agricultural and Food Chemistry*, **47**, 5267-5272.

Gordon, S.H., Schudy, R.B., Wheeler, B.C., Wicklow, D.T. & Greene, R.V. (1997). Identification of fourier transform infrared photoacoustic spectral features for detection of *Aspergillus flavus* infection in corn. *International Journal of Food Microbiology,* **35**, 179-186.

Gourama, H. & Bullerman, L.B. (1995). Detection of molds in foods and feeds: Potential rapid and selective methods. *Journal of Food Protection,* **58**, 1389-1394.

Gowen, A., Tiwari, B., Cullen, P., Mcdonnell, K. & O'donnell, C. (2010). Applications of thermal imaging in food quality and safety assessment. *Trends in Food Science & Technology,* **21**, 190-200.

Gowen, A.A., O'donnell, C.P., Cullen, P.J., Downey, G. & Frias, J.M. (2007). Hyperspectral imaging – an emerging process analytical tool for food quality and safety control. *Trends in Food Science & Technology,* **18**, 590-598.

Greene, R.V., Gordon, S.H., Jackson, M.A., Bennett, G.A., Mcclelland, J.F. & Jones, R.W. (1992). Detection of fungal contamination in corn: Potential of FTIR-PAS and-DRS. *Journal of Agricultural and Food Chemistry*, **40**, 1144-1149.

Gunasekaran, S. (1996). Computer vision technology for food quality assurance. *Trends in Food Science & Technology*, **7**, 245-256.

Haard, N.F. (1999). Fermented cereals: A global perspective. FAO Agricultural services bulletin 138.

Haff, P.R. & Toyofuku, N. (2008). X-ray detection of detects and contamination in food industry. *Sensing and Instrument Food Quality*, **2**, 262-273.

Hamid Muhammed, H. & Larsolle, A. (2003). Feature vector based analysis of hyperspectral crop reflectance data for discrimination and quantification of fungal disease severity in wheat. *Biosystems Engineering*, **86**, 125-134.

Hussein, H.S. & Brasel, J.M. (2001). Toxicity, metabolism, and impact of mycotoxins on humans and animals. *Toxicology*, **167**, 101-134.

Irudayaraj, J., Sivakesava, S., Kamath, S. & Yang, H. (2001). Monitoring chemical changes in some foods using fourier transform photoacoustic spectroscopy. *Journal of Food Science*, **66**, 1416-1421.

Irudayaraj, J., Yang, H. & Sakhamuri, S. (2002). Differentiation and detection of microorganisms using fourier transform infrared photoacoustic spectroscopy. *Journal of Molecular Structure*, **606**, 181-188.

Jiang, E.Y. & Palmer, R.A. (1997). Comparison of phase rotation, phase spectrum, and two-dimensional correlation methods in step-scan fourier transform infrared photoacoustic spectral depth profiling. *Analytical Chemistry*, **69**, 1931-1935.

Jirsa, O. & Polišenská, I. (2014). Identification of *Fusarium* damaged wheat kernels using image analysis. *Acta Universitatis Agriculturae Et Silviculturae Mendelianae Brunensis*, **59**, 125-130.

Jonsson, A., Winquist, F., Schnürer, J., Sundgren, H. & Lundström, I. (1997). Electronic nose for microbial quality classification of grains. *International Journal of Food Microbiology*, **35**, 187-193.

Kandpal, L.M., Lee, S., Kim, M.S., Bae, H. & Cho, B.-K. (2015). Short wave infrared (SWIR) hyperspectral imaging technique for examination of aflatoxin B1 (afB1) on corn kernels. *Food Control*, **51**, 171-176.

Karuppiah, K., Senthilkumar, T., Jayas, D.S. & White, N.D.G. (2016). Detection of fungal infection in five different pulses using near-infrared hyperspectral imaging. *Journal of Stored Products Research*, **65**, 13-18.

Kotwaliwale, N., Singh, K., Kalne, A., Narayan Jha, S., Seth, N. & Kar, A. (2014). X-ray imaging methods for internal quality evaluation of agricultural produce. *Journal of Food Science and Technology*, **51**, 1-15.

Landis, E.N. & Keane, D.T. (2010). X-ray microtomography. *Materials Characterization*, **61**, 1305-1316.

Lehmann, E., Hartmann, S. & Wyer, P. (2005). Neutron radiography as visualization and quantification method for conservation measures of wood firmness enhancement. *Nuclear Instruments and Methods in Physics Research Section A: Accelerators, Spectrometers, Detectors and Associated Equipment*, **542**, 87-94.

Lehmann, E.H., Vontobel, P., Frei, G. & Brönnimann, C. (2004). Neutron imaging—detector options and practical results. *Nuclear Instruments and Methods in Physics Research Section A: Accelerators, Spectrometers, Detectors and Associated Equipment*, **531**, 228-237.

Letzelter, N.S., Wilson, R.H., Jones, A.D. & Sinnaeve, G. (1995). Quantitative determination of the composition of individual pea seeds by fourier transform infrared photoacoustic spectroscopy. *Journal of the Science of Food and Agriculture*, **67**, 239-245.

Levasseur-Garcia, C., Bailly, S., Kleiber, D. & Bailly, J.-D. (2015). Assessing risk of fumonisin contamination in maize using near-infrared spectroscopy. *Journal of Chemistry*, **2015**, 485864.

Lewis, L., Onsongo, M., Njapau, H., Schurz-Rogers, H., Luber, G., Kieszak, S., Nyamongo, J., Backer, L., Dahiye, A.M. & Misore, A. (2005). Aflatoxin contamination of commercial maize products during an outbreak of acute aflatoxicosis in Eastern and Central Kenya. *Environmental Health Perspectives*, **113**, 1763-1767.

Lim, K.S. & Barigou, M. (2004). X-ray micro-computed tomography of cellular food products. *Food Research International*, **37**, 1001-1012.

Lin, H. & Cousin, M. (1985). Detection of mold in processed foods by high performance liquid chromatography. *Journal of Food Protection*, **48**, 671-678.

Lippolis, V., Pascale, M., Cervellieri, S., Damascelli, A. & Visconti, A. (2014). Screening of deoxynivalenol contamination in durum wheat by mos-based electronic nose and identification of the relevant pattern of volatile compounds. *Food Control*, **37**, 263-271.

Liu, M., Han, X., Tu, K., Pan, L., Tu, J., Tang, L., Liu, P., Zhan, G., Zhong, Q. & Xiong, Z. (2012). Application of electronic nose in Chinese spirits quality control and flavour assessment. *Food Control*, **26**, 564-570.

Lu, Y., Du, C., Yu, C. & Zhou, J. (2014). Classifying rapeseed varieties using fourier transform infrared photoacoustic spectroscopy (FTIR-PAS). *Computers and Electronics in Agriculture*, **107**, 58-63.

Luo, X., Jayas, D.S. & Symons, S.J. (1999). Identification of damaged kernels in wheat using a colour machine vision system. *Journal of Cereal Science,* **30**, 49-59.

Magan, N. & Evans, P. (2000). Volatiles as an indicator of fungal activity and differentiation between species, and the potential use of electronic nose technology for early detection of grain spoilage. *Journal of Stored Products Research,* **36**, 319-340.

Majumdar, S. (1998). Classification of cereal grains using machine vision. PhD thesis, University of Manitoba.

Manley, M. (2014). Near-infrared spectroscopy and hyperspectral imaging: Non-destructive analysis of biological materials. *Chemical Society Reviews*, **43**, 8200-8214.

Meirelles, P.G., Ono, M.A., Ohe, M.C.T., Maroneze, D.M., Itano, E.N., Garcia, G.T., Sugiura, Y., Ueno, Y., Hirooka, E.Y. & Ono, E.Y. (2006). Detection of *Fusarium* spp. contamination in corn by enzyme-linked immunosorbent assay. *Food and Agricultural Immunology,* **17**, 79-89.

Naresh, M., David, A. & Sanchis, V. (2004). The role of spoilage fungi in seed deterioration. In: Fungal biotechnology in agricultural, food and environmental application. pp. 311-322. New York City: Marcel Dekker.

Narvankar, D.S., Singh, D.S. & White, N.D.G. (2009). Assessment of soft X-ray imaging for detection of fungal infection in wheat. *Biosystems Engineering- Postharvest Technology,* **81**, 49-56.

Neethirajan, S., Jayas, D.S. & White, N.D.G. (2007). Detection of sprouted wheat kernels using soft X-ray image analysis. *Journal of Food Engineering*, **81**, 509-513.

Ng, H., Wilcke, W., Morey, R. & Lang, J. (1998). Machine vision color calibration in assessing corn kernel damage. *Transactions of the ASAE-American Society of Agricultural Engineers*, **41**, 727-732.

Nicolaï, B.M., Beullens, K., Bobelyn, E., Peirs, A., Saeys, W., Theron, K.I. & Lammertyn, J. (2007). Nondestructive measurement of fruit and vegetable quality by means of NIR spectroscopy: A review. *Postharvest Biology and Technology*, **46**, 99-118.

Norris, K. (2009). Letter to the editor: Hazards with near infrared spectroscopy in detecting contamination. *Journal of Near Infrared Spectroscopy,* **17**, 165-166.

Okuni, Y., Furukawa, J., Matsubayashi, M. & Nakanishi, T. (2002). Water accumulation in the vicinity of a soybean root imbedded in soil revealed by neutron beam. *Analytical Sciences/Supplements*, **17**, i1499-i1501.

Olsson, J., Börjesson, T., Lundstedt, T. & Schnürer, J. (2000). Volatiles for mycological quality grading of barley grains: Determinations using gas chromatography–mass spectrometry and electronic nose. *International Journal of Food Microbiology,* **59**, 167-178.

Olsson, J., Börjesson, T., Lundstedt, T. & Schnürer, J. (2002). Detection and quantification of ochratoxin a and deoxynivalenol in barley grains by GC-MS and electronic nose. *International Journal of Food Microbiology*, **72**, 203-214.

Orina, I., Manley, M. & Williams, P.J. (2017). Use of high-resolution X-ray micro-computed tomography for the analysis of internal structural changes in maize infected with *Fusarium verticillioides*. *Food Analytical Methods*, **10**, 2919-2933.

Paolesse, R., Alimelli, A., Martinelli, E., Di Natale, C., D'amico, A., D'egidio, M.G., Aureli, G., Ricelli, A. & Fanelli, C. (2006). Detection of fungal contamination of cereal grain samples by an electronic nose. *Sensors and Actuators B: Chemical*, **119**, 425-430.

Pascale, M.N. (2009). Detection methods for mycotoxins in cereal grains and cereal products. *Zbornik Matice srpske za prirodne nauke*, **117**, 15-25.

Pasikatan, M. & Dowell, F. (2001). Sorting systems based on optical methods for detecting and removing seeds infested internally by insects or fungi: A review*. *Applied Spectroscopy Review*, **36**, 399-416.

Patel, K.K., Kar, A., Jha, S. & Khan, M. (2012). Machine vision system: A tool for quality inspection of food and agricultural products. *Journal of Food Science and Technology*, **49**, 123-141.

Pearson, T. & Wicklow, D. (2006). Detection of corn kernels infected by fungi. *Transactions of the ASABE*, **49**, 1235-1245.

Pearson, T., Wicklow, D. & Pasikatan, M. (2004). Reduction of aflatoxin and fumonisin contamination in yellow corn by high-speed dual-wavelength sorting. *Cereal Chemistry*, **81**, 490-498.

Pearson, T.C., Wicklow, D.T., Maghirang, E.B., Xie, F. & Dowell, F.E. (2001). Detecting aflatoxin in single corn kernels by transmittance and reflectance spectroscopy. *Transactions of the ASAE*, **44**, 1247.

Peiris, K., Pumphrey, M., Dong, Y., Maghirang, E., Berzonsky, W. & Dowell, F. (2010). Near-infrared spectroscopic method for identification of *Fusarium* head blight damage and prediction of deoxynivalenol in single wheat kernels. *Cereal Chemistry*, **87**, 511-517.

Peiris, K.H., Pumphrey, M.O. & Dowell, F.E. (2009). NIR absorbance characteristics of deoxynivalenol and of sound and *Fusarium*-damaged wheat kernels. *Journal of Near Infrared Spectroscopy*, **17**, 213-221.

Pereira, V., Fernandes, J. & Cunha, S. (2014). Mycotoxins in cereals and related foodstuffs: A review on occurrence and recent methods of analysis. *Trends in Food Science & Technology*, **36**, 96-136.

Perfect, E., Cheng, C.L., Kang, M., Bilheux, H.Z., Lamanna, J.M., Gragg, M.J. & Wright, D.M. (2014). Neutron imaging of hydrogen-rich fluids in geomaterials and engineered porous media: A review. *Earth-Science Reviews,* **129**, 120-135.

Perkowski, J., Buśko, M., Chmielewski, J., Góral, T. & Tyrakowska, B. (2008). Content of trichodiene and analysis of fungal volatiles (electronic nose) in wheat and triticale grain naturally infected and inoculated with *Fusarium culmorum*. *International Journal of Food Microbiology,* **126**, 127-134.

Pettersson, H. & Åberg, L. (2003). Near infrared spectroscopy for determination of mycotoxins in cereals. *Food Control,* **14**, 229-232.

Polder, G., Van Der Heijden, G., Waalwijk, C. & Young, I. (2005). Detection of *Fusarium* in single wheat kernels using spectral imaging. *Seed Science and Technology,* **33**, 655-668.

Qiang, Z., Fuguo, J., Chenghai, L., Jingkun, S. & Xianzhe, Z. (2014). Rapid detection of aflatoxin B sub 1 in paddy rice as analytical quality assessment by near infrared spectroscopy. *International Journal of Agricultural and Biological Engineering,* **7**, 127-133.

Ramjee, G., Berjak, P., Adhikari, M. & Dutton, M. (1992). Aflatoxins and kwashiorkor in Durban, South Africa. *Annals of Tropical Paediatrics,* **12**, 241-247.

Ruan, R., Li, Y., Lin, X. & Chen, P. (2002). Non–destructive determination of deoxynivalenol levels in barley using near–infrared spectroscopy. *Applied Engineering in Agriculture,* **18**, 549-553.

Ruan, R., Ning, S., Song, A., Ning, A., Jones, R. & Chen, P. (1998). Estimation of *Fusarium* scab in wheat using machine vision and a neural network. *Cereal Chemistry,* **75**, 455-459.

Ryczkowski, J. (2010). Infrared photoacoustic spectroscopy in catalysis and surface science. *Applied Surface Science,* **256**, 5545-5550.

Schaller, E., Bosset, J.O. & Escher, F. (1998). 'Electronic noses' and their application to food. *LWT-Food Science and Technology,* **31**, 305-316.

Schnürer, J., Olsson, J. & Börjesson, T. (1999). Fungal volatiles as indicators of food and feeds spoilage. *Fungal Genetics and Biology,* **27**, 209-217.

Schoeman, L., Williams, P., Du Plessis, A. & Manley, M. (2016). X-ray micro-computed tomography (μCT) for non-destructive characterisation of food microstructure. *Trends in Food Science & Technology,* **47**, 10-24.

Senthilkumar, T., Jayas, D.S., White, N.D.G., Fields, P.G. & Gräfenhan, T. (2016a). Detection of fungal infection and ochratoxin A contamination in stored barley using near-infrared hyperspectral imaging. *Biosystems Engineering,* **147**, 162-173.

Senthilkumar, T., Jayas, D.S., White, N.D.G., Fields, P.G. & Gräfenhan, T. (2016b). Detection of fungal infection and ochratoxin A contamination in stored wheat using near-infrared hyperspectral imaging. *Journal of Stored Products Research,* **65**, 30-39.

Serranti, S., Cesare, D. & Bonifazi, G. (2013). The development of a hyperspectral imaging method for the detection of *Fusarium*-damaged, yellow berry and vitreous Italian durum wheat kernels. *Biosystems Engineering*, **115**, 20-30.

Shah, M.A. & Khan, A.A. (2014). Imaging techniques for the detection of stored product pests. *Applied Entomology and Zoology*, **49**, 201-212.

Shahin, M.A. & Symons, S.J. (2011). Detection of *Fusarium* damaged kernels in Canada western red spring wheat using visible/near-infrared hyperspectral imaging and principal component analysis. *Computers and Electronics in Agriculture*, **75**, 107-112.

Shahin, M.A. & Symons, S.J. (2012). Detection of *Fusarium* damage in Canadian wheat using visible/near-infrared hyperspectral imaging. *Journal of Food Measurement & Characterization*, **6,** 3-11.

Shahin, M.A., Symons, S.J. & Hatcher, D.W. (2014). Quantification of mildew damage in soft red winter wheat based on spectral characteristics of bulk samples: A comparison of visible-near-infrared imaging and near-infrared spectroscopy. *Food and Bioprocess Technology*, **7**, 224-234.

Singh, C., Jayas, D., Paliwal, J. & White, N. (2007). Fungal detection in wheat using near-infrared hyperspectral imaging. *Transactions of the ASABE*, **50**, 2171-2176.

Singh, C., Jayas, D., Paliwal, J. & White, N. (2012). Fungal damage detection in wheat using short-wave near-infrared hyperspectral and digital colour imaging. *International Journal of Food Properties*, **15**, 11-24.

Siripatrawan, U. & Makino, Y. (2015). Monitoring fungal growth on brown rice grains using rapid and non-destructive hyperspectral imaging. *International Journal of Food Microbiology*, **199**, 93-100.

Sivakesava, S. & Irudayaraj, J. (2000). Analysis of potato chips using FTIR photoacoustic spectroscopy. *Journal of the Science of Food and Agriculture*, **80**, 1805-1810.

Steenoek, L., Misra, M.K., Hurburgh, C. & Bern, C.J. (2001). Implementing a computer vision system for corn kernel damage evaluation. *Applied Engineering in Agriculture*, **17**, 235-240.

Stetter, J.R., Findlay, M.W., Schroeder, K.M., Yue, C. & Penrose, W.R. (1993). Quality classification of grain using a sensor array and pattern recognition. *Analytica Chimica Acta*, **284**, 1-11.

Strobl, M., Manke, I., Kardjilov, N., Hilger, A., Dawson, M. & Banhart, J. (2009). Advances in neutron radiography and tomography. *Journal of Physics D: Applied Physics*, **42**, 243001.

Tallada, J., Wicklow, D., Pearson, T. & Armstrong, P. (2011). Detection of fungus-infected corn kernels using near-infrared reflectance spectroscopy and color imaging. *Transactions of the ASABE*, **54**, 1151-1158.

Tekle, S., Måge, I., Segtnan, V.H. & Bjørnstad, Å. (2015). Near-infrared hyperspectral imaging of *Fusarium*-damaged oats (*Avena sativa* L.). *Cereal Chemistry,* **92**, 73-80.

Tognon, G., Campagnoli, A., Pinotti, L., Dell'orto, V. & Cheli, F. (2005). Implementation of the electronic nose for the identification of mycotoxins in durum wheat (*Triticum durum*). *Veterinary Research Communications,* **29**, 391-393.

Vadivambal, R. & Jayas, D.S. (2011). Applications of thermal imaging in agriculture and food industry—a review. *Food and Bioprocess Technology,* **4**, 186-199.

Van Der Gaag, B., Spath, S., Dietrich, H., Stigter, E., Boonzaaijer, G., Van Osenbruggen, T. & Koopal, K. (2003). Biosensors and multiple mycotoxin analysis. *Food Control,* **14**, 251-254.

Vithu, P. & Moses, J. (2016). Machine vision system for food grain quality evaluation: A review. *Trends in Food Science & Technology,* **56**, 13-20.

Vontobel, P., Lehmann, E.H., Hassanein, R. & Frei, G. (2006). Neutron tomography: Method and applications. *Physica B: Condensed Matter,* **385**, 475-480.

Wagacha, J. & Muthomi, J. (2008). Mycotoxin problem in Africa: Current status, implications to food safety and health and possible management strategies. *International Journal of Food Microbiology,* **124**, 1-12.

Wang, D., Dowell, F., Ram, M. & Schapaugh, W. (2004). Classification of fungal-damaged soybean seeds using near-infrared spectroscopy. *International Journal of Food Properties,* **7**, 75-82.

Wang, W., Heitschmidt, G.W., Ni, X., Windham, W.R., Hawkins, S. & Chu, X. (2014). Identification of aflatoxin B1 on maize kernel surfaces using hyperspectral imaging. *Food Control,* **42**, 78-86.

Wang, W., Heitschmidt, G.W., Windham, W.R., Feldner, P., Ni, X. & Chu, X. (2015a). Feasibility of detecting aflatoxin B1 on inoculated maize kernels surface using vis/NIR hyperspectral imaging. *Journal of Food Science,* **80**, M116-M122.

Wang, W., Lawrence, K.C., Ni, X., Yoon, S.-C., Heitschmidt, G.W. & Feldner, P. (2015b). Near-infrared hyperspectral imaging for detecting aflatoxin B1 of maize kernels. *Food Control,* **51**, 347-355.

Wang, W., Ni, X., Lawrence, K.C., Yoon, S.-C., Heitschmidt, G.W. & Feldner, P. (2015c). Feasibility of detecting aflatoxin B1 in single maize kernels using hyperspectral imaging. *Journal of Food Engineering,* **166**, 182-192.

Wegulo, S.N. & Dowell, F.E. (2008). Near-infrared versus visual sorting of *Fusarium*-damaged kernels in winter wheat. *Canadian Journal of Plant Science,* **88**, 1087-1089.

Williams, J.H., Phillips, T.D., Jolly, P.E., Stiles, J.K., Jolly, C.M. & Aggarwal, D. (2004). Human aflatoxicosis in developing countries: A review of toxicology, exposure, potential health consequences, and interventions. *The American Journal of Clinical Nutrition,* **80**, 1106-1122.

Williams, P., Manley, M., Fox, G. & Geladi, P. (2009). Indirect detection of *Fusarium verticillioides* in maize (*Zea maize* L.) kernels by NIR hyperspectral imaging. *Journal of Near Infrared Spectroscopy*, **18**, 49-58.

Williams, P.J., Geladi, P., Britz, T.J. & Manley, M. (2012). Investigation of fungal development in maize kernels using NIR hyperspectral imaging and multivariate data analysis. *Journal of Cereal Science,* **55**, 272-278.

Wiwart, M., Koczowska, I. & Borusiewicz, A. (2001). Estimation of *Fusarium* head blight of triticale using digital image analysis of grain. *Computer Analysis of Images and Patterns. Lecturer notes in compter science,* **2124**, 563-569.

Wu, D. & Sun, D.-W. (2013). Colour measurements by computer vision for food quality control–a review. *Trends in Food Science & Technology,* **29**, 5-20.

Yang, Y., Chai, R. & He, Y. (2012). Early detection of rice blast (*pyricularia*) at seedling stage in nipponbare rice variety using near-infrared hyper-spectral image. *African Journal of Biotechnology,* **11**, 6809-6817.

Yao, H., Hruska, Z. & Di Mavungu, J.D. (2015). Developments in detection and determination of aflatoxins. *World Mycotoxin Journal,* **8**, 181-191.

Yorulmaz, O., Pearson, T.C. & Çetin, A.E. (2012). Detection of fungal damaged popcorn using image property covariance features. *Computers and Electronics in Agriculture,* **84**, 47-52.

Zhang, J.-C., Pu, R.-L., Wang, J.-H., Huang, W.-J., Yuan, L. & Luo, J.-H. (2012). Detecting powdery mildew of winter wheat using leaf level hyperspectral measurements. *Computers and Electronics in Agriculture,* **85**, 13-23.

Zwiggelaar, R., Bull, R.C. & Mooney, M., J. Mooney (1996). X-ray simulation for imaging applications in the agricultural and food industries. *Journal of Agricultural Engineering Research,* **51**, 161-170.

Declaration by student

With regard to Chapter 3 (pp 53 - 77) the nature and scope of my contribution were as follows:

Nature of contribution	Extent of contribution (%)
Research, analysis and writing of chapter	70%

The following co-authors have contributed to Chapter 3:

Name	e-mail address	Nature of contribution	Extent of contribution (%)
Dr Paul J. Williams	pauljw@sun.ac.za	Research inputs, editorial suggestions and proofreading	15%
Prof Marena Manley	mman@sun.ac.za	Research inputs, editorial suggestions and proof reading	15%

Signature of student: I. Orina

Date: 13/12/2017

The undersigned hereby confirm that:

1. the declaration above accurately reflects the nature and extent of the contributions of the candidate and the co-authors to Chapter 3 (pp 53- 77),
2. no other authors contributed to Chapter 3 (pp 53- 77) besides those specified above, and
3. potential conflicts of interest have been revealed to all interested parties and that the necessary arrangements have been made to use the material in Chapter 3 (pp 53 -77) of this dissertation.

Signature	Institutional affiliation	Date
Dr Paul J. Williams	Department of Food Science, Stellenbosch University	13/12/2017
Prof Marena Manley	Department of Food Science, Stellenbosch University	13/12/2017

Chapter 3

Use of high resolution X-ray micro-computed tomography for the analysis of internal structural changes in maize infected with *Fusarium verticillioides**

Abstract

X-ray micro-computed tomography (X-ray micro-CT) is a non-destructive, three-dimensional (3D) imaging and analysis technique for the investigation of internal structure of a large variety of materials, including agricultural produce. As a relatively new method in the field of food science, X-ray micro-CT has been applied successfully to obtain microstructural information of foods undergoing different physical and chemical changes. In this study, high resolution X-ray micro-CT was used for non-destructive analysis of the internal structure of maize kernels infected with *Fusarium verticillioides.* The major anatomical features of the maize kernel were identified based on their differences in X-ray attenuation i.e. the germ, scutellum, vitreous and floury endosperm. Fungal infection caused changes in the internal structure of the kernels over time, which included a decrease in total kernel volume and an increase in total volume of void space, with more voids observed in the germ and floury endosperm regions. No significant ($P > 0.05$) difference was observed between the control and the infected kernels, it was apparent that the changes observed in the infected kernels were not solely as a result of fungal growth. The grey level histograms of the control and infected kernels shifted to the lower grey value intensity range over time indicating an increase in void space within the kernels. In the 3D images the increase in total volume of void space with fungal progression was clearer and the effect of fungal damage on the internal structure was evident.

Keywords: X-ray micro computed tomography; maize; internal structure; *Fusarium verticillioides.*

---

*Published as: Irene Orina, Marena Manley & Paul J. Williams (2017). Use of high resolution X-ray micro computed tomography for the analysis of internal structural changes in maize infected by *Fusarium verticillioides*, *Food Analytical Methods*, **10**, 2919-2933.

Introduction

X-ray micro-computed tomography is an emerging technique in the field of food science for non-destructive analysis of the internal structure characteristics and the detection of internal defects. X-ray micro-CT has been widely used to study the internal structure of many food materials such as coffee beans (Frisullo *et al.*, 2012), wheat (Suresh & Neethirajan, 2015a; Schoeman *et al.*, 2016a), rice (Zhu *et al.*, 2012), apples (Mendoza *et al.*, 2007) and bread (Van Dyck *et al.*, 2014). It provides a means to acquire a complete 3D image of the structure, visualising the internal architecture at the microscopic level in a non-destructive way. Additionally, the X-ray micro-CT images enable subsequent image analysis resulting in 3D quantification of the internal structure (Kerckhofs *et al.*, 2008). Therefore, the technique is used not only for qualitative visualisation of internal features but also for quantitative data acquisition.

X-ray micro-CT uses the difference in X-ray attenuation, arising principally from differences in density and atomic composition within the sample (Landis & Keane, 2010). The variation in X-ray attenuation within a sample creates a contrast in the X-ray image to differentiate lower density regions from higher density regions (Schoeman *et al.*, 2016b). The sample is rotated either 180 or 360 degrees and multiple two-dimensional (2D) projections are progressively collected as the X-ray beam passes through the rotating object. The numerous 2D projections covering the entire sample are then reconstructed into a 3D image using dedicated computer algorithms (du Plessis *et al.*, 2016). For a particular sample (at a specific energy), the X-ray attenuation is approximately proportional to the material density (Sinka *et al.*, 2004; Kelkar *et al.*, 2015).

The internal structure of foods, including cereal grains, is generally studied by means of microscopic techniques such as optical or scanning electron microscopy (SEM) with a suitable resolution. These techniques are 2D in nature and require sample preparation which involves cutting to expose the cross-section to be viewed, which can alter structural features (Trater *et al.*, 2005). X-ray micro-CT can be an important complementary technique for the microscopy laboratory as the data obtained is a result of virtual rendering of the object under investigation, allowing one to scroll through the volume in any direction and angle, revealing complex hidden structures within the object non-destructively (Singhal *et al.*, 2013). The non-destructive nature of this technique also allows one to investigate structural changes in the same sample under influence of environmental changes or mechanical stress or high-speed time lapse monitoring (Cnudde *et al.*, 2006).

Maize is an important cereal crop and is primarily used for direct consumption in developing countries. In the field as well as during storage, maize is particularly vulnerable to degradation due to mycotoxigenic fungi belonging to *Aspergillus*, *Fusarium* and *Penicillium* genera (Lillehoj, 1987). Infection of the kernel by these fungal pathogens often results in a decrease in dry matter content and

thus kernel density. Of major concern is mycotoxin contamination which are carcinogenic secondary metabolites harmful to humans and animals (Pomeranz, 1982; Seitz *et al.*, 1982; Cardwell *et al.*, 2000).

Very little work has been undertaken to study the effect of fungal contamination on the internal maize kernel structure non-destructively. Cleveland *et al.* (2008) used neutron tomography to study the internal process of *Aspergillus flavus* infection and invasion of maize kernels. Unlike X-rays, neutrons do not interact (or at most interact negligibly) with the electronic charge of the electrons, instead they interact strongly with the atomic nucleus (Strobl *et al.*, 2009). With neutron tomography, they were able to identify the different anatomical features of the kernel. Differences were also detected between susceptible kernels that had been inoculated with *Aspergillus flavus* and those that had not. Infected kernels were found to have a lower neutron attenuation in the scutellum and embryo region, possibly caused by lower hydrogen concentration due to fungal degradation. Pearson and Wicklow (2006) in their study using X-ray imaging, detected a significantly lower mean X-ray intensity in the fungal infected kernels than in the undamaged kernels. This indicated lower density, as the fungal infected kernels absorbed less X-ray energy. Narvankar *et al.* (2009) used soft X-ray imaging to detect fungal infection in wheat with the common storage fungi namely *Aspergillus niger*, *A. glaucus* group and *Pencilluim* spp. Accuracies of between 92.2 and 98.9% were obtained using a two-class Mahalanobis discriminant classifier.

The aim of this study was to determine whether high resolution X-ray micro-CT was able to distinguish the anatomical features of the maize kernel, to investigate the changes in the internal structure of maize kernels infected with *Fusarium verticillioides* over time and, to distinguish between infected and uninfected maize kernels

Materials and methods

Maize kernel preparation

A South African maize variety, I16, supplied by the Department of Plant Pathology (Stellenbosch University, South Africa), was used for experiment 1 and 2. It is important to note that the two experiments were not done simultaneously. Maize kernel preparation was similar in both experiments. A batch of 50 kernels were chosen in both experiments and first soaked overnight (*ca.* 15 h) in sterile distilled water. The kernels were then surface-sterilised by rinsing in 70% ethanol, then in 1% sodium hypochlorite solution, followed by double rinsing with sterile distilled water. Finally, the surface sterilised kernels were imbibed in a water bath at 60°C for 5 min, immediately placed in ice for 1 min then left to dry in a laminar flow hood for 1 h. The kernels were considered sterile and ready for inoculation.

Spore preparation

Fusarium verticillioides (MRC 0826) obtained from the Department of Plant Pathology (Stellenbosch University, South Africa) was used for both experiments. Prior to spore preparation, the culture was transferred onto potato dextrose agar (PDA) (Merck, Cape Town, South Africa) and incubated at 25°C. After 4 days, sterile water with Tween 20 (three drops. L^{-1}) was used to wash spores from the agar surface. The spore suspension was poured through sterile cheesecloth to remove mycelium, thereafter the suspension was adjusted to 1×10^6 conidia per millilitre using a haemocytometer. *F. verticillioides* was chosen because it is a well-known and problematic fungus in maize. *F. verticillioides* infects maize at all stages of plant development, either via infected seeds, the silk channel or wounds, causing grain rot during both pre- and postharvest periods (Munkvold & Desjardins, 1997). Infection of maize kernels by toxigenic fungi remains a challenging problem despite decades of research (Munkvold, 2003).

Experiment 1

To obtain high resolution X-ray images, only one kernel could be scanned at a time; however, due to high cost of scanning per hour and image analysis, only six kernels were selected. The six kernels were randomly selected from the batch of sterilised kernels and injured using a sterile needle at random positions on the kernel. Injury of the kernel was important to facilitate entry of the fungus into the kernel. Three of the kernels were dipped into *F. verticillioides* spore suspension for 1 min (infected) and the other three were dipped into sterile distilled water for 1 min (controls). Both sets were allowed to dry at room temperature. Each dry kernel was placed in a 5-mL plastic pipette tip with sterilised cotton wool on both ends of the pipette tip (see sample setup in Fig. 3.1a). This enabled holding the kernel in a fixed position during X-ray scanning and to avoid contamination.

Experiment 2

Moisture and temperature are the most important factors that influence the rate of fungal growth and deterioration (Sauer, 1988). In the second experiment, relative humidity of the storage environment of the maize kernels was increased to facilitate the growth of the fungus within the kernels. Six kernels were randomly selected from the batch of sterilized maize kernels; to facilitate entry of the fungus into the kernel, injury using a sterilised needle on random positions on the kernels was done. Three of the kernels were dipped into *F. verticillioides* spore suspension for 1 min (infected kernels) and the other three were dipped into sterile distilled water for 1 min (control kernels); both were allowed to dry at room temperature. Each dry kernel was then placed in a 5-mL pipette tip; a sterilised polymeric disc (0.29-0.371g) was included below each maize kernel inside the pipette tip, then sterilised cotton wool was added on both ends of the pipette tip. The polymeric disc had a higher

density than the maize kernel and was used as a reference standard for relative density determinations (results are not shown).

Previous studies have reported a relative humidity of 92-95% and temperature of 25-30ºC to be optimum for the growth of *F. verticillioides* in maize (Marin *et al.*, 1995a; Marín *et al.*, 2004). Constant relative humidity was produced and maintained using a saturated solution of potassium nitrate (KNO_3) in an airtight plastic container (Winston & Bates, 1960). Approximately 250 mL of saturated solution of KNO_3 in a beaker was placed inside an airtight plastic container (25 cm × 25 cm × 14.5 cm) and the relative humidity was monitored using a LogTag® (Haxo-8) humidity and temperature recorder. An equilibrium relative humidity of 90-92% was obtained before placing the six maize kernels inside the airtight plastic container and incubated at 25°C.

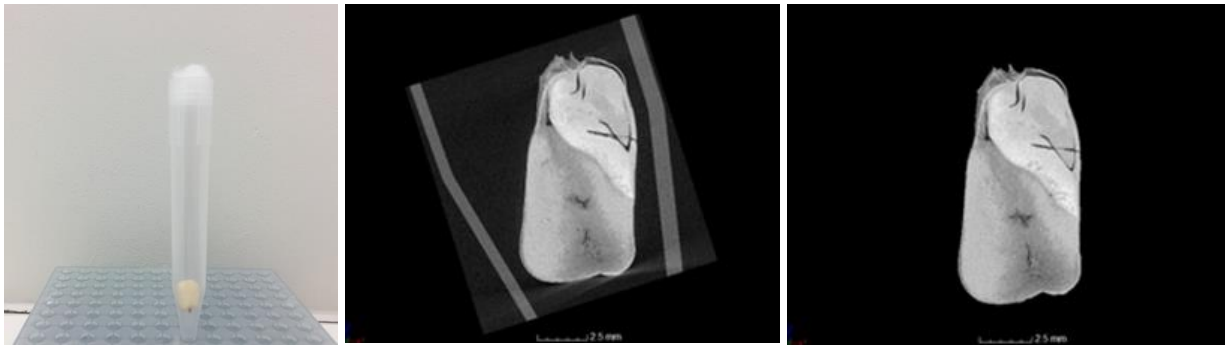

Figure 3.1. (a) Digital image of the maize kernel in the plastic pipette tip and cotton wool, (b) 2D sagittal view image of maize kernel with plastic pipette tip and surrounding air, and (c) maize kernel after removal of the plastic pipette pit and surrounding air.

X-ray micro-computed tomography image acquisition

X-ray scans were acquired using a General Electric phoenix Nanotom S (GE Sensing & Inspection Technologies. GmbH, Phoenix, Wunstorff, Germany) high-resolution X-ray computed tomography system, equipped with a 180 kV nanofocus tube, located at the Stellenbosch University CT Scanner Facility. The power setting of 50 kV and 250 µA were used. The system was equipped with a 0.1 mm copper filter to reduce beam hardening artefacts. In experiment 1, each maize kernel, in a 5-mL pipette tip, was placed on the specimen stage (the pipette tip had a lower density than the maize kernel) at a physical distance of 30 mm from the X-ray radiation source and 200 mm from the detector with a scanning resolution of 7.5 µm. The cotton wool on both ends of the pipette tips was not within the field-of-view (FOV). The control and infected maize kernels were scanned on the following days after inoculation: 1, 2, 3, 4, 8, 9, 10 and 14 using similar instrument settings.

In experiment 2, each maize kernel, in a 5-ml pipette tip with a polymer disc included, was placed on the specimen stage (the polymeric disc had a higher density than the maize kernel) at a physical distance 35 mm from the X-ray radiation source and 200 mm from the detector. The

polymeric disc was included in the field of view, resulting in CT scans with a resolution of 8.75 µm. Both the control and infected maize kernels were scanned on the following days after inoculation: 1, 2, 3 and 4 using similar instrument settings.

A series of 2D X-ray images were obtained as the maize kernel was rotated 360 degrees. The exposure time was set at 0.5 s per image with 2000 images recorded in one rotation of the sample along the axis, perpendicular to the beam direction. Each maize kernel scan (three controls and three infected) in both experiments took approximately 1 h to complete. The 2D radiographs, covering the entire sample were acquired using a fully automated data acquisition system and saved onto a processing workstation, operated by system-supplied reconstruction software (datos x ® 2.1 GE Sensing & Inspection Technologies GmbH, Phoenix, Wunstorf, Germany). The 3D volumes were reconstructed using the integrated Phoenix datos x 3D computed tomography acquisition and reconstruction software (GE Sensing & Inspection Technologies. GmbH, Phoenix, Wunstorf, Germany). The instrument is standardized using unsigned 16-bit data, which results in grey values between 0 and 65,535 (2^{16} for 16-bit data). Beam hardening corrections was not necessary in experiment 1, due to the high quality of the images. In experiment 2, beam hardening correction (2 units or low) was applied using Volume Graphic Studio MAX 2.2 software (VGStudio MAX 2.2, Heidelberg, Germany) to improve the quality of the images.

Image processing and analysis

The 3D volumes of the maize kernels from both experiments were further analysed using the VGStudio Max 2.2 software. Each kernel was analysed independently using similar image processing and analysis procedure. The first step in image processing was to remove the plastic pipette tips, the background pixels (i.e. surrounding air) and the polymeric disc (for the second experiment). This was done using the Region growing tool by choosing an appropriate thresholding grey value tolerance ranging from 2000-2500 for the plastic pipette tip, 800-2000 for the surrounding air (Fig. 3.1) and 16,000-16,500 for the polymeric disc, these regions were then inverted and extracted from the image.

The total kernel volume and mean grey value of the whole maize kernels were determined automatically using the Volume analyser function of VGStudio Max 2.2. The total volume of voids space (intergranular voids) within the kernels was calculated automatically using the Volume analyser tool after thresholding all the voids within the maize kernel using the whole kernel grey level histogram in the Volume analyser tool. The thresholding value for the total volume of void within the kernels were different for each kernel and on each day.

Scanning electron microscopy

Scanning electron microscopy (SEM) micrographs were obtained from the maize kernels of the first experiment on day 15 post inoculation. The control and infected kernels were cut into two using a surgical blade, and one half of each was mounted onto double sided carbon tape. This was coated with gold dust, using a 5150A sputter coater (HHV, Crawley, UK). The SEM micrographs were taken with a LEO1430 VP scanning microscope (Zeiss, Germany). The remaining halves were plated onto PDA to confirm presence of *F. verticillioides*.

The maize kernels (control and uninfected) of the second experiment were viewed under a Stemi 508 stereomicroscope (Zeiss, Germany) on day 4 post inoculation to view presence of hyphae on the surface of the maize kernels.

Statistical analysis

Analysis of variance (ANOVA) was used to compare the means for the respective quantitative measurements (total volume, mean grey value and total volume of void space) with respect to time and treatment (control and infected). Data analyses were carried out using STATISTICA version 12 (Statsoft Inc., Tulsa, USA). *P* values less than 0.05 were deemed to be statistically significant.

Results

The grey level 2D cross-sectional images of the uninfected maize kernel in the three orthogonal views, i.e. sagittal, horizontal and frontal are shown in Fig. 3.2. The 3D image generated by the X-ray micro-CT could be sliced in any direction revealing information in 2D as a slice in the 3D image. The contrast in 2D cross-sectional images is based on the differences in X-ray attenuation by the constituents of the sample (i.e. structure and air), which is a result of variation in density of the maize kernel constituents. The images thus serve as a map of the spatial distribution of the X-ray attenuation in which the brighter regions correspond to higher levels of attenuation, which is attributed to denser regions and the darkest areas represent the voids (air) as it has a lower absorption coefficient with respect to material. The different structural components within the kernel were distinguished based on X-ray attenuation with the brightest grey region representing the germ and scutellum (Fig. 3.2).

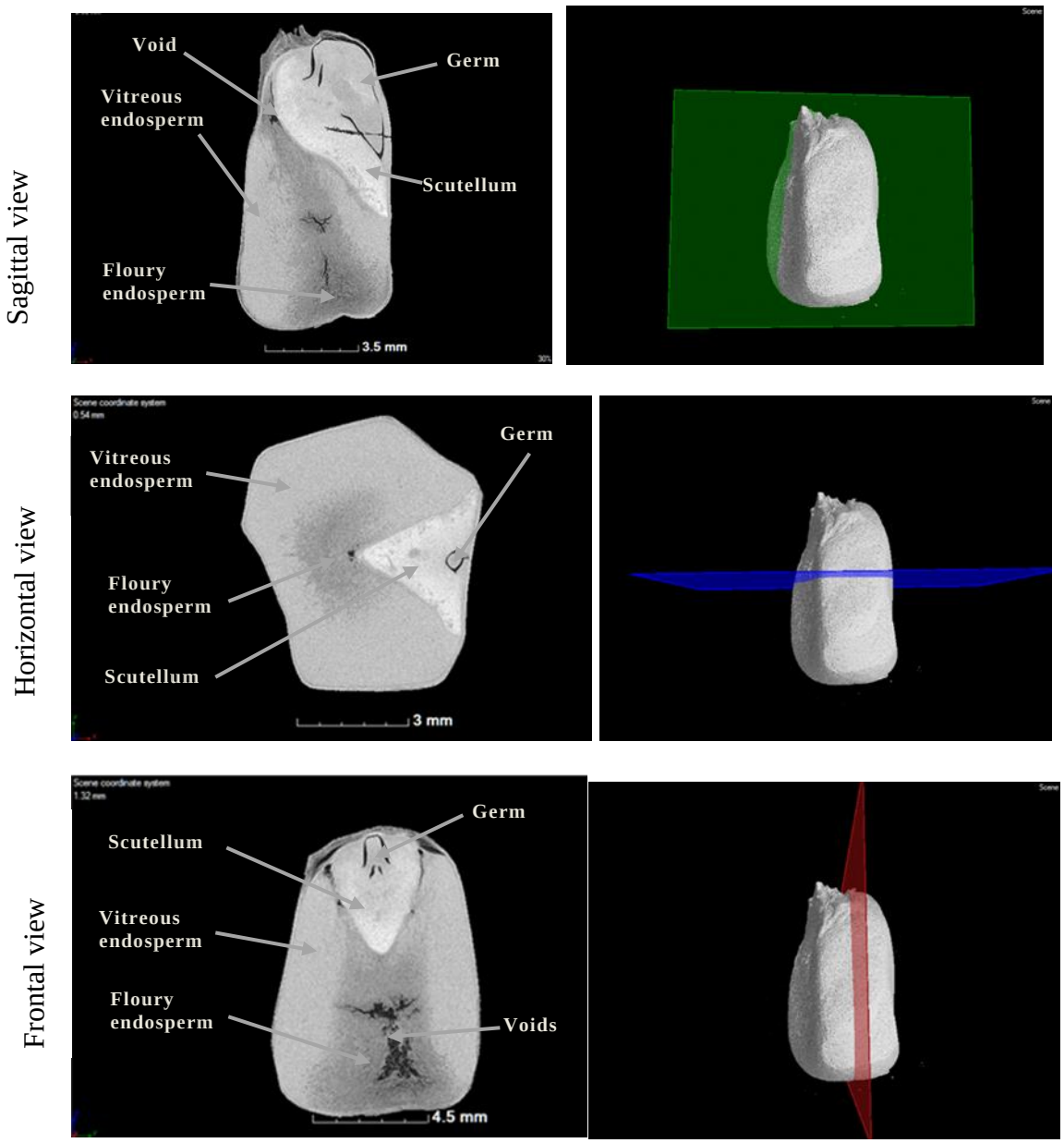

Figure 3.2. Illustration of the different X-ray views (sagittal, horizontal, frontal view). 2D views are shown on the left and the corresponding section of 3D view on the right. The different constituents within the maize kernel are also shown based on the X-ray attenuation.

The 2D cross-sectional images of the control and infected maize kernels became less bright with time and this was due to less material in the kernel to attenuate the X-rays as shown in Fig. 3.3 (only the results of one control and one infected kernel are shown, since similar results were obtained for the other kernels). The germ and scutellum regions of both the control and the infected kernels developed more voids with time, as visually illustrated in Fig. 3.3. The widening of the existing voids as well as the presence of additional ones were observed. The presence of voids depended on the structural part (and thus, on the position and depth in the kernel) as well as the sample kernel under investigation.

(a)

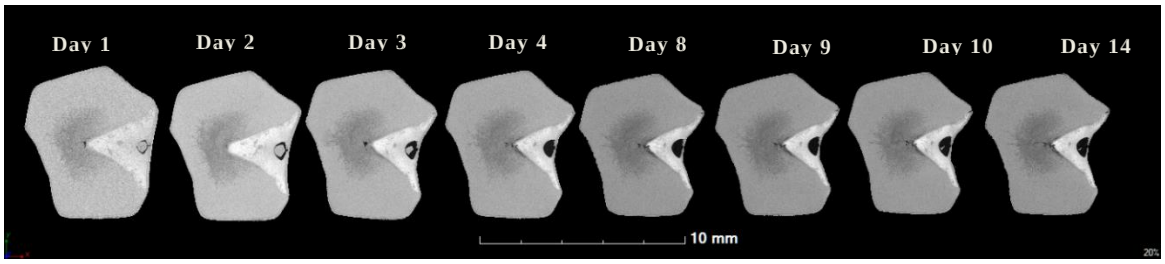

(b)

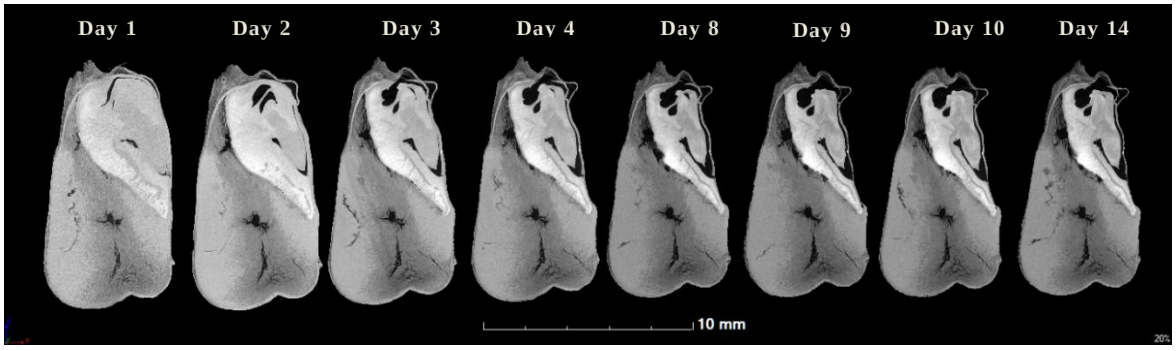

(c)

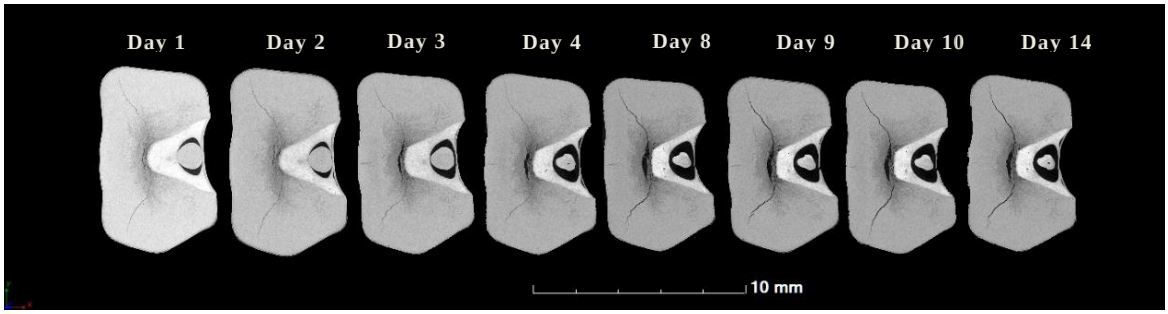

(d)

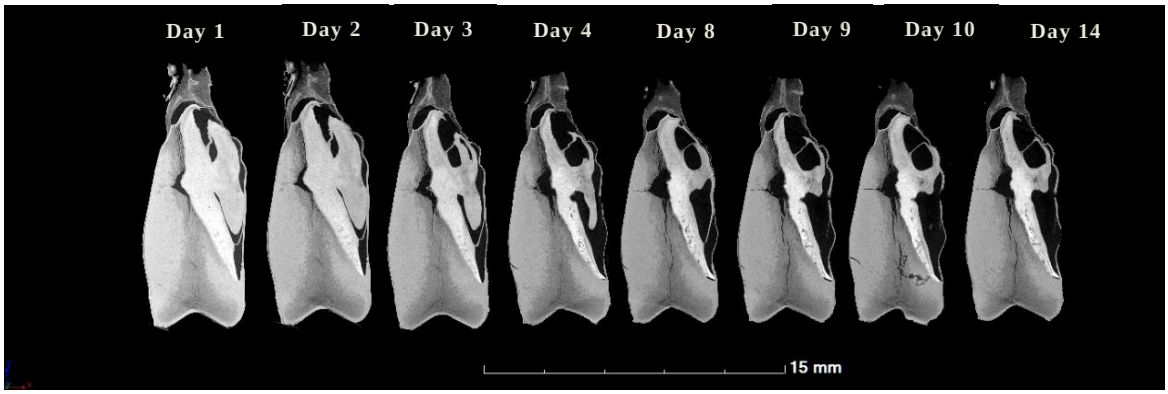

Figure 3.3. 2D X-ray images of approximately the same slice in the image stack of the control and infected maize kernels over the period of days scanned demonstrating internal structural changes, with (a) horizontal and (b) sagittal views of a control kernel; and (c) horizontal and (d) sagittal views of an infected kernel.

There were more voids in the floury endosperm region of both the control and infected kernels compared to the vitreous endosperm and these increased with time (Fig. 3.4).

Grey value histograms plot the frequency, or number of occurrence of pixels or voxels of a particular intensity (Landis & Keane, 2010). The different peaks in the grey value histogram of the whole maize kernel correspond to the different phases within the kernel, with the lower grey value corresponding to internal air while the higher values correspond to the kernel structure. On day 14, in both the control and the infected kernels, there was a general shift to the lower intensity grey values end of the grey level spectrum (Fig. 3.5). These were attributed to less material and more voids in the kernel on day 14 compared to day 1 (only the results of one control and one infected kernel are shown).

The total kernel volume is the amount of space occupied by the 3D object (Herremans *et al.*, 2013). The total kernel volume decreased with time in both the control and the infected kernels in both experiments. There was a significant difference in the total volume of the kernels in the first 8 days but no significant difference ($P > 0.05$) between the control and the infected kernels in the first experiment (Fig. 3.6a). In the second experiment (Fig. 3.6b), the infected kernels had a significant difference in kernel volume between day 1, 2 and 3 but no significant difference between day 3 and 4. There was also no significant difference ($P > 0.05$) observed in the kernel volume between the control and infected kernel.

Total volume of void space is a measure of space occupied by all the voids/air within the kernel (intergranular space). An increase in total volume of void space with time was observed in both the control and infected kernels in the first experiment, a significant difference in total voids is observed in the first three days and no significant difference ($P > 0.05$) between the control and infected kernels (Fig. 3.7a). An increase in total volume of voids was observed in both the control and infected kernels with time in the second experiment (Fig. 3.7b). There was no significant difference in total volume of voids between the days in the control kernels while there was a significant difference between day 3 and 4 in the infected kernel. There was no significant difference between the control and infected kernels in the second experiment.

(a)

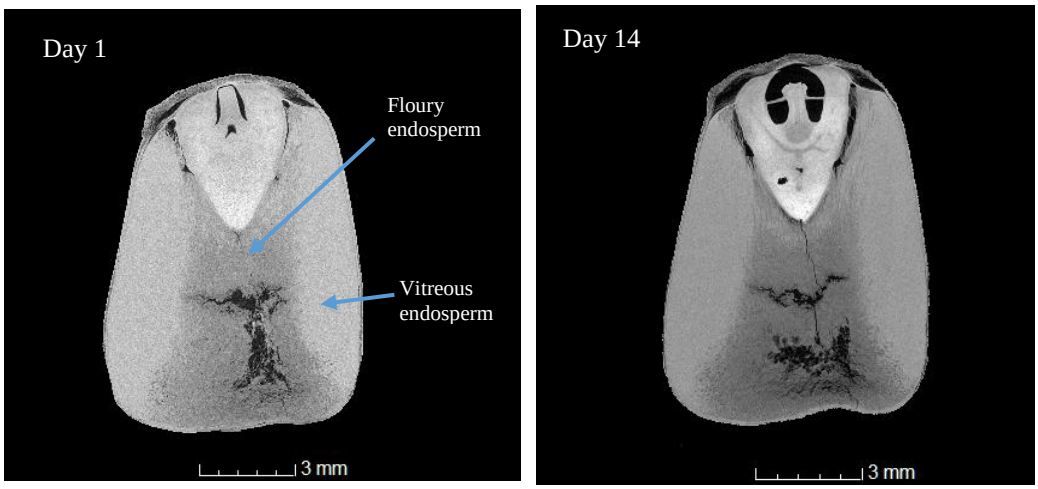

(b)

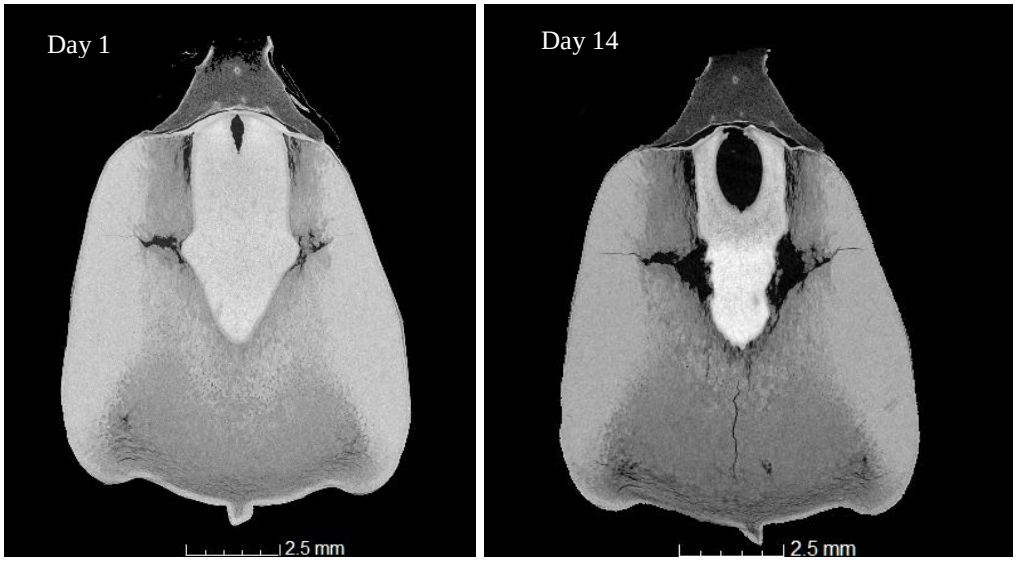

Figure 3.4. 2D X-ray images (approximately the same slice in the image stack) from the frontal view of (a) control maize kernel and (b) an infected kernel on days 1 and 14, showing internal structural changes.

The mean grey values for the control and infected kernels for both experiments are shown in Fig. 3.8. The mean grey value is the pixel intensity of the image which correspond to the attenuation coefficient of the sample (Van Geet *et al.*, 2000). A higher mean grey value corresponds to higher density due to a higher attenuation coefficient while lower grey values correspond to lower attenuation coefficient. In the first experiment, there was a decrease in the mean grey value with time in both the control and the infected kernels, implying that the kernels were becoming less dense with time as they were attenuating less X-rays. Significant differences were observed from day 1 to day 8, but no significant change in mean grey values from day eight onwards. There was no significant difference ($P > 0.05$) in mean grey values between the control and the infected kernels (Fig 3.8a).

While in the second experiment, there was also a decrease in the mean grey value with time in the control and the infected kernels, there was a significant difference in the days but no significant difference between the control and infected kernel (Fig 3.8b).

(a)

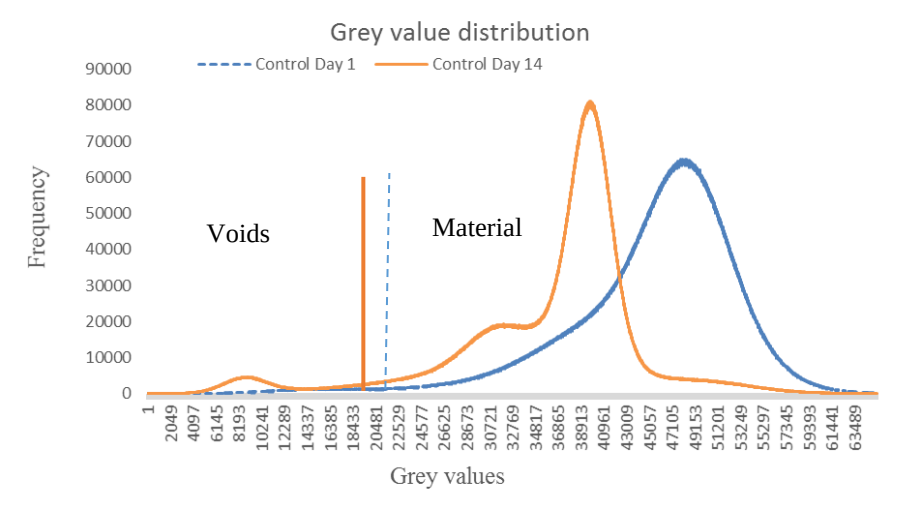

(b)

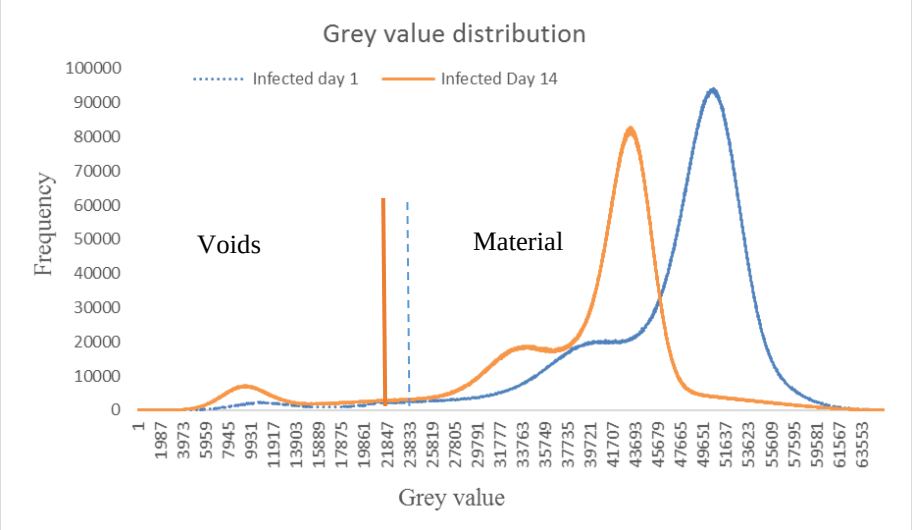

Figure 3.5. Grey level distribution histograms of (a) control kernel on day 1 and day 14 and (b) infected kernel on day 1 and day 14 illustrating the shift to the low grey level intensity with time and the different thresholding levels of the intergranular air for the respective days (vertical blue dotted line is the threshold level for day 1 and orange line is for day 14).

A 3D visualisation of the reconstructed volume through 3D rendering procedures is necessary to observe and visualise the internal microstructure. The 3D-rendered images enable the visualisation of the morphology and microstructure such as pore shape, size, position and distribution (Suresh & Neethirajan, 2015; Schoeman *et al.*, 2016b). Figure 3.9 shows 3D visualisation of the voids/pores (in red) in the control and the infected maize kernel on day 1 and day 14 (images of only one control and

one infected kernel are shown). There were more voids on day 14 compared to day 1, and the voids were distributed more around the germ region and the floury endosperm.

(a)

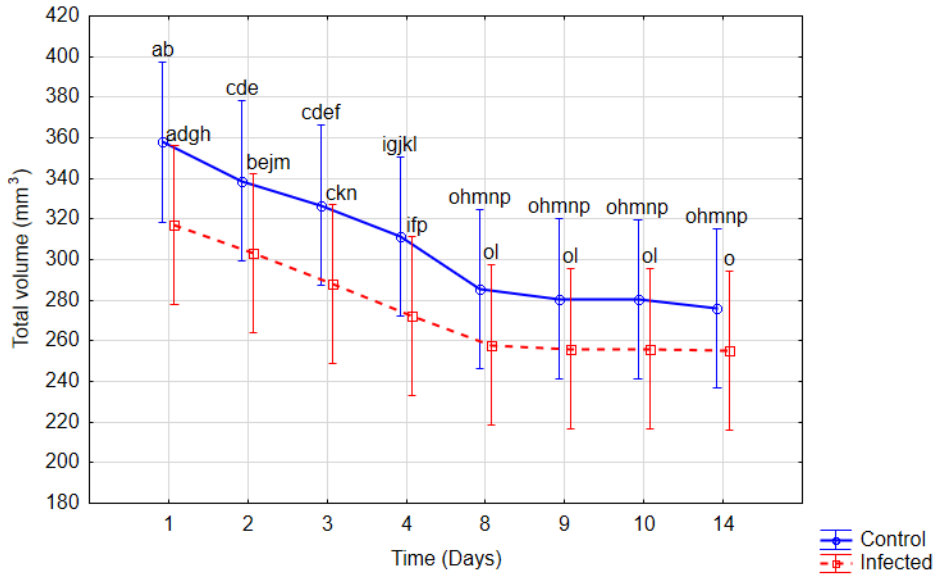

(b)

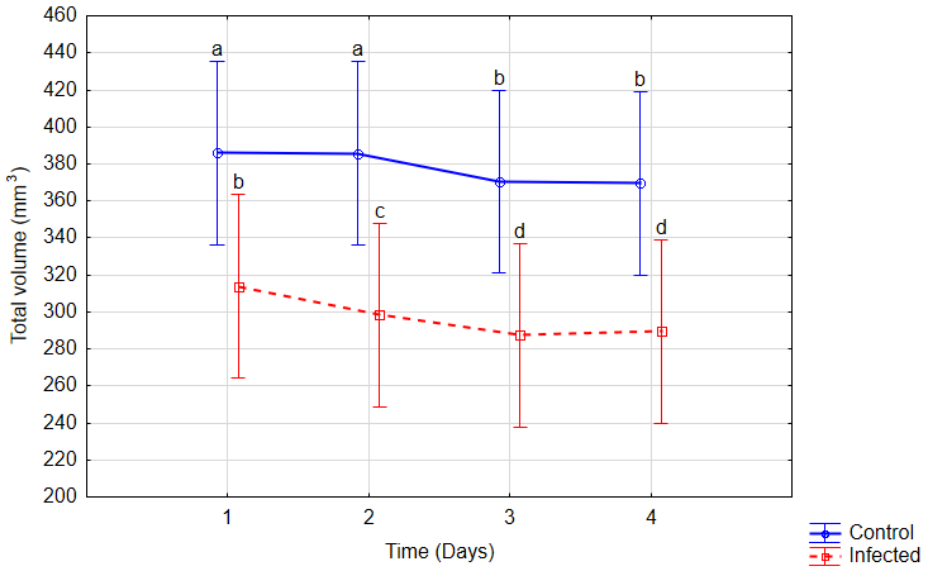

Figure 3.6. Total kernel volume in cubic millimetres of control (n =3) and infected kernels (n =3) over time (days) for (a) experiment one for the 8 days scanned and (b) experiment two the four days scanned. The letters (a-m) represent the statistical significant difference.

The SEM micrographs revealed hyphae of *F. verticillioides* in the infected kernel of the first experiment on day 15 after X-ray scanning (Fig. 3.10). The infected kernels were plated on PDA on day 15 after X-ray scanning, they also confirmed the presence of *F. verticillioides* (Fig. 3.11a). The infected kernels from the second experiment were viewed with a stereomicroscope on day 4 post

inoculation and hyphae were observed growing on the surface of the maize kernels (Fig. 3.11b, only photographs of one infected kernel is shown).

(a)

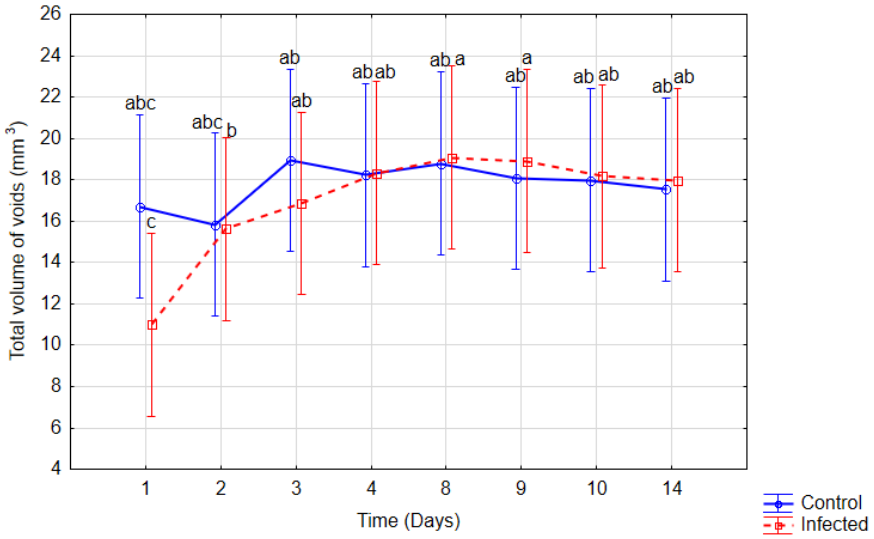

(b)

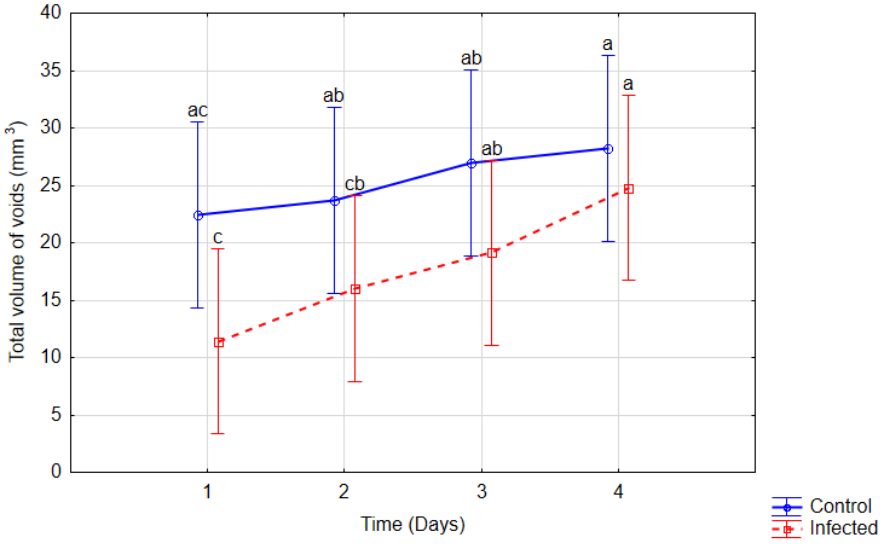

Figure 3.7. Total volume of void space in cubic millimetres for control (n=3) and infected kernels (n=3) over time for (a) experiment one for the 8 days scanned and (b) experiment two for the four days scanned. The letters (a, b, c,) on the line graphs represent the statistical significant differences.

Discussion

X-ray micro-CT is based on image contrast that is created by variation in the X-ray attenuation within the sample. When an X-ray beam passes through a sample, it is attenuated and the differences in X-ray attenuation are attributable to density and compositional differences within a sample (Schoeman *et al.*, 2016b). The denser regions within a sample will appear brighter on the 2D cross-

sectional X-ray image due to a higher X-ray attenuation. A maize kernel consists of important anatomical structures that include; the tip cap, germ, scutellum and endosperm, which possess different chemical compositions (Fernandez-Munoz *et al.*, 2004). The X-ray micro-CT was able to distinguish these structural components within the kernel on the basis of their differences in X-ray attenuation, with dense regions appearing brighter (Fig. 3.2). The germ appeared brigther on the 2D image of the maize kernel indicating it was more dense than the endosperm region (Fig. 3.2). Gustin *et al.* (2013) and Guelpa *et al.* (2015) were also able to distiguish the different morphological structures, in addition to density determinations, in maize kernels based on X-ray attenuation in their studies using X-ray micro-CT.

Maize kernels have both vitreous and floury endosperm in different proportions, with the vitreous endosperm contained on the periphery of the kernel (Dombrink-Kurtzman & Bietz, 1993; Landry *et al.*, 2004). In the 2D X-ray images (Fig 3.2), these two regions in the grain are distinguished based on their difference in X-ray attenuation, the vitreous endosperm appears more brighter than the floury endosperm hence it is more dense. Pores and voids are inherent to maize kernels due to the porous nature of the endosperm that influences kernel hardness (Chang, 1988). Maize kernels differ in the amount of void space within the endosperm in relation to the starch/protein ratio, so floury endosperm has less protein hence more air space than vitreous endosperm (Cardwell *et al.*, 2000). The voids in the maize kernels on day 1 were assumed to be natural and inherent to the kernels and were used for comparison with the rest of the days. There were more void space observed in the floury endosperm with time compared to the vitreous endosperm region of the kernel in both the control and the infected kernel and this could be attributed to breakdown of kernel reserves (Fig 3.4). The floury endosperm has been reported to be more susceptible to damage compared to the vitreous endosperm due to the presence of voids (Dombrink-Kurtzman & Knutson, 1997).

The mean grey value of the maize kernels in both the control and the infected kernels decreased with time, meaning that the kernels were getting less dense as there was less material to attenuate the X-rays. This can be attributed to breakdown of starch and other chemical components within the kernel. Pearson and Wicklow (2006) reported a significantly lower mean X-ray intensity in the fungal infected maize kernels compared to the undamaged kernels at 95% confidence level. This was attributed to lower density as the fungal infected kernels absorbed less X-ray energy. Neethirajan *et al.* (2007) also used mean total grey values to differentiate between healthy and sprouted wheat kernels. The sprouted wheat kernels had a significantly lower mean total grey value compared to the healthy kernel and this was attributed to the lower attenuation in the sprouted kernel due to breakdown of starch by α-amylase.

(a)

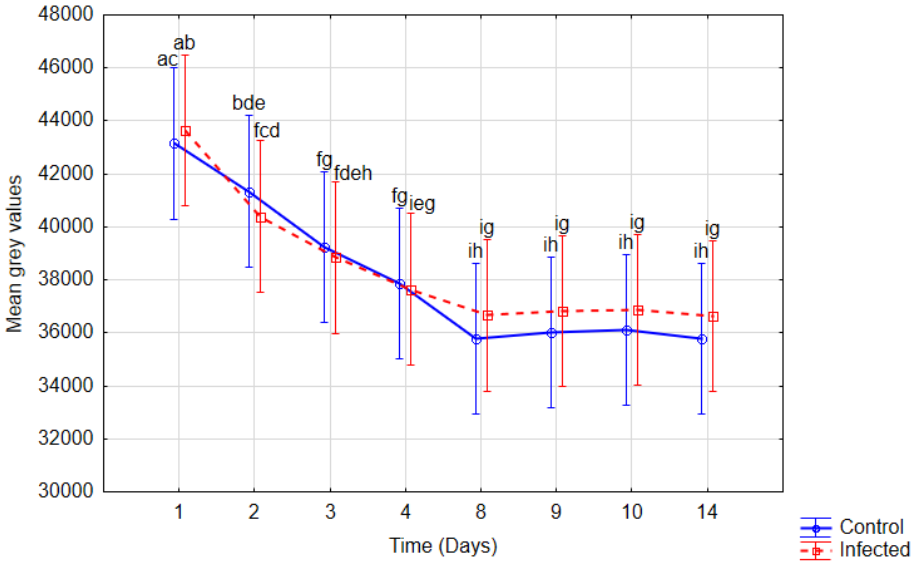

(b)

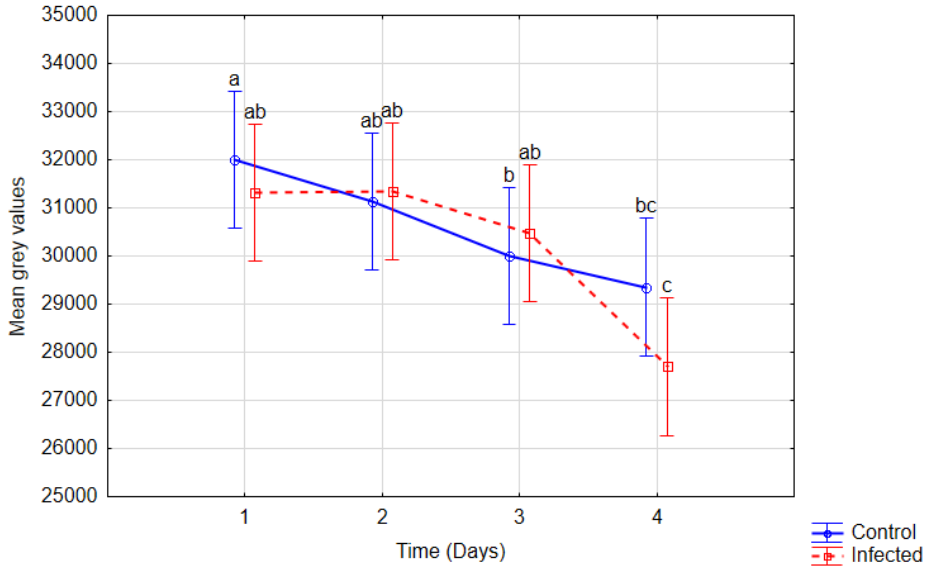

Figure 3.8. Mean grey values of the control kernels (n =3) and infected kernel (n =3) over time (days) for (a) experiment one for the 8 days scanned and (b) experiment two for the four days scanned. The letters (a-i) on the line graphs represent the statistical significant difference.

The grey level histogram is the distribution of grey levels in an image. The shape of the histogram provides information about the nature of the image and hence the object. An image with its histogram grouped at the low end of the grey value range appears darker probably due to more voids and vice versa (Thum, 1983; Umbaugh, 2010). In the grey value histogram, there was a general shift to the lower intensity grey values on day 14 in both the control and the infected kernels, this indicates that the images were getting darker (less bright) with time (Fig. 3.5).The grey value histogram on day 14 in both the control and infected kernels had more distinct peaks, indicating the

increase in intergranular voids due to the increase of low grey value intensities. The higher grey intensity level corresponds to the solid/material region within the kernel, the shift to lower intensity grey levels on day 14 can be attributed to breakdown of kernel reserves with time, thereby causing less material within the kernel and more pores, hence making the kernel less dense.

(a) (b)

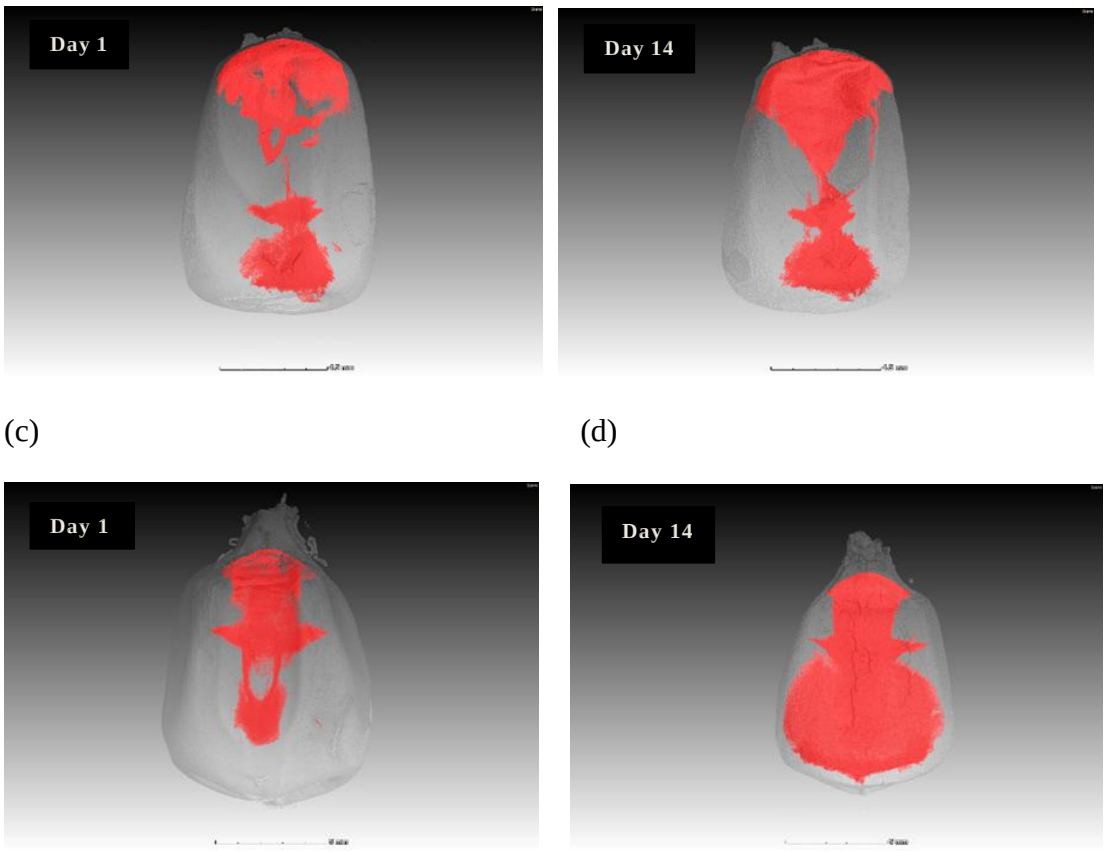

(c) (d)

Figure 3.9. 3D visualisation of the total volume of void space (red) in the control maize kernel (a) day 1 and (b) day 14; infected kernel (c) day 1 and (d) day 14 displaying the changes in intergranular void space.

Fungal growth has been reported to cause loss in kernel integrity and ultimately the decrease in density of the kernel (Hesseltine & Shotwell, 1973; Lillehoj *et al.*, 1976). As the fungi grow, they convert some of the grain reserves to heat, carbon dioxide and fungal material (Sauer, 1988). Thus, an increase in the existing pores and/or the appearance of additional pores within the kernel leading to a decrease in total volume and density due to the growing fungi is expected. However, for successful infection and dissemination of the fungus within the kernel, water activity, relative humidity and temperature are critical (Torres *et al.*, 2003). In the first experiment, both the control and infected kernels decreased in total kernel volume and increased in total volume of void space with time, and there were no significant differences between the control and the infected kernels. Therefore, it was apparent that the changes observed in the infected kernel were not solely as a result of fungal growth. Seitz *et al.* (1982) reported that respiration of both the maize itself and fungi in the

grain contribute to a loss of dry matter, however, the contribution to dry matter loss by the fungi increases at a rate dependent on moisture, temperature, amount and type of damage, and the amount and type of fungal inoculum on the grain.

(a) (b) (c)

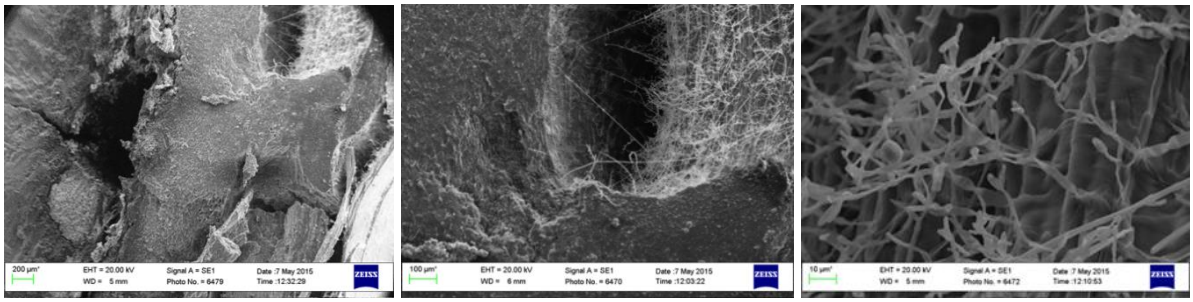

Figure 3.10. Scanning Electron micrographs (SEM) of one of the infected maize kernels on day 15 after X-ray scanning. (a) Scale bar =200 µm (b) Scale bar =100 µm (c) Scale bar = 10 µm.

Under uncontrolled storage environment, as in the case during the first experiment, most grains will take up or release moisture until they reach a dynamic equilibrium with the surrounding environment (Naresh *et al.*, 2004). Fungi utilise intergranular water vapour, the concentration of which is determined by the state of equilibrium between free water within the grain (the grain moisture content) and water in the vapour phase immediately surrounding the granular particle (Proctor, 1994). From the SEM micrographs of the infected kernel (Fig. 3.10), the *F. verticillioides* spores germinated but they were not able to cause significant changes in the internal structure due to the decrease in moisture content with time, thereby causing a decrease in the growth of the fungi. It should be noted that the kernels were also plated on PDA on day 15 post inoculation and their growth on the agar (Fig 3.11a) was evidence that the fungi were not affected by the X-ray radiations.

Previous studies on *F. verticillioides* growth on maize kernels have demonstrated that water activity (a_w) and temperature are very critical for their germination and growth. Samapundo *et al.* (2005) showed that fungal growth was hindered by low a_w and/or temperature. Similar trends were also reported by Le Bars *et al.* (1994), Cahagnier *et al.* (1995), Marin *et al.* (1995b) and Marin *et al.* (1999). Woods and Duniway (1986) found that optimum and minimum a_w values for growth of *F. verticillioides* were 0.98 and 0.87, respectively. Similarly, Marin *et al.* (1995a) demonstrated the influence of temperature and a_w on *F. verticillioides* and concluded that the minimum a_w for growth of this species was 0.89-0.90 a_w at 25-30°C.

In the second experiment, relative humidity of the storage environment was increased to approximately 90-92% to create a conducive environment for the fungus to grow in the maize kernels. There was visual evidence of fungal growth (hyphae) on the infected maize kernels on day 4 post inoculation as shown in Fig. 11b. The results from the second experiment for the four days scanned were similar to the first experiment that is the total kernel volume and mean grey value decreased

while the total volume of voids increased with no significant difference between the control and infected kernels.

(a) (b)

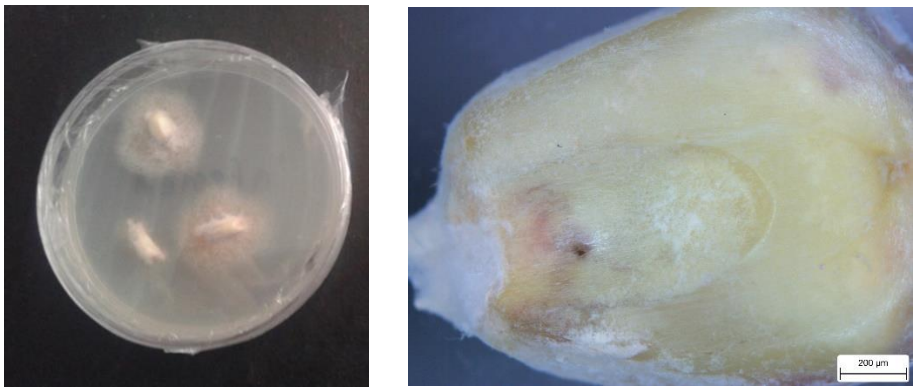

Figure 3.11. (a) Digital image of the infected maize kernels from experiment one plated on PDA agar on day 15 after X-ray scanning, visible fungal growth was evident (b) Stereomicroscope photograph of one of infected maize kernel from experiment two taken on day 4 post inoculation to reveal presence of hyphae on the surface of the maize kernel, scale bar =200 µm.

The maize kernels used in both experiments were soaked overnight (ca. 15 h) during sterilisation to facilitate the removal of internally borne microorganisms. The soaking overnight increased moisture content of the maize kernels (moisture content of the maize kernels was measured after soaking overnight using a Delmhorst G-7 Grain moisture meter (Towaco, USA) and ranged from 20-23%). Water uptake by seeds activates respiration, protein synthesis and other metabolic activities due to increased enzyme activity in the dry seeds (Helland *et al.*, 2002). One of the first changes upon imbibition is the resumption of respiration activity which can be detected within minutes (Bewley, 1997). These activities will result in disintegration of the kernel and thus lead to a decrease in volume of the maize kernel with time. Therefore, the combined activity of respiration and fungal growth was expected to result in a significantly higher reduction in total kernel volume (dry matter loss) with time in the infected kernels than in the control kernels. This was not observed in both experiments despite increasing the relative humidity in the second experiment. Seitz *et al.* (1982) and Christensen and Meronuck (1989) in their respective studies stated that contribution to dry matter loss by fungi is usually minimal at the start of storage and increases slowly and consistently depending on the storage conditions.

The X-ray 2D images showed most structural changes in the germ and scutellum regions of the maize kernels (Fig 3.3 and Fig. 3.4). The germ and the scutellum have been reported to be the regions preferred by most fungi including *F. verticillioides* (Duncan & Howard, 2010; Dolezal *et al.*, 2013). These regions (germ and scutellum) are high in nutrients especially lipids (Evers & Millar, 2002) and the fungus colonises these regions to produce hydrolytic enzymes for degrading the kernel

(Naresh *et al.*, 2004). According to Duncan and Howard (2010), depending on the point of entry, *F. verticillioides* will grow laterally in the various spaces that can be found between the "nucellar membrane". Differences in inoculation techniques would also influence the route of infection and, potentially, disease severity by altering how the fungus enters the kernel and which tissues it comes into contact with initally (Dolezal *et al.*, 2013). Koehler (1942) reported that if the fungus enters the kernels via wounds, hyphae should not be uniformly localised but randomly distributed within the kernel. Shu *et al.* (2015), observed initial colonisation of *F. verticillioides* in the aleurone and endosperm at the site of inoculation at 48 h post inoculation and at 96 h post inoculation the fungus was observed in all tissues of the kernel. They also observed extensive colonisation and degradation of tissues of the endosperm with the fungus creating cavities that often contained mycelia and conidia. The more voids observed in the germ and scutellum region of the infected kernel with time (Fig. 3.3 c and d) could be attributed to fungal activity, this agrees with Shu *et al.* (2015) who observed colonisation of *F. verticillioides* in the scutellum of kernels at 96 h post inoculation.

It should also be noted that during water uptake by the maize kernels, enzymatic synthesis and secretion into the starchy endosperm occurs first in the scutellelar epithelial cells (Young *et al.*, 1997). The germ and the scutellum which constituent the embryo are the live tissues within the maize seed and are involved in reserve mobilisation (Mayer & Poljakoff-Mayber, 1982). This region secretes enzymes which hydrolysis the kernel reserve for energy use (Thevenot *et al.*, 1992). The scutellum carbohydrate, protein and lipid reserves are used to nourish the embryo in preparation for germination (Sánchez-Linares *et al.*, 2012). This will lead to the increase in pores observed in the scutellum region with time, as seen in the control kernels (Fig. 3.4 a).

Conclusion

This study demonstrates the potential of high resolution X-ray micro-CT to investigate internal structural changes in maize kernels infected by *F. verticillioides* over time. The anatomical structures of the maize kernel were distinguished based on their differences in X-ray attenuation, with the germ and the scutellum being the dense regions within the kernel. Details of the structural alterations in the maize kernel could be visualised by the 2D and 3D images; and quantified in terms of total kernel volume, total volume of void space and mean grey value. There was a decrease of total volume and an increase in the total volume of voids of the kernel with time and this was atributed to breakdown of the maize reserves. The 2D X-ray images showed more voids in the germ and scutellum regions of the kernels with time. The mean grey value of the control and the infected kernels decreased with time meaning the kernels were becoming less dense as they were attenuating less X-rays over time. There was a general shift to the lower intensity range of the grey value in the whole kernel grey value

histograms of both the control and the infected kernel with time. This suggests the kernel was getting less bright with an increase in voids/pores and was due to degradation of the kernel.

There was no significant difference($P > 0.05$) in total kernel volume, mean grey value and total volume of void space between the control and the infected maize kernels in both experiments, this could be due to slow fungal activity at the start of infection. Further studies should be carried out using image texture analyis to aid in discrimination of the control and infected kernels.

References

Bewley, J.D. (1997). Seed germination and dormancy. *The Plant Cell*, **9**, 1055-1066.

Cahagnier, B., Melcion, D. & Richard-Molard, D. (1995). Growth of *Fusarium moniliforme* and its biosynthesis of fumonisin B1 on maize grain as a function of different water activities. *Letters in Applied Microbiology*, **20**, 247-251.

Cardwell, K.F., Kling, J.G., Maziya-Dixon, B. & Bosque-Perez (2000). Interaction between *Fusarium verticillioides*, *Aspergillus flavus* and insect infestation in four maize genotype in lowland Africa. *Phytopathology*, **90**, 276-284.

Chang, C. (1988). Measuring density and porosity of grain kernels using a gas pycnometer. *Cereal Chemistry*, **65**, 13-15**.**

Christensen, C.M. & Meronick, R.A. (1989). Dry matter loss in yellow dent corn resulting from invasion by storage fungi. *Plant Disease*, **73**, 501-503.

Cleveland, T., Hussey, D., Chen, Z.-Y., Jacobson, D., Brown, R., Carter-Wientjes, C. & Arif, M. (2008). The use of neutron tomography for the structural analysis of corn kernels. *Journal of Cereal Science*, **48**, 517-525.

Cnudde, V., Massachaele, B., Dierick, M., Vlassenbroeck, J., Van Hoorebeke, L. & Jacobs, P. (2006). Recent progress in X-ray CT as a geosciences tool. *Applied Geochemistry*, **21**, 826-832.

Dolezal, A.L., Obrian, G.R., Nielsen, D.M., Woloshuk, C.P., Boston, R.S. & Payne, G.A. (2013). Localization, morphology and transcriptional profile of *Aspergillus flavus* during seed colonization. *Molecular Plant Pathology*, **14**, 898-909.

Dombrink-Kurtzman, M. & Bietz, J. (1993). Zein composition in hard and soft endosperm of maize. *Cereal Chemistry*, **70**, 105-108.

Dombrink-Kurtzman, M. & Knutson, C. (1997). A study of maize endosperm hardness in relation to amylose content and susceptibility to damage. *Cereal Chemistry*, **74**, 776-780.

Du Plessis, A., Le Roux, S.G. & Guelpa, A. (2016). The CT scanner facility at Stellenbosch University: An open access X-ray computed tomography laboratory. *Nuclear Instruments and Methods in Physics Research Section B: Beam Interactions with Materials and Atoms*, **384**, 42-49.

Duncan, E.K. & Howard, J.R. (2010). Biology of maize kernel infection by *Fusarium verticillioides*. *The American Phytopathology Society*, **23**, 6-16.

Evers, T. & Millar, S. (2002). Cereal grain structure and development: Some implications for quality. *Journal of Cereal Science*, **36**, 261-284.

Fernandez-Munoz, J.L., Rojas-Molina, I., Gonzalez-Davalos, M.L., Leal, M., Valtierra, M.E., San Martin-Martinez, E. & Rodriguez, M.E. (2004). Study of calcium ion diffusion in components of maize kernels during traditional nixtamalization process. *Cereal Chemistry*, **81**, 65-69.

Frisullo, P., Barnabà, M., Navarini, L. & Del Nobile, M.A. (2012). Coffea arabica beans microstructural changes induced by roasting: An X-ray microtomographic investigation. *Journal of Food Engineering*, **108**, 232-237.

Guelpa, A., Plessis, A.D., Kidd, M. & Manley, M. (2015). Non-destructive estimation of maize kernel hardness by means of an X-ray micro-computed tomography density calibration. *Food Bioprocess Technology*, **8**, 1419-1429.

Gustin, J.L., Jackson, S., Williams, C., Patel, A., Armstrong, P., Peter, G.F. & Settles, A.M. (2013). Analysis of maize (*Zea mays*) kernel density and volume using microcomputed tomography and single-kernel near-infrared spectroscopy. *Journal of Agricultural and Food Chemistry*, **61**, 10872-10880.

Helland, M.H., Wicklund, T. & Narvhus, J.A. (2002). Effect of germination time on alpha-amylase production and viscosity of maize porridge. *Food Research International*, **35**, 315-321.

Herremans, E., Verboven, P., Bongaers, E., Estrade, P., Verlinden, B.E., Wevers, M., Hertog, M.L.A.T.M. & Nicolai, B.M. (2013). Characterisation of 'braeburn' browning disorder by means of X-ray micro-CT. *Postharvest Biology and Technology*, **75**, 114-124.

Hesseltine, C.W. & Shotwell, O. (1973). New methods for rapid detection of aflatoxins. *Pure and Applied Chemistry*, **35**, 259-266.

Kelkar, S., Boushey, C.J. & Okos, M. (2015). A method to determine the density of foods using X-ray imaging. *Journal of Food Engineering*, **159**, 36-41.

Kerckhofs, G., Schrooten, J., Van Cleynenbreugel, T., Lomov, S.V. & Wevers, M. (2008). Validation of X-ray microfocus computed tomography as an imaging tool for porous structures. *Review of Scientific Instruments*, **79**, 013711.

Koehler, B. (1942). Natural mode of entrance of fungi into corn ears and some symptoms that indicate infection. *Journal of Agricultural Research*, **64**, 421-442.

Landis, E.N. & Keane, D.T. (2010). X-ray microtomography. *Materials Characterization*, **61**, 1305-1316.

Landry, J., Delhaye, S. & Damerval, C. (2004). Protein distribution pattern in floury and vitreous endosperm of maize grain. *Cereal Chemistry*, **81**, 153-158.

Le Bars, L., Le Bars, P., Dupuy, J., Boudra, H & Casini, R. (1994). Biotic and abiotcs factors in fumonisin B1 production and stability. *Journal of Association of Official Analytical Chemists International*, **77**, 517-521.

Lillehoj, E., Kwolek, W., Peterson, R., Shotwell, O., H & Hesseltine, C. (1976). Aflatoxin contamination, flourescence, and insect damage in corn infected with *Aspergillus flavus* before harvest. *Cereal Chemistry*, **53**, 505-512.

Lillehoj, E.B. (1987). The aflatoxin in maize problem: The historical persepective. US University CIMMYT maize aflatoxin workshop, pp. 13-33. El Batan, Mexico.

Marín, S., Magan, N., Ramos, A.J. & Sanchis, V. (2004). Fumonisin-producing strains of *Fusarium*: A review of their ecophysiology. *Journal of Food Protection*, **67**, 1792-1805.

Marin, S., Magan, N., Sena, J., Ramos, A.J., Canela, R. & Sanchis, V. (1999). Fumonisin B1 production and growth of *Fusarium moniliforme* and *Fusarium proliferatum* on maize,wheat and barley grain. *Journal of Food Science*, **64**, 921-924.

Marin, S., Sanchis, V. & Magan, N. (1995a). Water activity, temperature and pH effects on growth of *Fusarium moniliforme* and *F. proliferatum* isolates from maize. *Canadian Journal of Microbiology*, **41**, 1063-1070.

Marin, S., Sanchis, V., Vinas, I., Canela, R. & Magan, N. (1995b). Effect of water activity and temperature on growth and fumonisin B1 and B2 production by *Fusarium proliferatum* and *F. moniliforme* on maize grain. *Letter in Applied Microbiology*, **21**, 298-301.

Mayer, A.M. & Poljakoff-Mayber, A. (1982). The germination of seeds. Pergamon International Library of Science, Technology, Engineering and Social Studies, Elsevier.

Mendoza, F., Verboven, P., Mebastsion, H.K., Kerckhofs, G., Wevers, M. & Nicolai, B.M. (2007). Three dimensional pore space quantification of apple tissue using X-ray computed microtomography *Planta*, **226**, 559-570.

Munkvold, G.P. (2003). Cultural and genetic approaches to managing mycotoxins in maize. *Annual Review of Phytopathology*, **41**, 99-116.

Munkvold, G.P. & Desjardins, A. (1997). Fumoninins in maize. Can we reduce their occurence? *Plant Disease*, **81**, 556-564.

Naresh, M., David, A. & Sanchis, V. (2004). The role of spoilage fungi in seed deterioration. In: Fungal biotechnology in agricultural, food and environmental application. pp. 311-322. Marcel Dekker, New York City.

Narvankar, D.S., Singh, D.S. & White, N.D.G. (2009). Assessment of soft X-ray imaging for detection of fungal infection in wheat. *Biosystems Engineering- Postharvest Technology*, **81**, 49-56.

Neethirajan, S., Jayas, D.S. & White, N.D.G. (2007). Detection of sprouted wheat kernels using soft X-ray image analysis. *Journal of Food Engineering,* **81**, 509-513.

Pearson, T. & Wicklow, D. (2006). Detection of corn kernels infected by fungi. *Transactions of the ASABE,* **49**, 1235-1245.

Pomeranz, Y. (1982). Biochemical, functional and nutritional changes during storage. Storage of cereal grains and their products. 3rd edn. pp. 145-217. St Paul, MN.

Proctor, D.L. (1994). Grain storage techniques: Evolution and trends in developing countries. Food agricultural organisation agricultural services bulletin 109, United Nations, Rome.

Samapundo, S., Dev Lieghene, F., De Meulenaer, B., Geeraerd, A.H., Van Impe, J.F. & Debevere, J.M. (2005). Predictive modelling of individual and combined effect of water activity and temperature on the radical growth of *Fusarium verticillioides* and *Fusarium proliferatum* on corn. *International Journal of Food Microbilogy,* **105**, 35-52.

Sánchez-Linares, L., Gavilanes-Ruíz, M., Díaz-Pontones, D., Guzmán-Chávez, F., Calzada-Alejo, V., Zurita-Villegas, V., Luna-Loaiza, V., Moreno-Sánchez, R., Bernal-Lugo, I. & Sánchez-Nieto, S. (2012). Early carbon mobilization and radicle protrusion in maize germination. *Journal of Experimental Botany,* **63,** 4513-4526.

Sauer, B.D. (1988). Effects of fungal deterioration on grain: Nutritional value, toxicity, germination. *International Journal of Food Microbiology,* **7**, 267-275.

Schoeman, L., Du Plessis, A. & Manley, M. (2016a). Non-destructive characterisation and quantification of the effect of conventional oven and forced convection continuous tumble (FCCT) roasting on the three-dimensional microstructure of whole wheat kernels using X-ray micro-computed tomography (µCT). *Journal of Food Engineering,* **187**, 1-13.

Schoeman, L., Williams, P., Du Plessis, A. & Manley, M. (2016b). X-ray micro-computed tomography (µCT) for non-destructive characterisation of food microstructure. *Trends in Food Science & Technology,* **47**, 10-24.

Seitz, L., Sauer, D., Mohr, H. & Aldis, D. (1982). Fungal growth and dry matter loss during bin storage of high-moisture corn. *Cereal Chemistry,* **59**, 9-14.

Shu, X., Livingston III, P.D., Franks, G.R., Boston, S.R., Woloshuk, P.C. & Payne, A.G. (2015). Tissue-specific gene expression in maize seeds during colonisation by *Aspergilus flavus* and *Fusarium verticilliodes*. *Molecular Plant Pathology,* **16**, 662-674.

Singhal, A., Grande, J.C. & Zhou, Y. (2013). Micro/nano CT for visualisation of interal structures. *Microscopy Today,* **21**, 16-22.

Sinka, I.C., Burch, S.F., Tweed, J.H. & Cunningham, J.C. (2004). Measurement of density variations in tablets using X-ray computed tomography. *International Journal of Pharmaceutics,* **271**, 215-224.

Strobl, M., Manke, I., Kardjilov, N., Hilger, A., Dawson, M. & Banhart, J. (2009). Advances in neutron radiography and tomography. *Journal of Physics D: Applied Physics*, **42**, 243001.

Suresh, A. & Neethirajan, S. (2015). Real-time 3D visualisation and quantitative analysis of internal structure of wheat kernels. *Journal of Cereal Science*, **63**, 81-87.

Thevenot, C., Lauriere, C., Mayer, C., Simond-Cote, E. & Daussant, J. (1992). α-amylase changes during development and germination of maize kernels. *Journal of Plant Physiology*, **140**, 61-65.

Thum, C. (1983). Hybrid measurements of image histograms, with an application to texture discrimination. *Journal of Modern Optics*, **30**, 1665-1673.

Torres, M., Ramos, A., Soler, J., Sanchis, V. & Marın, S. (2003). SEM study of water activity and temperature effects on the initial growth of *Aspergillus ochraceus*, *Alternaria alternata* and *Fusarium verticillioides* on maize grain. *International Journal of Food Microbiology*, **81**, 185-193.

Trater, A.M., Alavi, S. & Rizvi, S.S.H. (2005). Use of non-invasive X-ray microtomography for characterizing microstructure of extruded biopolymer foams. *Food Research International*, **38**, 709-719.

Umbaugh, S.E. (2010). Digital image processing and analysis: Human and computer vision applications with CVIP tools. CRC press, Boca, Raton, pp 456-463.

Van Dyck, T., Verboven, P., Herremans, E., Defraeye, T., Van Campenhout, L., Wevers, M., Claes, J. & Nicolaï, B. (2014). Characterisation of structural patterns in bread as evaluated by X-ray computer tomography. *Journal of Food Engineering*, **123**, 67-77.

Van Geet, M., Swennen, R. & Wevers, M. (2000). Quantitative analysis of reservoir rocks by microfocus X-ray computerised tomography. *Sedimentary Geology*, **132**, 25-36.

Winston, P.W. & Bates, D.H. (1960). Saturated solutions for the control of humidity in biological research. *Ecology*, **41**, 232-237.

Woods, D. & Duniway, J. (1986). Some effects of water potential on growth, turgor, and respiration of *phytophthora cryptgea* and *Fusarium moniliforme*. *Phytopathology*, **76**, 1248-1254.

Young, T.E., Juvik, J.A. & Demason, D.A. (1997). Changes in carbohydrate composition and α-amylase expression during germination and seedling growth of starch-deficient endosperm mutants of maize. *Plant Science*, **129**, 175-189.

Zhu, L.-J., Hulya, D., Gajula, H., Gu, M.-H., Qiao-Quan, L. & Yong-Cheng, S. (2012). Study of kernel structure of high-amylose and wild-type rice by X-ray microtomography and SEM. *Journal of Cereal Science*, **51**, 1-5.

Declaration by student

With regard to Chapter 4 (pp 79 - 104) the nature and scope of my contribution were as follows:

Nature of contribution	Extent of contribution (%)
Research, analysis and writing of chapter	65%

The following co-authors have contributed to Chapter 4:

Name	e-mail address	Nature of contribution	Extent of contribution (%)
Dr Paul J. Williams	pauljw@sun.ac.za	Research inputs, image texture analysis, editorial suggestions and proofreading	20%
Prof Marena Manley	mman@sun.ac.za	Research inputs, editorial suggestions and proof reading	10%
Prof Sergey Kucheryaskiy	svk@bio.aau.dk	Writing image texture analysis codes in Matlab, proof reading	5%

Signature of student: I. Orina

Date: 13/12/2017

The undersigned hereby confirm that:

1. the declaration above accurately reflects the nature and extent of the contributions of the candidate and the co-authors to Chapter 4 (pp 79 - 104),
2. no other authors contributed to Chapter 4 (pp 79 -104) besides those specified above, and
3. potential conflicts of interest have been revealed to all interested parties and that the necessary arrangements have been made to use the material in Chapter 4 (pp 79 -104) of this dissertation.

Signature	Institutional affiliation	Date
Dr Paul J. Williams	Department of Food Science, Stellenbosch University	13/12/2017
Prof Marena Manley	Department of Food Science, Stellenbosch University	13/12/2017
Prof Sergey Kucheryaskiy	Department of Chemistry and Bioscience, Aalborg University, Esbjerg, Denmark	13/12/2017

Chapter 4

Application of image texture analysis for evaluation of X-ray images of fungal infected maize kernels*

Abstract

The feasibility of image texture analysis to evaluate X-ray images of fungal infected maize kernels was investigated. X-ray images of maize kernels infected with *Fusarium verticillioides* and control kernels were acquired using high-resolution X-ray micro-computed tomography daily for a period of four days after inoculation. After image acquisition and pre-processing, several algorithms were developed to extract image textural features from selected two-dimensional (2D) images of the kernels. Four first order statistics (mean, standard deviation, kurtosis and skewness) and four grey level co-occurrence matrix (GLCM) features (correlation, energy, homogeneity and contrast) were extracted from the side, front and top views of each kernel, and used as inputs for principal component analysis (PCA). No clear grouping was observed between the infected and control kernels, this was attributed to similar changes in the kernels internal structure, however there was separation in the days of the individual kernels. The top view gave better results compared to the side and front view. GLCM features were used to develop a classification model using partial least squares discriminant analysis (PLS-DA). Classification accuracies of 75% for the control and 41.67% for infected kernels were achieved. This work provides information on the possible application of image texture analysis to aid is discrimination of fungal infected maize kernels from uninfected kernels.

Key words: Image texture analysis; fungal invasion; X-ray micro-computed tomography; maize; grey level co-occurrence matrix.

---

*Submitted for publication as: Irene Orina, Marena Manley, Sergey Kucheryaskiy & Paul J. Williams, (2017). Application of image texture analysis for evaluation of X-ray images of fungal infected maize kernels. *Food Analytical Methods.*

Introduction

Image texture analysis has become a relevant tool in the field of food science for quality evaluation of agricultural and food products, particularly in grading and inspection. This is due to advancements in computer vision systems and image processing techniques that allow characterisation of foods from their images (Brosnan & Sun, 2004; Zheng *et al.*, 2006b). Images are acquired using an image sensor, and then dedicated computing hardware and software are used to analyse the images with the aim of finding association between different image features and characteristics of the investigated food product (Du & Sun, 2004). Image texture analysis, therefore, involves extracting meaningful information from the images which results in quantitative measurements useful for characterising the food product (Gunasekaran, 1996).

The meaning of the term texture in image analysis is completely different from the usual meaning of texture in foods. Food texture refers to the manner in which the human mouth/senses responses to food, and is described by properties such as hardness, elasticity, chewiness, viscosity and gumminess (Bourne, 2002). On the other hand, image texture can be defined as the spatial organisation of intensity of pixels on digitised images (Prats-Montalbán *et al.*, 2011). Pixels are the basic components of images and each pixel is usually represented by one (for monochrome) or several (for colour images) intensities (Zheng *et al.*, 2006a). Several techniques are available for calculating image texture properties such as statistical texture, structural texture, model-based texture and transform-based texture (Bharati *et al.*, 2004). In food applications, statistical texture is the most widely used method for quality evaluation (Zheng *et al.*, 2006a). The statistical approach tries to characterise the texture of an image region using statistical measures. This includes first and second order statistics. First order statistics are based on statistical properties of the pixel intensity distribution histogram of an image region and do not provide any information about the relative position of pixels and the correlation of their intensities. Examples include mean, variance, skewness and kurtosis (Prats-Montalbán *et al.*, 2011; Patel *et al.*, 2012). Second order statistics, on the other hand, are based on spatial arrangement and interrelation of grey levels of the pixels in a region of an image (Bharati *et al.*, 2004). The most commonly used second order statistics in image texture analysis is that related to grey level co-occurrence matrix (GLCM) (Haralick & Shanmugam, 1973).

Image texture analysis has been applied in food quality evaluation (Zheng *et al.*, 2006a). For example, in characterisation of bread breakdown during mastication (Tournier *et al.*, 2012), classification of bovine meat (Basset *et al.*, 2000), classification of commercial potato chips (Mendoza & Aguilera, 2004), to study dehydration of apple discs (Fernandez *et al.*, 2005), to evaluate image texture features as indicators of beef tenderness (Li *et al.*, 1999), to discriminate crumb grain visual appearance of organic and non-organic bread loaves (Gonzales-Barron & Butler, 2008) and

classification and dockage identification of cereal grains (Majumdar & Jayas, 2000; Paliwal *et al.*, 2003).

X-ray micro-computed tomography (X-ray micro-CT) is a powerful technique for visualisation and characterisation of the internal microstructure of food products at high resolution (Suresh & Neethirajan, 2015). X-ray micro-CT offers unique insights, either by its ability to reveal internal structure of an object in a non-destructive way, thereby allowing one to monitor structural changes over time, or due to its three dimensional (3D) imaging capability which enables viewing of the object from different angles (Cnudde & Boone, 2013). X-ray micro-CT is based on the differences in X-ray attenuation that arises mainly from differences in density within a sample (Cnudde & Boone, 2013). During image acquisition the sample is mounted on a rotary stage and illuminated with X-rays. The X-rays pass through the sample in different directions and along different pathways to yield an image that reflects variation in density at numerous points in a two dimensional (2D) slice (Lim & Barigou, 2004). The difference in X-ray attenuation creates a contrast in the X-ray images to distinguish various components within a sample. High density regions correspond to areas of high attenuation and will appear brighter on the 2D cross-sectional image and vice versa (Schoeman *et al.*, 2016b). A series of 2D projections are obtained at fixed angular increments as the sample is rotated either at 180º or 360º. The numerous 2D projections, covering the entire sample, are then rendered/reconstructed into a 3D volume (Baker *et al.*, 2012). The resultant 3D-rendered volume can be presented as a whole or as virtual slices of the sample at different depths and in different directions (Schoeman *et al.*, 2016b).

Image analysis in X-ray micro-CT involves extraction of qualitative and quantitative information from the 2D images and 3D volume to characterise the microstructure of the product. This technique has found wide application in the field of food science as recently reviewed by Schoeman *et al.* (2016b). In cereal grains, X-ray micro-CT has been used to determine volume and density of maize kernels (Gustin *et al.*, 2013; Guelpa *et al.*, 2015; Guelpa *et al.*, 2016), 3D visualisation and quantification of the internal structure of single wheat kernels damaged by sprouting and insect infestation (Suresh & Neethirajan, 2015), characterisation of rice strains by differences in pore size and distribution (Zhu *et al.*, 2012), the effect of heat treatment on rice kernel structure (Mohoric *et al.*, 2009) and effect of roasting on the 3D microstructure of whole wheat and maize kernels (Schoeman *et al.*, 2016a; Schoeman *et al.*, 2017).

To date, limited studies have applied image texture analysis to characterise X-ray micro-CT images. It has found application in the characterisation of images obtained from traditional X-ray imaging, where only one projection image (X-ray transmission through a sample) is acquired per object of interest. Pearson and Wicklow (2006) used traditional X-ray imaging to detect fungal

infection in maize kernels. A maximum of three image features i.e. mean, standard deviation and maximum pixel intensity were selected and used for classification of the kernels using stepwise discriminant analysis. Classification accuracies of 100% and 82%, for undamaged and fungal infected kernels respectively, were achieved. In another study, X-ray imaging was used for the detection of fungal infection in wheat kernels (Narvankar *et al.*, 2009). Single images of fungal infected and healthy kernels were acquired then analysed. A total of 34 image features (maximum, minimum, mean, median, variance, standard deviation, and 28 grey-level co-occurrence matrix (GLCM) features) were extracted from the images and given as input to statistical discriminant classifiers (linear, quadratic and Mahalanobis) and back-propagation neural network (BPNN) classifier. They reported better classification accuracies with lower false positives with the statistical classifiers than with the BPNN classifier (Narvankar *et al.*, 2009).

Recently, Orina *et al.* (2017) used X-ray micro-CT to monitor internal structural changes in maize kernels infected with *Fusarium verticillioides*. They observed more voids especially in the germ and floury endosperm regions of the kernel over time. Quantitative measurements including total kernel volume, mean grey value and total volume of voids were calculated from the rendered 3D volumes of the kernels. Total kernel volume and mean grey volume decreased while total volume of voids increased in both the control and infected kernels over time. No significant difference was reported between the control and infected kernels.

The aim of this study was to evaluate the potential of image textural features extracted from 2D X-ray images coupled with multivariate statistical analysis to discriminate maize kernels infected with *F. verticillioides* from uninfected kernels.

Materials and methods

Maize kernel preparation

Sample preparation was done as described by Orina *et al.* (2017). A batch of 50 maize kernels (I16, a South African variety) kindly supplied by the Department of Plant Pathology, (Stellenbosch University, South Africa), were initially soaked overnight (*ca.* 15 h) in sterile distilled water. The kernels were then surface sterilised by rinsing in 70% ethanol. Thereafter, surface sterilised kernels were imbibed in a water bath at 60° C for 5 min, immediately placed in ice for 1 min, then left to dry in a laminar flow hood for 1 h. The kernels were considered sterile and ready for inoculation.

Spore suspension was prepared by first plating *Fusarium verticillioides* (MRC 0826) culture (kindly supplied by the Department of Plant Pathology, Stellenbosch University) onto potato dextrose agar (PDA) and incubating at 25°C. After 4 days, sterile water with Tween 20 (3 drops. L^{-1}) was used

to wash spores from the agar surface. The spore suspension was poured through sterile cheesecloth to remove mycelium, thereafter the suspension was adjusted to 1×10^6 conidia.ml^{-1} using a haemocytometer.

The six kernels (3 controls and 3 infected) were randomly selected from the sterilised maize samples. Three of the kernels were dipped into the spore suspension for 1 min (infected) and the other three were dipped into sterile distilled water for 1 min (control). Each kernel was placed into a 5-mL pipette tip (this was for holding the kernel during scanning) with sterilised cotton wool on both ends to avoid contamination. The six kernels were then placed in an airtight container (25 cm × 25 cm × 14.5 cm) which contained saturated solution of potassium nitrate (KNO_3) in a beaker for creating a high relative humidity of above 90% to facilitate growth of the fungus. They were then incubated at 28ºC for four days.

X-ray micro-CT image acquisition

The control and infected kernels were individually scanned daily for four days (Day 1 to 4) using similar instrument conditons X-ray scanning was done using a General Electric Phoenix nanotom S (General Electric Sensing & Inspection Technologies. GmbH, Phoenix, Wunstorf, Germany), at the Stellenbosch University CT Scanner Facility, equipped with a 180 kV nano-focus tube. The scans were obtained using the scanning parameters described by Orina *et al.* (2017). A Power setting of 50 kV and 250 µA was used. The instrument was equipped with a 0.1 mm copper filter which suppresses low energy X-rays from the source, hence reducing beam hardening artefacts. Individual maize kernels, each in a 5-mL pipette tip, was placed on a specimen stage at a physical distance of 35 mm from the X-ray radiation source and 200 mm from the detector resulting in a scanning resolution of 8.75 µm. The cotton wool on both ends of the pipette tip were not in the field of view. Figure 4.1 illustrates the basic setup for X-ray micro-CT.

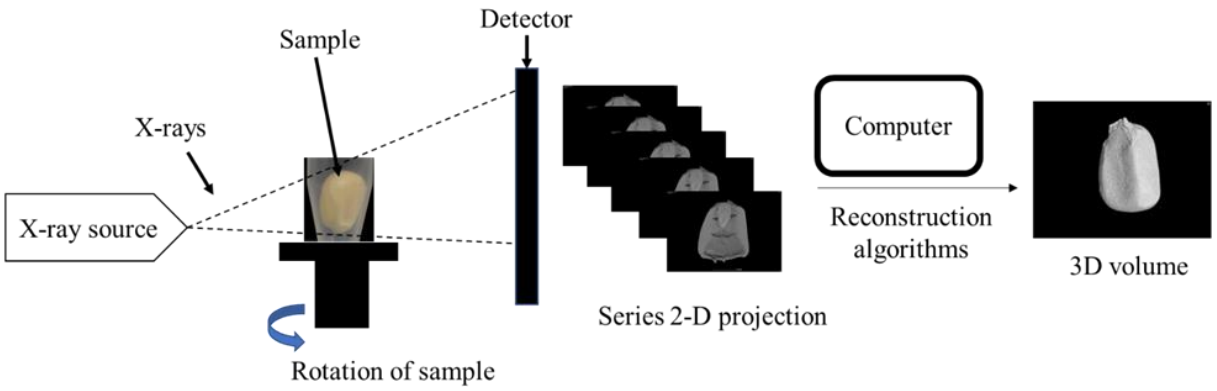

Figure 4.1. Schematic illustration of the sample and X-ray micro-computed tomography setup. The series of 2D images acquired of the sample were rendered into a 3D volume.

The maize kernels were rotated 360º with each kernel scan (3 controls and 3 infected) taking approximately 1 h to complete. Image acquisition was set at 0.5 s per image with 2000 images recorded in one rotation of the sample along the axis, perpendicular to the beam direction. The 2D image radiographs, covering the entire sample were acquired using a fully automated data acquisition system and saved onto a processing workstation, operated by system-supplied reconstruction software (Dato|x ® 2.1 General Electric Sensing and Inspection Technologies GmbH Phoenix, Wunstorf, Germany). The multiple 2D projection images of each kernel were reconstructed to create a 3D volume using the integrated Phoenix datos|x 3D computed tomography acquisition and reconstruction software (General Electric Sensing & Inspection Technologies. GmbH, Phoenix, Wunstorf, Germany). The instrument was standardised using 16-bit data, which resulted in grey values between 0 and 65,535 (2^{16} for 16-bit data). To improve the quality of the images a beam hardening correction of 2 units was applied.

Image processing

Image processing was performed as described by Orina *et al.* (2017). The raw 3D volumes of the maize kernels were analysed further using Volume Graphic Studio Max 2.2 software (VGStudio Max 2.2, Heidelberg, Germany) by first removing the plastic pipette tip and the surrounding air (background). This was done by selecting the region of interest (ROI) belonging to the pipette tip and surrounding air using appropriate tolerances ranging from 800 to 2500 in the Region growing tool function. The ROI was then inverted and extracted. The image registration technique in the VGStudio software was used to align the data sets representing volumes of each kernel on the four days scanned into the same coordinate system. This was done to ensure all images of an individual kernel for the four days scanned were the same size and similar regions within the kernels were chosen. It is important to mention that the resultant 3D rendered volume allowed for multidirectional examination of each kernel, i.e. from the top, side and front views. One hundred images from each kernel, from each of the three views were manually selected from the centre of the kernels to include regions mostly comprising of the germ and endosperms for image texture analysis.

Image feature extraction

First-order statistical features

First-order features are based on statistical properties of the intensity distribution histogram of an image. They consider the intensity of individual pixels independent of their neighbouring pixels (Patel *et al.*, 2012). A feature extraction algorithm was implemented in MATLAB (R2017a) to separate the kernel image from the background. Calculation of mean, standard deviation, kurtosis and skewness of 100 X-ray images selected in the different orientation (i.e. top, side and front view) for

each kernel (3 controls and 3 infected) for the four days was then done. That is 6 kernels × 4 days × 3 views × 100 images × 4 statistics. These outputs were used as inputs to calculate principal component analysis (PCA).

Texture analysis using grey level co-occurrence matrices

The most commonly used statistical texture analysis method is the grey level co-occurrence matrix (GLCM) (Zheng *et al.*, 2006a). The GLCM of an image is a square matrix whose elements correspond to the relative frequency of occurrence $P(i,j)$ of two pixels (one with intensity of i and other with intensity j), separated by a certain distance d in a given direction Θ (Fernandez *et al.*, 2005). Several features can be derived from GLCM. Haralick and Shanmugam (1973) proposed 14, however, only the four most commonly used features were computed in this study, i.e. contrast, correlation, energy and homogeneity. More detailed information on matrix computation and textural feature definitions are given by Haralick and Shanmugam (1973) and Zheng *et al.* (2006a). Equations for the four textural features used in this study are given in Table 4.1.

Table 4.1. Textural features extracted from GLCM

Texture features	Equation
Contrast	$f_1 = \sum_{n=1}^{n_g-1} n^2 \left[\sum_{i=1}^{n_g}\sum_{j=1}^{n_g} P(i,j)\right] \lvert i-j\rvert = n$
Energy (angular second moment)	$f_2 = \sum_i \sum_j \{P(i,j)\}^2$
Correlation	$f_3 = \frac{\sum_i \sum_j (i,j)\, P(i,j) - \mu_i\, \mu_j}{\sigma_i \sigma_j}$
Homogeneity (inverse difference moment)	$f_4 = \sum_{i,j} \frac{P(i,j)}{1+\lvert i-j\rvert}$

Where: i, j: neighbouring grey level values; P (i, j): i, jth entry in the normalized GLCM; μ mean; σ: standard deviation (Haralick & Shanmugam, 1973).

For the GLCM, an area of approximately 957×666 pixels in the front view and 644×612 pixels in the top view were cropped automatically from the centre of each kernel (this is the region where changes were observed) using algorithms developed in MATLAB (R2017a) (Fig. 4.2). The four textural features (contrast, correlation, energy and homogeneity) were then calculated from the GLCM matrix for directions Θ = 0º, 45º, 90º and 135º and distance of 1. Thus, a set of four values (one per angle) for each textural feature was obtained, these four values were averaged and used as input to calculate PCA. Based on the results obtained from the first order statistics, only day one and day four of the top and front view of the control and infected kernels were analysed in the PCA (6 kernels × 2 views × 2 days × 100 images × 4 textural features).

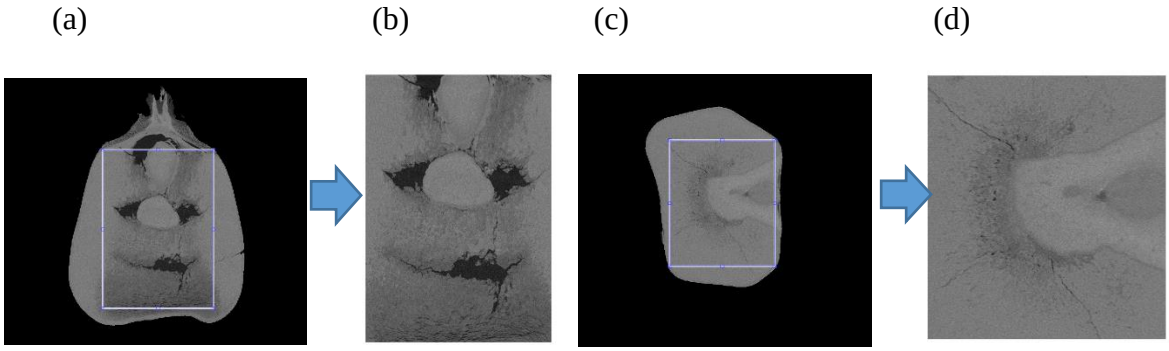

Figure 4.2. Illustration of the cropped region from the centre of the kernel in the (a) front view and (c) top view. The cropped regions (b) and (d) were used in calculation of the GLCM matrix.

Principal component analysis (PCA)

PCA is an unsupervised multivariate pattern recognition method (Abdi & Williams, 2010). With PCA, the original measured variables are transformed to a set of new latent variables called principal components (PCs) (Wold *et al.*, 1987). Each component of a PCA model is characterised by two complimentary sets of attributes; one is the loading of the PC which defines the direction of greatest variability; and the other is the score value which represents the projection of each object onto PCs (i.e. the properties, difference or similarities of the samples) (Liu *et al.*, 2006; Li *et al.*, 2007). The PCs are linear combinations of the original variables, with the first PC lying along the direction of maximum variance in the data set. The second PC is orthogonal to the first one and explains the second greatest variance. All other PCs calculated, represent successively smaller variance along the higher-order component direction (Esbensen *et al.*, 2002). PCA was performed on the data set using the PLS_Toolbox from Eigenvector Research in MATLAB (R2017a).

Classification model development

Partial least square discriminant analysis (PLS-DA) was used to develop a model for distinguishing between infected and control kernels. Only the GLCM textural features were used for development of the classification model. PLS-DA is a supervised classification technique that is based on partial least square regression (PLSR) approach, for the optimum separation of classes by encoding dependant variables of PLSR with dummy variables describing the classes (Brereton & Lloyd, 2014). Therefore, the aim of PLS-DA is to find a straight line that divides the samples into two groups, and thus decide which of the two groups a sample is most likely to belong to from a set of analytical measurements (Brereton & Lloyd, 2014). MATLAB (R2017a) was used for calibrating the PLS-DA model. Pre-processing was set at autoscale and venetian blinds was used for cross-validation in building the PLS-DA model.

Classification accuracy was calculated using the following equation:

$$\%\ Classification\ accuracy = \frac{number\ of\ positive\ classified\ images\ per\ class}{total\ number\ of\ images\ per\ class} \times 100$$

Results and discussion

Visual assessment

Digital images of the maize kernels taken on day 4 post inoculation are shown in Fig. 4.3. Control kernels showed no signs of infection (Fig. 4.3a) while infected maize kernels (Fig. 4.3b) were covered with white/pinkish hyphae, which are a typical symptom of infection by *F. verticillioides* (Afolabi *et al.*, 2007). A successful fungal spore germination will result in the formation of extending hyphae that are able to colonise the kernel (Naresh *et al.*, 2004). There was variation in the degree of infection of the individual kernels (Fig. 4.3b), with infected kernel 3 being severely damaged by the fungus. This was expected because maize kernels are biological materials and they react differently to infection.

(a)

(b)

Figure 4.3. Digital images of (a) the three control kernels and (b) the three infected kernels taken on day 4 post inoculation.

Qualitative image analysis

The X-ray micro-CT enabled visualisation of the internal structure of the maize kernels for the four days scanned. Due to the non-destructive nature of the technique, it was possible to scan the same kernel repeatedly, thereby monitoring the changes in the internal structure of the kernels over time. The differences in grey level intensities (image contrast) on the 2D cross-sectional images correspond to density variations within the kernel (Fig. 4.4). The contrast in these images is a result of the difference in X-ray attenuation by the voids and the different anatomical features (germ, floury and vitreous endosperm) within the maize kernel. The brighter regions correspond to the higher level of attenuation, hence denser regions, whereas the dark areas represent voids/pores as they have a lower attenuation with respect to the solid fraction.

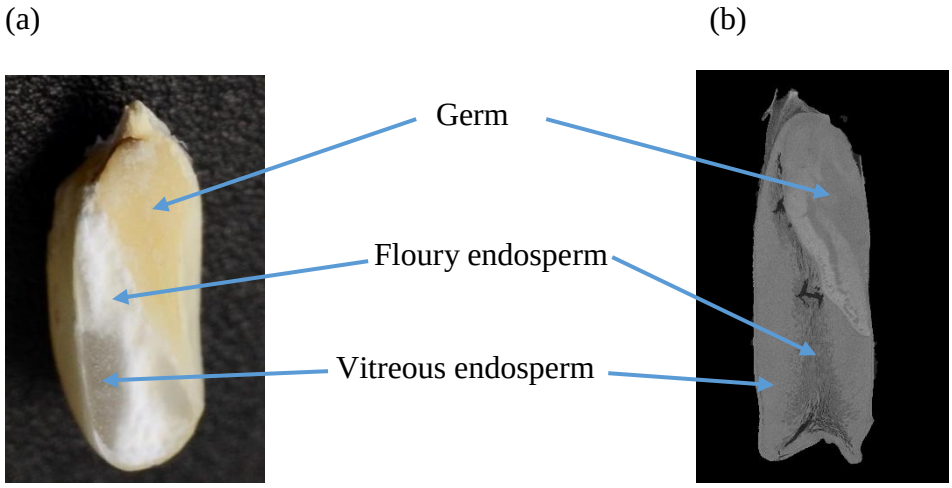

Figure 4.4. (a) A longitudinal digital image and (b) 2D X-ray image, showing the internal structure of a maize kernel i.e. germ, floury and vitreous endosperm.

The 2D cross-sectional images of the maize kernels for the four days scanned illustrated internal structural changes with time (Fig. 4.5). Images of only one control and one infected maize kernel on day 1 and day 4 are shown. There were more voids in the both the control and infected kernel over time especially in the germ and floury endosperm. The voids and airspaces that appeared on day 1 in both the control and infected kernels were expected since voids are natural and inherent to the kernel and could be attributed to the drying process after harvesting (Chang, 1988; Watson *et al.*, 2003). Although it was previously reported that conidia and hyphae infection were detected in maize kernels as early as 24 h post inoculation (Duncan & Howard, 2010), this was only found on the surface of the kernels. Williams *et al.* (2012) also reported little fungal activity in maize kernels after 20 h post inoculation in their study using near infrared (NIR) hyperspectral imaging. Hence, it was not expected to observe structural damage on day 1. Day 1 was therefore used for comparison with the rest of the time points.

Sample	Top view	Front view	Side view
Control day 1	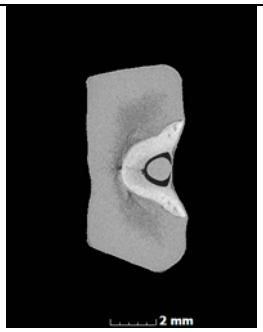	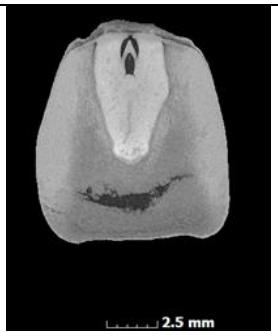	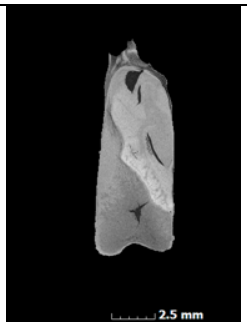
Control day 4	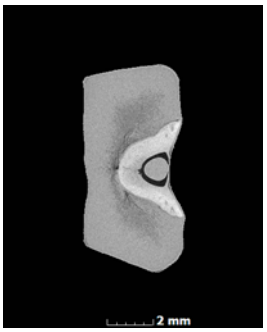	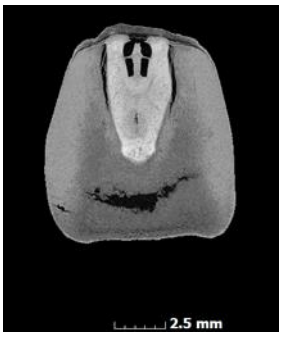	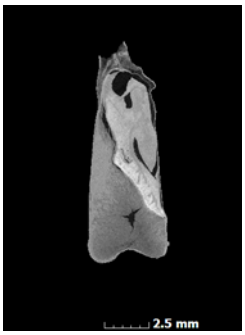
Infected day 1	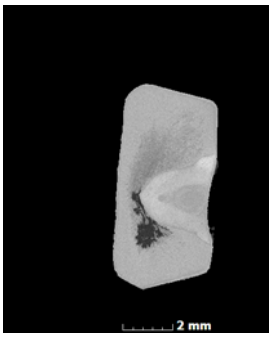	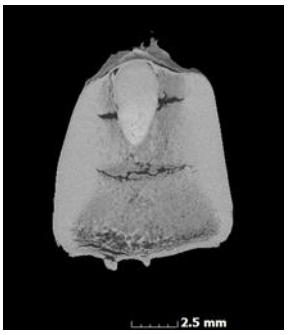	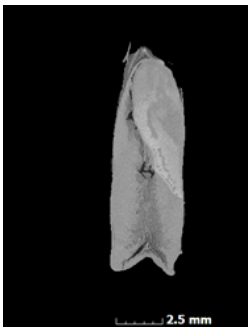
Infected day 4	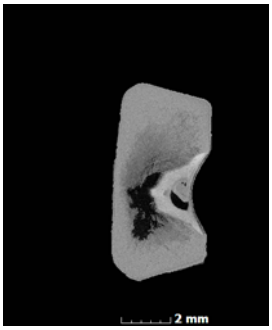		

Figure 4.5. Grey scale 2D X-ray images of the different views (top, front, side) of one control and one infected maize kernel on day 1 and day 4 illustrating internal structural changes over time.

The presence of more voids with time in both the control and infected kernel could be attributed to breakdown of kernel reserves. Respiration of the grain itself and the fungi in the grain contribute to breakdown of kernel reserves for energy use (Seitz *et al.*, 1982), this could alter the structural integrity of the kernel resulting in less attenuation of X-rays over time. Theoretically, the combined activity of the fungus and the respiration of the grain itself was expected to cause more

structural damage (more pores) in the infected kernels compared to the control kernels. However, the activity of fungi in the grain is usually minimal at the start of infection and increases at a rate dependent on moisture, temperature and host vulnerability (Seitz *et al.*, 1982; Popovski & Celar, 2013).

The germ and scutellum have been reported to be the regions preferred by most fungi including *F. verticillioides* (Duncan & Howard, 2010; Dolezal *et al.*, 2013). These regions (germ and scutellum) are high in nutrients, especially lipids (Evers & Millar, 2002) and the fungus colonises these regions to produce hydrolytic enzymes for degrading the kernel (Naresh *et al.*, 2004). The germ and the scutellum which constitute the embryo are also the live tissues within the maize seed and are involved in reserve mobilisation (Mayer & Poljakoff-Mayber, 1982). This region secretes enzymes which break the kernel reserve down for energy use (Thevenot *et al.*, 1992). This explains why more pores were observed in the control maize kernel with time.

More voids were observed in the floury endosperm over time compared to the vitreous endosperm (Fig. 4.5). Less structural damage in the vitreous endosperm could be attributed to it being harder and having fewer intercellular spaces, making this region less susceptible to damage (Schoeman *et al.*, 2017). The presence of voids/pores in the floury endosperm makes it more susceptible to damage compared to the vitreous endosperm (Dombrink-Kurtzman & Knutson, 1997).

Grey level histogram

An intensity histogram illustrates the variation of intensities in an image. The shape of the histogram gives information about the nature of the image and thus the object (Umbaugh, 2010). The histogram can illustrate the different parts within an object based on the grey level frequency distribution values, with the lower grey values corresponding to internal air while the higher values correspond to the object structure (Magwaza & Opara, 2014; Schoeman *et al.*, 2016a). An image with its grey level histogram grouped at the low end of the grey level intensity is dark and corresponds to more voids within the sample; while a grey level histogram with values concentrated at the high end of the grey level intensity corresponds to a brighter image or dense region within the sample (Scott, 2010; Schoeman *et al.*, 2016a). Figure 4.6 shows the grey value distribution of one control and one infected maize kernel for the four days scanned. There was a shift to the lower intensity grey value end of the grey level spectrum with time in both the control and the infected kernels. The shift in the grey values with time is an indication of the kernel becoming less dense with time probably due to increase in voids within the kernel because of breakdown of kernel reserve.

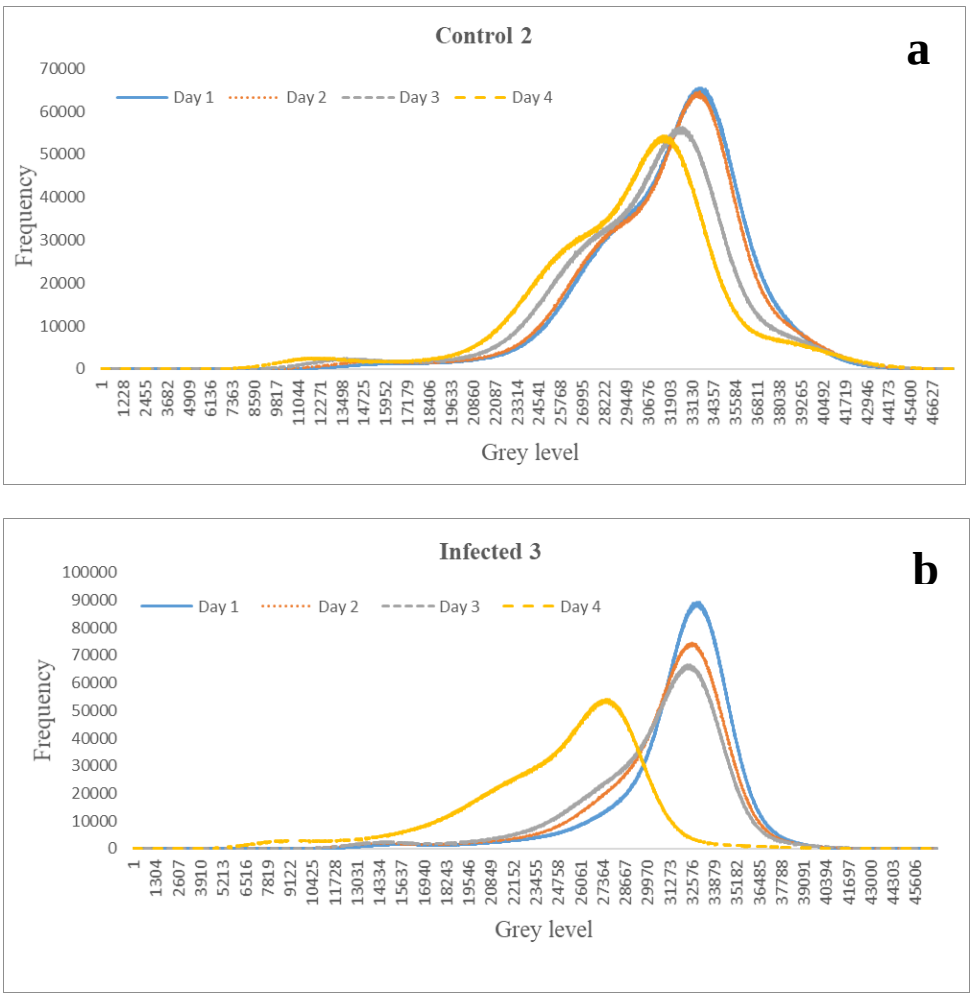

Figure 4.6. Grey value distribution histograms of (a) one control and (b) one infected maize kernel for the four days scanned, depicting the shift in grey level intensity over time.

First order statistics and principal component analysis

The calculated values of mean, standard deviation, kurtosis and skewness for 100 images of each kernel in the three views for the four days scanned were used as inputs for PCA. PCA was applied to determine relationships between variables measured and samples, and thus reveal natural patterns and clustering in the samples. The results of PCA score and loading plots from the front view orientation of the kernels is shown in Fig. 4.7. The first two principal components (PCs) explained 72.51% of the total variance in the data set, with PC1 describing the largest portion (57.47%). Maize kernels located on the positive side of PC1 were correlated to mean and kurtosis and negatively correlated to skewness. Mean measures the average grey level intensity (brightness) while kurtosis is a measure of flatness of the histogram, i.e. the 'peakedness' of the distribution relative to the length and size of the tails. Increased kurtosis values signify increased 'peakedness' of the distribution while decreased kurtosis values signify flattening and broadening of the distribution (Skorton *et al.*, 1983).

(a)

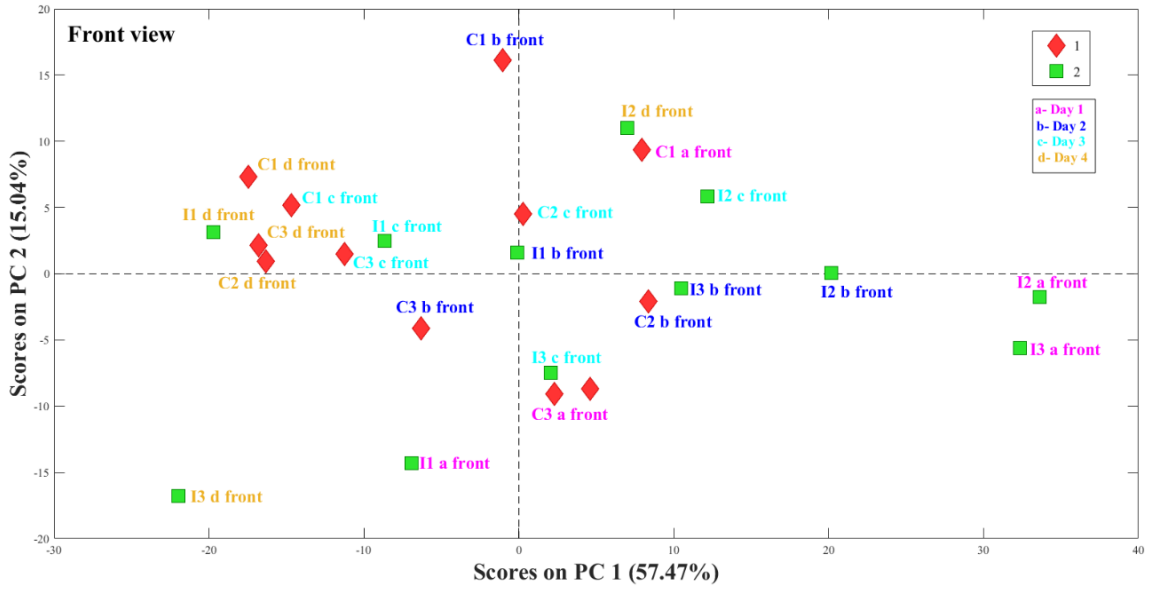

(b)

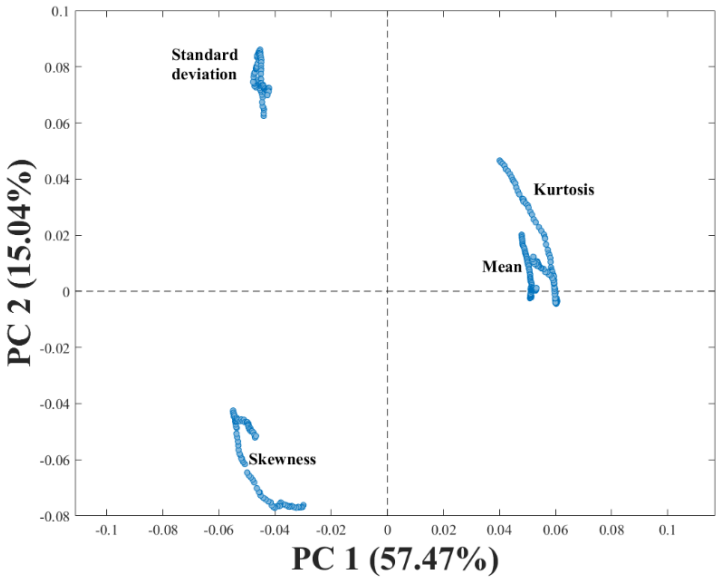

Figure 4.7. PCA (a) score plot (b) loadings plot for control (C1, C2, C3) and infected (I1, I2, I3) kernels in the front view for the four days scanned with the first order statistics as inputs, where red is control, and green is infected kernels.

The score plot for the front view (Fig 4.7a) did not show any clear grouping/clustering of the control kernels from the infected kernels; however, clear differences were seen within the days of the individual kernels. The lack of clear grouping could be attributed to similar structural changes in the

control and infected kernels on the days scanned, variation in the rate of infection of the individual kernels, minimum changes in the kernel structure in the earlier stage of fungal infection and the small sample size used in this study. Mean and kurtosis of both the control and infected kernels decreased over time, meaning the kernels were becoming less bright and this is attributed to lower density due to breakdown of kernel reserves by the fungi and grain respiration. In an earlier study conducted using the same kernels as in this experiment, (Orina *et al.*, 2017) found no significant difference between the control and infected kernels. However, differences were observed within the days.

Kernels situated in the quadrant where PC1 and PC2 was negative, were positively correlated to skewness. Skewness measures if there is any change in the direction of the distribution of the brightness/grey level intensity. This measure is 0 if the histogram is symmetrical about the mean, otherwise positive or negative depending on whether it has been skewed above or below the mean (Materka & Strzelecki, 1998). There was a shift to the lower grey level intensities over time in both the controls and infected kernels.

In the side view score plot (Fig 4.8a), PC1 explained 76.26% of the total variation and samples with positive score values along PC1 were correlated to standard deviation and skewness (Fig. 4.8b). Standard deviation measures the average contrast in the image (variability in the brightness) (Patel *et al.*, 2012). This demonstrates that contrast (difference between the highest and lowest grey values) in the images and shift in the grey value intensity were the main discriminating factors in this direction/orientation, however no clear grouping was observed between the control and infected kernels. Both the control and infected kernels had a higher standard deviation and skewness on day 4 compared to day 1.

(a)

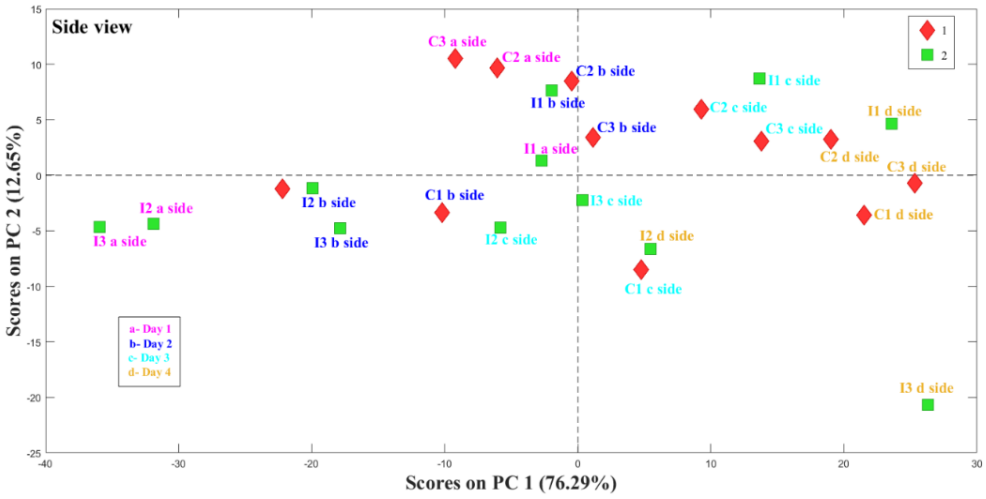

(b)

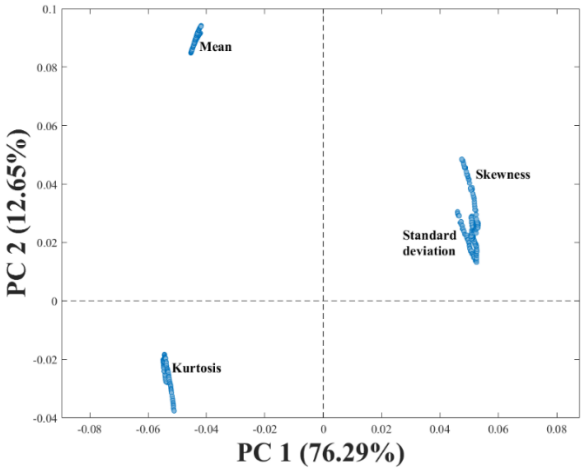

Figure 4.8. PCA (a) score plot (b) loadings plot for control (C1, C2, C3) and infected (I1, I2, I3) kernels in the side view for the four days scanned with the first order statistics as inputs, where red is control, and green is infected kernel.

The variable that was positively correlated to PC1 in the top view was skewness as shown in Fig 4.9b. Some sort of kernel grouping was observed in this orientation (Fig 4.9a, boundaries were manually drawn to illustrate the groupings). Similar trends were observed in this view as with the other views (side and front view), that is mean and kurtosis of the both control and infected kernels were high on day one and decreased with time. The change in skewness of the kernels with time is an indication of an increase in low grey value intensities, due to the breakdown of kernel reserves creating more pores. Looking at the score plots (Fig 4.9a) along PC2, a separation of day 1 and day 2 from day 3 and 4 could be seen. The kernels (both control and infected) on day 1 and 2 located on the positive side of PC2 were positively correlated to mean and negatively correlated to standard deviation. The top view gave a better grouping of the samples compared to the other two views.

(a)

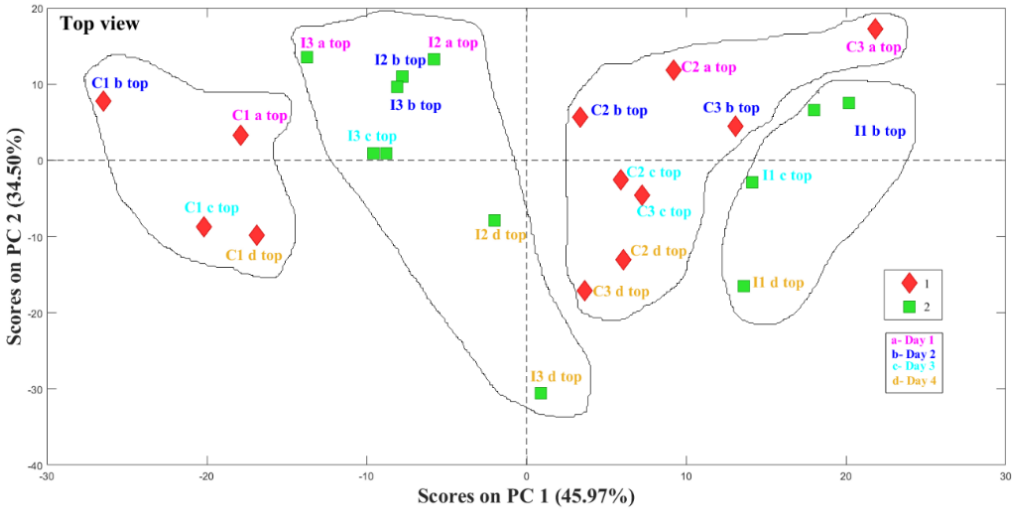

(b)

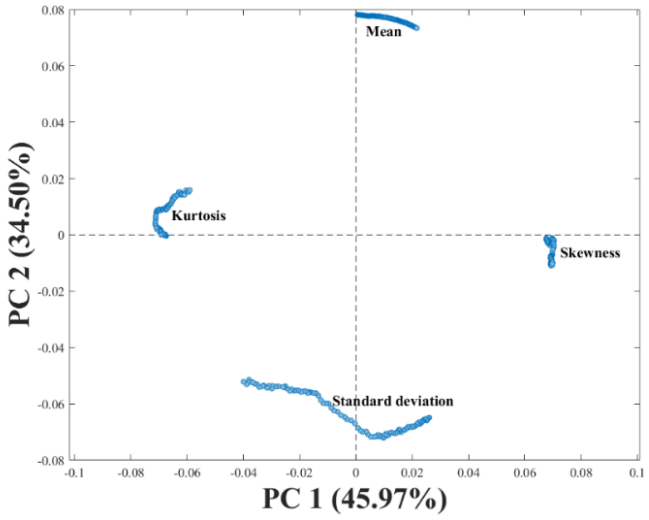

Figure 4.9. PCA (a) score plot (b) loadings plot for control (C1, C2, C3) and infected (I1, I2, I3) kernels in the top view for the four days scanned with the first order statistics as inputs, where red is control, and green is infected kernel.

Image texture analysis using grey level co-occurrence matrices and PCA

The outputs of texture analysis for the front view are shown in Figure 4.10. The textural features that had accounted for the maximum variation were homogeneity and correlation (Fig. 4.10b). Correlation is a measure of the grey tone linear dependencies in the image (Haralick & Shanmugam, 1973), while homogeneity, also known as inverse difference moment, measures image homogeneity as it assumes larger values for smaller grey tone differences in pair elements (Gadkari, 2004). There was no clear separation of the control from infected kernels, however changes were

observed in the days of the individual kernels in both the control and infected kernels. Most of the control and infected kernels grouped together (Fig 4.10a) on day 1, this could be attributed to minimal fungal effect in the kernel on this day. There was an increase in correlation and homogeneity over time in both the control and infected kernels, meaning neighbouring pixels became more correlated with each other over time. This indicates large areas in the images on day 4 had similar grey level intensities compared to day 1. And this could be attributed to increase in the presence of voids and airspaces because of destruction of the kernel structure caused by breakdown of kernel reserves.

(a)

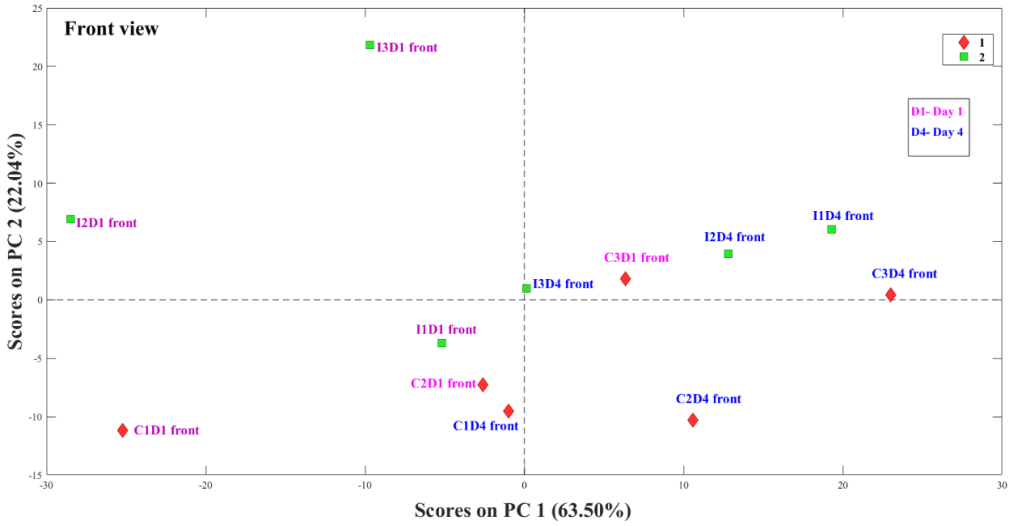

(b)

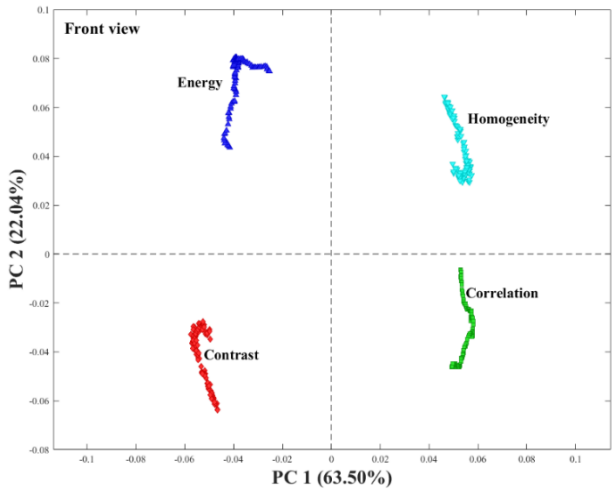

Figure 4.10. PCA (a) score plot (b) loadings plot for control (C1, C2, C3) and infected (I1, I2, I3) kernels in the front view for day 1 and day 4 scanned with the extracted textural features as inputs, where red is control, and green is infected kernel.

In the top view, energy, correlation and homogeneity were positively correlated to PC1, while contrast was negatively correlated (Fig. 4.11b). Energy is also called angular second moment and it measures textural uniformity of an image, it detects disorder in textures. Energy values close to or equal 1 indicates a homogenous image (Fernandez *et al.*, 2005). The energy of the kernels increases over time meaning the images were becoming more homogenous as pixels with lower grey level intensities increases due to kernel degradation. Contrast on the other hand is a measure of the local variation present in an image. A high contrast value indicates a high degree of local variation (Haralick & Shanmugam, 1973). Most kernels had a higher contrast on day 1 which decreases over time as the kernels deteriorated. Similar trend was also observed in this view where most control and infected kernels clustered together on day 1 (Fig 4.11a). Contrast and homogeneity are inversely correlated (Gadkari, 2004), meaning contrast decreases if homogeneity increases, and this was evident in this study. As the kernel deteriorates, its ability to attenuate X-rays is affected leading to changes in the grey value intensity which are detected by the image textural features.

(a)

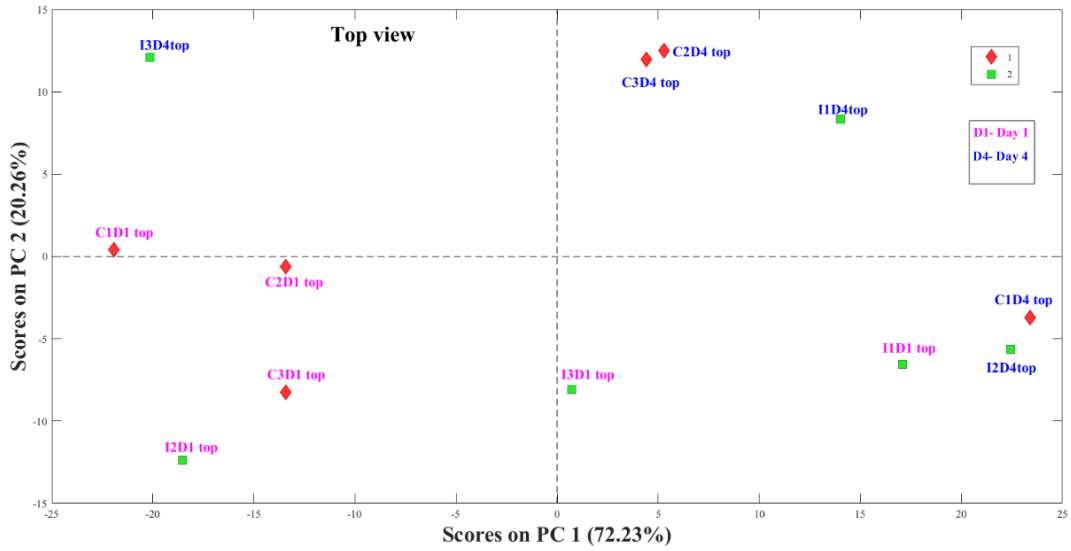

(b)

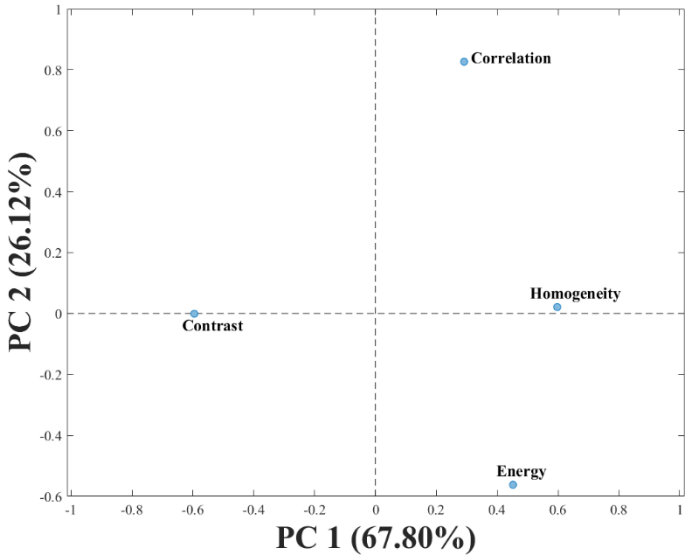

Figure 4.11. PCA (a) score plot (b) loadings plot for control (C1, C2, C3) and infected (I1, I2, I3) kernels in the top view for day 1 and day 4 scanned with the extracted textural features as inputs, where red is control, and green is infected kernels.

Classification

PLS-DA was used to determine whether it was possible to discriminate between the control and infected kernels, and hence possibly build a model that could be used to predict future images. Table 4.1 shows the classification results in the form of a confusion matrix. The classification accuracy of each class (control or infected) was determined by the number of correctly classified samples in each class divided by the total number of samples in such a class. It is seen that 3 control images were misclassified as infected, and 7 infected images were misclassified as control, resulting in a classification accuracy of 72.25% for control and 54.17% for infected samples. Misclassification between the control and infected could be attributed to similar changes observed in both kernels due to breakdown of kernel reserves. The high number of infected kernels misclassified as control could also be attributed to minimum structural changes due to fungal infection on day 1, therefore the infected kernels on day 1 are likely to classified as control kernels (as evident in Fig 4.10a and Fig 4. 11a). Using non-linear methods like support vector machine (SVM) allowed to improve the classification accuracy up to 99.9% and 100% for the control and infected samples respectively. However, the results are not shown here since non-linear methods require bigger calibration and test sets (a large sample size).

Table 4.2. Classification results from PLS-DA model using the extracted textural features in both top and front view on day 1 and day 4.

Model used		Class		Accuracy (%)
		Control (12)	Infected (12)	
PLS-DA	Predicted as control	9	7	75%
	Predicted as infected	3	5	41.67%

Conclusion

X-ray micro-CT enabled qualitative assessment of the internal structure of maize kernels using 2D cross sectional images, with more voids especially in the germ and floury endosperm regions over time in both the control and infected kernels. The grey level histogram of the whole kernels shifted to the lower level grey value intensity over time in both the control and infected samples, meaning the kernels were becoming less dense with time. The changes in the kernel internal structure with time were attributed to breakdown of kernel reserves by the kernel itself during respiration and fungal activities within the kernel.

There was no clear grouping between the control and infected kernels using the first order statistics and GLCM features as inputs in PCA. PCA was used to aid in understanding the relationship between the extracted image texture features and the treatments (control and infected), and how they changed over time. Though no grouping was observed, there was separation in the days of individual kernels. Mean and kurtosis decreased over time implying that the kernels were becoming less dense, while correlation increased indicating more regions in the images on day 4 had similar grey level intensities compared to day 1 due to presence of more voids because of kernel degradation. The top view showed some sort of kernel grouping compared to side and front view of the kernel. The GLCM features were used to develop a classification model using PLS-DA. The PLS-DA model gave high false positives, and this was attributed to similar changes observed in both the control and infected kernels over time.

Image texture analysis is an effective technique for extraction of quantitative features from images for characterisation of a food product. The results from this study proves that image texture analysis coupled with multivariate analysis could be used to evaluate X-ray images and hence aid in discriminating control from infected maize kernels. Further studies should be conducted using more maize kernels to account for variability and scan kernels for more days after inoculation (e.g. Day 1, 4, 8).

References

Abdi, H. & Williams, L.J. (2010). Principal component analysis. *Wiley Interdisciplinary Reviews: Computational Statistics*, **2**, 433-459.

Afolabi, C., Ojiambo, P., Ekpo, E., Menkir, A. & Bandyopadhyay, R. (2007). Evaluation of maize inbred lines for resistance to *Fusarium* ear rot and fumonisin accumulation in grain in tropical Africa. *Plant Disease*, **91**, 279-286.

Baker, D.R., Mancini, L., Polacci, M., Higgins, M.D., Gualda, G.A.R., Hill, R.J. & Rivers, M.L. (2012). An introduction to the application of X-ray microtomography to the three-dimensional study of igneous rocks. *Lithos*, **148**, 262-276.

Basset, O., Buquet, B., Abouelkaram, S.d., Delachartre, P. & Culioli, J. (2000). Application of texture image analysis for the classification of bovine meat. *Food Chemistry*, **69**, 437-445.

Bharati, M.H., Liu, J.J. & MacGregor, J.F. (2004). Image texture analysis: methods and comparisons. *Chemometrics and Intelligent Laboratory Systems*, **72**, 57-71.

Bourne, M. (2002). *Food texture and viscosity: concept and measurement.* Academic press, Geneva, New York.

Brereton, R.G. & Lloyd, G.R. (2014). Partial least squares discriminant analysis: taking the magic away. *Journal of Chemometrics*, **28**, 213-225.

Brosnan, T. & Sun, D.W. (2004). Improving quality inspection of food products by computer vision––a review. *Journal of Food Engineering*, **61**, 3-16.

Chang, C. (1988). Measuring density and porosity of grain kernels using a gas pycnometer. *Cereal Chemistry*, **65**, 13-15.

Cnudde, V. & Boone, M. (2013). High-resolution X-ray computed tomography in geosciences: a review of the current technology and applications. *Earth-Science Reviews*, **123**, 1-17.

Dolezal, A.L., Obrian, G.R., Nielsen, D.M., Woloshuk, C.P., Boston, R.S. & Payne, G.A. (2013). Localization, morphology and transcriptional profile of *Aspergillus flavus* during seed colonization. *Molecular Plant Pathology*, **14**, 898-909.

Dombrink-Kurtzman, M. & Knutson, C. (1997). A study of maize endosperm hardness in relation to amylose content and susceptibility to damage. *Cereal Chemistry*, **74**, 776-780.

Du, C.J. & Sun, D.W. (2004). Recent developments in the applications of image processing techniques for food quality evaluation. *Trends in Food Science & Technology*, **15**, 230-249.

Duncan, E.K. & Howard, J.R. (2010). Biology of maize kernel infection by *Fusarium verticillioides*. *The American Phytopathology Society*, **23**, 6-16.

Esbensen, K.H., Guyot, D., Westad, F. & Houmoller, L.P. (2002). *Multivariate data analysis: in practice: An introduction to multivariate data analysis and experimental design.* Multivariate Data Analysis. 5th edition, CAMO process AS, Oslo, Norway.

Evers, T. & Millar, S. (2002). Cereal Grain Structure and Development: Some Implications for Quality. *Journal of Cereal Science*, **36**, 261-284.

Fernandez, L., Castillero, C. & Aguilera, J. (2005). An application of image analysis to dehydration of apple discs. *Journal of Food Engineering*, **67**, 185-193.

Gadkari, D. (2004). Image quality analysis using GLCM. MSc thesis, University of Central Florida.

Gonzales-Barron, U. & Butler, F. (2008). Discrimination of crumb grain visual appearance of organic and non-organic bread loaves by image texture analysis. *Journal of Food Engineering*, **84**, 480-488.

Guelpa, A., du Plessis, A., Kidd, M. & Manley, M. (2015). Non-destructive estimation of maize (*Zea mays* L.) kernel hardness by means of an X-ray micro-computed tomography (µCT) density calibration. *Food and Bioprocess Technology*, **8**, 1419-1429.

Guelpa, A., du Plessis, A. & Manley, M. (2016). A high-throughput X-ray micro-computed tomography (µCT) approach for measuring single kernel maize (*Zea mays* L.) volumes and densities. *Journal of Cereal Science*, **69**, 321-328.

Gunasekaran, S. (1996). Computer vision technology for food quality assurance. *Trends in Food Science & Technology*, **7**, 245-256.

Gustin, J.L., Jackson, S., Williams, C., Patel, A., Armstrong, P., Peter, G.F. & Settles, A.M. (2013). Analysis of maize (*Zea mays*) kernel density and volume using microcomputed tomography and single-kernel near-infrared spectroscopy. *Journal of Agricultural and Food Chemistry*, **61**, 10872-10880.

Haralick, R.M. & Shanmugam, K. (1973). Textural features for image classification. *IEEE Transactions on Systems, Man, and Cybernetics*, **3**, 610-621.

Li, J., Tan, J., Martz, F. & Heymann, H. (1999). Image texture features as indicators of beef tenderness. *Meat Science*, **53**, 17-22.

Li, X., He, Y. & Fang, H. (2007). Non-destructive discrimination of Chinese bayberry varieties using Vis/NIR spectroscopy. *Journal of Food Engineering*, **81**, 357-363.

Lim, K.S. & Barigou, M. (2004). X-ray micro-computed tomography of cellular food products. *Food Research International*, **37**, 1001-1012.

Liu, H.F., Wu, B.H., Fan, P.G., Li, S.H. & Li, L.S. (2006). Sugar and acid concentrations in 98 grape cultivars analyzed by principal component analysis. *Journal of the Science of Food and Agriculture*, **86**, 1526-1536.

Magwaza, L.S. & Opara, U.L. (2014). Investigating non-destructive quantification and characterization of pomegranate fruit internal structure using X-ray computed tomography. *Postharvest Biology and Technology*, **95**, 1-6.

Majumdar, S. & Jayas, D. (2000). Classification of cereal grains using machine vision: III. Texture models. *Transactions of the ASAE*, **43**, 1681-1687.

Materka, A. & Strzelecki, M. (1998). Texture analysis methods–a review. Technical University of Lodz, Institute of Electronics, COST B11 report, Brussels, pp. 9-11.

Mayer, A.M. & Poljakoff-Mayber, A. (1982). *The germination of seeds.* Pergamon International Library of Science, Technology, Engineering and Social Studies: Elsevier.

Mendoza, F. & Aguilera, J. (2004). Application of image analysis for classification of ripening bananas. *Journal of Food Science*, **69**, E471-E477.

Mohoric, A., Vergeldt, F, Gerkerma, E., Dalen, G.v., Doel, J.R.v.d., Vliet, L.J.v., As, H.V. & Duynhoven, J.v. (2009). The effect of rice kernel microstructure on cooking behaivour:a combined microCT and MRI study. *Food Chemistry*, **115**, 1491-1499.

Naresh, M., David, A. & Sanchis, V. (2004). The Role of spoilage fungi in seed deterioration. In: *Fungal Biotechnology in Agricultural, Food and Environmental Application.* pp. 311-322. New York City: Marcel Dekker.

Narvankar, D.S., Singh, D.S. & White, N.D.G. (2009). Assessment of soft X-ray imaging for detection of fungal infection in wheat. *Biosystems Engineering- Postharvest Technology*, **81**, 49-56.

Orina, I., Manley, M. & Williams, P.J. (2017). Use of High-Resolution X-Ray Micro-Computed Tomography for the Analysis of Internal Structural Changes in Maize Infected with *Fusarium verticillioides*. *Food Analytical Methods*, **10**, 2919-2933.

Paliwal, J., Visen, N., Jayas, D. & White, N. (2003). Cereal grain and dockage identification using machine vision. *Biosystems Engineering*, **85**, 51-57.

Patel, K.K., Kar, A., Jha, S. & Khan, M. (2012). Machine vision system: a tool for quality inspection of food and agricultural products. *Journal of Food Science and Technology*, **49**, 123-141.

Pearson, T. & Wicklow, D. (2006). Detection of corn kernels infected by fungi. *Transactions of the ASABE*, **49**, 1235-1245.

Popovski, S. & Celar, F.A. (2013). The impact of environmental factors on the infection of cereals with *Fusarium* species and mycotoxin production-a review/Vpliv okoljskih dejavnikov na okuzbo zit z glivami *Fusarium* spp. in tvorbo mikotoksinov-pregledni clanek. *Acta Agriculturae Slovenica*, **101**, 105-116.

Prats-Montalbán, J., De Juan, A. & Ferrer, A. (2011). Multivariate image analysis: a review with applications. *Chemometrics and Intelligent Laboratory Systems*, **107**, 1-23.

Schoeman, L., du Plessis, A. & Manley, M. (2016a). Non-destructive characterisation and quantification of the effect of conventional oven and forced convection continuous tumble (FCCT) roasting on the three-dimensional microstructure of whole wheat kernels using X-ray micro-computed tomography (µCT). *Journal of Food Engineering*, **187**, 1-13.

Schoeman, L., du Plessis, A., Verboven, P., Nicolaï, B.M., Cantre, D. & Manley, M. (2017). Effect of oven and forced convection continuous tumble (FCCT) roasting on the microstructure and dry milling properties of white maize. *Innovative Food Science & Emerging Technologies*, **44**, 54-66.

Schoeman, L., Williams, P., du Plessis, A. & Manley, M. (2016b). X-ray micro-computed tomography (µCT) for non-destructive characterisation of food microstructure. *Trends in Food Science & Technology*, **47**, 10-24.

Scott, E.U. (2010). Digital image processing and analysis: human and computer vision applications with CVIPtools. pp. 456-463. CRC press.

Seitz, L., Sauer, D., Mohr, H. & Aldis, D. (1982). Fungal growth and dry matter loss during bin storage of high-moisture corn. *Cereal Chemistry*, **59**, 9-14.

Skorton, D.J., Melton, H.E., Pandian, N.G., Nichols, J., Koyanagi, S., Marcus, M.L., Collins, S.M. & Kerber, R.E. (1983). Detection of acute myocardial infarction in closed-chest dogs by analysis of regional two-dimensional echocardiographic gray-level distributions. *Circulation Research*, **52**, 36-44.

Suresh, A. & Neethirajan, S. (2015). Real-time 3D visualisation and quantitative analysis of internal structure of wheat kernels. *Journal of Cereal Science*, **63**, 81-87.

Thevenot, C., Lauriere, C., Mayer, C., Simond-Cote, E. & Daussant, J. (1992). α-Amylase changes during development and germination of maize kernels. *Journal of Plant Physiology*, **140**, 61-65.

Tournier, C., Grass, M., Zope, D., Salles, C. & Bertrand, D. (2012). Characterization of bread breakdown during mastication by image texture analysis. *Journal of Food Engineering*, **113**, 615-622.

Umbaugh, S.E. (2010). Digital image processing and analysis: human and computer vision applications with CVIP tools. CRC press. Boca, Raton, pp 456-463.

Watson, S., White, P. & Johnson, L. (2003). Description, development, structure, and composition of the corn kernel. In: White P.J. Johnson LA (eds) Corn: Chemistry and Technology, 2nd edn. American Association of Cereal Chemists, St. Paul, pp 69-106.

Williams, P.J., Geladi, P., Britz, T.J. & Manley, M. (2012). Investigation of fungal development in maize kernels using NIR hyperspectral imaging and multivariate data analysis. *Journal of Cereal Science*, **55**, 272-278.

Wold, S., Esbensen, K. & Geladi, P. (1987). Principal component analysis. *Chemometrics and Intelligent Laboratory Systems*, **2**, 37-52.

Zheng, C., Sun, D.-W. & Zheng, L. (2006a). Recent applications of image texture for evaluation of food qualities-a review. *Trends in Food Science and Technology*, **17**, 113-128.

Zheng, C., Sun, D.-W. & Zheng, L. (2006b). Recent developments and applications of image features for food quality evaluation and inspection–a review. *Trends in Food Science & Technology*, **17**, 642-655.

Zhu, L.J., Hulya, D., Gajula, H., Gu, M.H., Qiao-Quan, L. & Yong-Cheng, S. (2012). Study of kernel structure of high-amylose and wild-type rice by X-ray microtomography and SEM. *Journal of Cereal Science*, **51**, 1-5.

Chapter 5

Fungal damage evaluation in maize using high resolution X-ray micro computed tomography and image texture analysis

Abstract

Contamination of maize by fungi leads to economic losses and they produce toxic secondary metabolites which are harmful to humans. In this study, high resolution X-ray micro-computed tomography was used to visualise the effect of fungal infection on the internal structure and discriminate infected from uninfected maize kernels using image textural features. More voids were observed in the two-dimensional (2D) X-ray images of the maize kernels over time, especially in the germ and floury endosperm regions. Algorithms were developed to extract image textural features from selected 2D images of the kernels. A total of eight image features (four first order statistics and four grey-level co-occurrence matrix (GLCM) features) were extracted and used as input to principal component analysis (PCA). The first order statistical image features gave a better separation of the control from infected on day 8 post-inoculation. Classification models were developed using partial least square discriminant analysis (PLS-DA). Classification accuracies of 97.22% for control and 55.56% for infected kernels were achieved using first order statistical features. The model developed using GLCM extracted features gave a better classification accuracy of 79.16% for infected kernels with less infected kernels classified as controls.

Introduction

Maize (*Zea mays* L.) is a staple food for millions of people worldwide especially in developing countries. It is consumed in various forms, i.e. fresh, roasted, boiled, fermented, milled or a combination of these (Kayode *et al.*, 2013); and can also be processed into speciality foods such as tortillas, bread, corn chips, snack bars and breakfast cereals (Velu *et al.*, 2006).

Depending on the environmental conditions, maize is vulnerable to fungal infection in the field and during storage. Fungal activity in maize results in reduced germination, discolouration, dry matter loss, chemical and nutritional changes, reduction of processing quality, and most importantly is the production of mycotoxins which are harmful to humans (Suleiman *et al.*, 2013). Mycotoxins have cancer promoting activity, and have been linked to oesophageal cancer in humans (Isaacson, 2005). Detection of fungal contamination is therefore essential in preventing contamination in the form of mycotoxins from entering the food chain.

Traditional methods including diagnostic media (Gourama & Bullerman, 1995), polymerase chain methods (Manonmani *et al.*, 2005), microscopy (Duncan & Howard, 2010) and immunological methods (Paepens *et al.*, 2004) have been utilised for detection of fungal contamination in maize and other cereal grains. These methods are effective but are invasive and require tedious sample preparation, while microscopic techniques are limited to two dimensional images and sectioning the sample is likely to disrupt the structure, causing imaging artefacts (Salvo *et al.*, 2010).

X-ray micro computed tomography (X-ray micro-CT) is a relatively new technique, which enables non-destructive visualisation and quantification of the internal microstructure of a product. Following its huge success in material science (Landis & Keane, 2010), geology (Cnudde & Boone, 2013b), industrial applications (De Chiffre *et al.*, 2014) and biological sciences (Mizutani & Suzuki, 2012), efforts have been made in recent years to extend this technique to the field of agriculture and food quality evaluation. X-ray micro-CT is based on the interaction of X-rays with matter. X-rays have a distinct advantage in non-destructive inspection because they can penetrate through most objects to visualise the internal structure, and hence aid in detection of internal defects non-destructively (Mathanker *et al.*, 2013).

During scanning, a sample is mounted on a rotary stage and illuminated with X-rays, the X-rays passes through the sample in many different directions and along different pathways to create an image displacing variation in density at numerous points in a two-dimensional slice (Lim & Barigou, 2004). The differences in density creates a contrast on the two-dimensional (2D) image to distinguish components within the sample. The denser regions, which are areas of higher X-ray attenuation, will appear brighter on the 2D image (Schoeman *et al.*, 2016b). The series of 2D projection images

acquired at different angles, using dedicated software, are reconstructed into a three-dimensional (3D) volume of the sample, which can provide qualitative and quantitative information about its internal structure (Cnudde & Boone, 2013).

X-ray micro-CT has proven to be a very useful technique for qualitative and quantitative assessment of the internal quality of agricultural products. It has been used to assess internal decay of fresh chestnut (Donis-González *et al.*, 2014), to characterise 'Braeburn' browning in apples (Herremans *et al.*, 2013), to study the effect of far-infrared radiation assisted drying on the microstructure of bananas (Léonard *et al.*, 2008) and in 3D visualisation and quantification of internal structure of wheat kernels damaged by sprouting and insect infestation (Suresh & Neethirajan, 2015). This technique has also been used to study the effect of heat on rice kernel microstructure (Mohorič *et al.*, 2009), to investigate the effect of roasting on the 3D microstructure of whole maize (Schoeman *et al.*, 2017) and wheat (Schoeman *et al.*, 2016a; Schoeman *et al.*, 2017) kernels and to measure maize kernel density and volume (Gustin *et al.*, 2013; Guelpa *et al.*, 2015). The various application of X-ray micro-CT in food and food products has recently been reviewed by Schoeman *et al.* (2016b).

Fusarium verticillioides is the most frequently isolated fungal species from maize in the field, stored maize and maize-based products (Popovski & Celar, 2013). A recent study demonstrated the potential of X-ray micro-CT to analyse the internal structural changes in maize kernels infected by *F. verticillioides* based on quantitative measurements that is total kernel volume, total volume of voids and mean grey value (Orina *et al.*, 2017). The major components of the kernel, i.e. germ, floury and vitreous endosperm were identified based on their differences in X-ray attenuation. The rendered 3D volumes of the kernels enabled visualisation of the kernel from different orientations, i.e. sagittal, horizontal and frontal views. More voids were observed in the germ and floury endosperm region over time in both the control and infected kernels. No significant differences were, however, reported between the control and infected kernels using the quantitative measurements taken (kernel volume, mean grey value and total volume of voids).

The aim of this study was thus to visualise the effect of fungal damage on the internal structure of maize using high resolution X-ray micro-CT and distinguish infected from uninfected kernels using image textural features.

Materials and methods

Maize kernel sterilization

This was done as described by Orina *et al.*, (2017), one hundred white maize kernels, kindly provided by the Department of Plant Pathology (Stellenbosch University, South Africa), were soaked

for approximately 15 h in sterile distilled water. They were then rinsed in 70% ethanol, imbibed in a water bath at 60°C for 5 min, then immediately placed in ice for 1 min. The kernels were sterile and ready for inoculation.

Spore suspension preparation

A *Fusarium verticillioides* (MRC 0826) culture, kindly supplied by the Department of Plant Pathology (Stellenbosch University, South Africa), was plated onto potato dextrose agar (PDA) and incubated at 25°C. Spore suspension preparation was as described by Orina *et al*., 2017. After 4 days, a small portion of *F. verticillioides* mycelium was taken from the surface of the PDA agar and transferred into Armstrong solution to facilitate growth of spores. The Armstrong solution, containing the mycelium, was placed in an incubator shaker at 25°C at 1000 rpm for four days. The fungal spores in the Armstrong solution were poured through sterile cheesecloth to remove mycelium, then washed three times using sterile distilled water. The concentration of the spore suspension was checked using a haemocytometer before adjusting to 1×10^6 conidia per millilitre using sterile distilled water.

Maize inoculation

Maize inoculation was done as described by Orina *et al.,* (2017). Sixteen kernels were randomly selected from the batch of sterilised kernels and injured with a needle at random positions, this was to facilitate entry of the fungus into the kernel. Eight of these kernels were dipped in *F. verticillioides* spore suspension for 1 min (infected), and the other eight were dipped into sterile distilled water for 1 min (control). Two kernels were then placed in one 5-ml plastic pipette tip with sterile cotton wool between to separate them from each other. Thus, eight pipette tips with two kernels each (four controls and four infected) were prepared. The pipette tip was used to hold the kernels during scanning and to avoid contamination.

The eight pipette tips with kernels were then placed inside an airtight container (25 × 25 × 14.5 cm) containing a saturated potassium nitrate (KNO_3) solution. The saturated KNO_3 solution was used to create a relative humidity of above 90% in the airtight container (Winston & Bates, 1960). Relative humidity and temperature are the most important factors that influence the growth of fungi on cereal grains. Studies have reported a relative humidity of 92-95% and a temperature of 25-30°C to be conducive for the growth of *F. verticillioides* (Fandohan *et al.*, 2003; Marin *et al.*, 2004). The airtight container with the kernels was incubated at 25°C for 8 days.

X-ray micro-CT image acquisition

Each pipette tip (four controls and four infected) containing two kernels was individually scanned on days 1, 4 and 8 post inoculation under similar conditions. The X-ray scans were obtained

using a General Electric Phoenix Nanotom S (GE Sensing & Inspection Technologies GmbH, Phoenix, Wunstorf, Germany) high-resolution X-ray computed system with a nanofocus tube, located at the CT Scanner Facility (Stellenbosch University, South Africa). Parameters used were optimised to ensure adequate image contrast as outlined by Orina *et al*., (2017) with slight modifications. X-ray radiation was generated from a source voltage of 60 kV and an electric current set at 200 µA. Each pipette was mounted on a translation stage which was at a fixed physical distance of 64 mm from the X-ray source and 230 mm from the detector, resulting in CT scans with a voxel size (resolution) of 14 µm. The pipette tip and cotton wool (used to separate the two kernels in the pipette) had a lower density than the kernels; therefore, the two kernels and cotton wool were scanned in the field of view. Fig. 5.1 illustrates the procedure used in X-ray scanning and image analysis.

Image acquisition was set at 1000 ms per image with 1200 images recorded in one rotation (360°). These 2D images, covering the entire sample were acquired using a fully automated data acquisition system and saved onto a processing workstation operated by system supplied reconstruction software (Datos|x®2.2, General Electric Sensing & Inspection Technologies GmbH, Phoenix, Wunstorf, Germany). A scan took approximately 45 min to complete. The series of projection images were reconstructed/rendered into a 3D volume using integrated Phoenix datos x 3D computed tomography acquisition and reconstruction software (GE Sensing & Inspection Technology GmbH, Phoenix, Wunstorf, Germany). The instrument was standardised using unsigned 16-bit data, which results in grey values between 0 and 65,535 (2^{16} for 16-bit data).

High resolution scan

One control and one infected kernel were scanned at high resolution on day 9 post inoculation. These two kernels were randomly selected, removed from the pipette tip and mounted on a piece of oasis (floral foam) and scanned using the General Electric Phoenix Nanotom S. A power setting of 60 kV and 250 µA was used, with the individual kernel placed at a physical distance of 28 mm from the X-ray source and 200 mm from the detector. Based on these system settings, the scan resolution was 7 µm. Multiple 2D projection images were obtained as the kernel was rotated at 360°, with 750 ms exposure time per image, recording 2000 images in one rotation. The scan took approximately 78 min to complete. The numerous 2D images were acquired using a fully automated data acquisition system, saved onto a processing workstation and reconstructed into 3D volume by system supplied reconstruction software (Datos|x®2.2, General Electric Sensing & Inspection Technologies GmbH, Phoenix, Wunstorf, Germany).

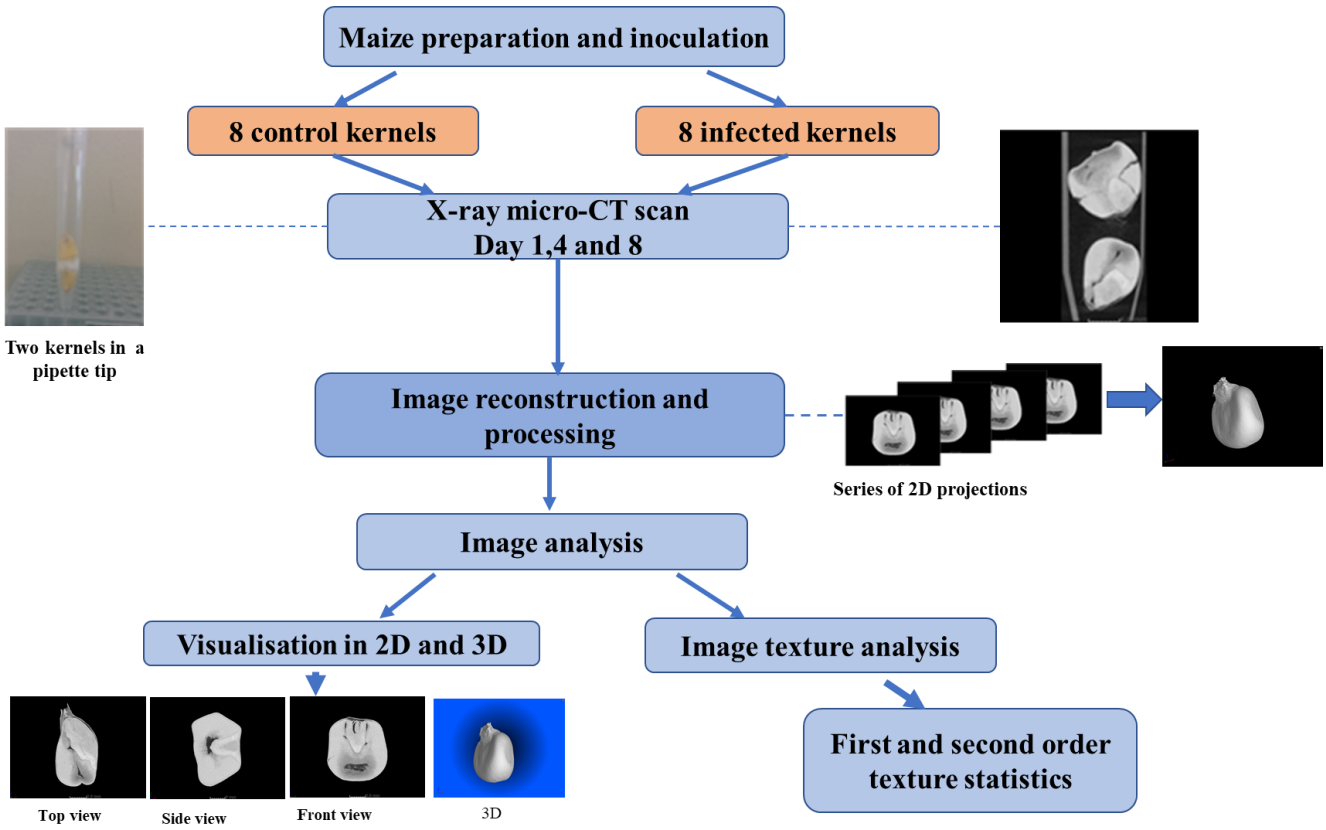

Figure 5.1 Flow diagram illustrating experimental design used during maize kernel X-ray scanning and image analysis.

Images processing

The 3D volumes were imported directly into image visualisation and analysis software, Volume Graphic Studio Max 2.2 (VGStudio Max 2.2, Heidelberg, Germany). The same procedure was used for all the kernels, scanned on the 3 days. Image processing involved first filtering the images using the Adaptive Gaussian method to remove random noise. Then removing the plastic pipette tip, background pixels (i.e. surrounding air), cotton wool separating the kernels and the oasis (for high resolution scans). This was done using the Region Growing Tool by choosing appropriate thresholding grey value tolerances ranging from 1000 to 2500. These regions (pipette tip, surrounding air and cotton wool) were than inverted and extracted from the images. Each kernel was then analysed individually. The resultant 3D volume enabled viewing of each kernels from different orientations, i.e. top, front and side view. One hundred 2D images were selected from each view of each kernel (8 controls and 8 infected kernels) for all 3 days scanned. The images selected were such as to include regions mostly comprised of the germ and endosperm.

Image features extraction

First order statistical features

Image first order statistical features consider the intensity of individual pixels in an image (Patel *et al.*, 2012). Pixels are basic components of images and each pixel contains information on the brightness value (intensity) and location in coordinates assigned to the pixels (Zheng *et al.*, 2006b). First order statistics do not extract any information about the relative location of pixels and the correlation of their intensities to neighbouring pixels (Prats-Montalbán *et al.*, 2011). Algorithms were applied in MATLAB (R2017a) to initially separate the kernel from the background before calculating the mean, standard deviation, kurtosis and skewness. These features were calculated on 100 images of each of the different views, i.e. top, side, front view for each kernel (8 infected and 8 controls) of the three days scanned, i.e. 16 kernels × 100 images × 3 views × 3 days (day 1, 4 and 8) × 4 statistical features. The outputs were converted into a matrix (144 × 400) and used as inputs for principal component analysis (PCA).

Image texture analysis using grey level co-occurrence matrix

Grey level co-occurrence matrix (GLCM) is presumably one of the most frequently cited method for texture analysis of images (Bharati *et al.*, 2004). GLCM describes the occurrence of grey levels between two pixels separated in the image by a given distance and angle. Details on GLCM matrix computation are given in Haralick and Shanmugam (1973). Up to 14 textural features can be calculated from the GLCM to represent textural characteristics of the image studied (Haralick & Shanmugam, 1973). In this study, only 4 textural features, homogeneity, contrast, correlation and entropy, were extracted from the images (equation and definitions are given in Table 5.1).

Algorithms written in MATLAB (R2017a) were implemented to automatically crop regions of approximately 280 × 250 pixels from the centre of each kernel image (100 images) in both the front and top views. The GLCM matrix was then computed followed by extraction of the four textural features (contrast, correlation, energy and homogeneity) in direction 0°, 45°, 90° and 135° and in the distance of 1. The mean of the four angles of each textural feature was computed. Only the top and front views of the kernels (control and infected) was considered, and thus 16 kernels × 100 images × 2 views × 3 days × 4 statistics, which was converted into a matrix of 96 × 400 and used as inputs to calculate PCA.

Table 5.1. Textural features extracted from GLCM

Texture features	Equation	Definition
Contrast	$f_1 = \sum_{n=1}^{n_g-1} n^2 \left[\sum_{i=1}^{n_g}\sum_{j=1}^{n_g} P(i,j)\right] \lvert i-j\rvert = n$	A measure of the amount of local variation present in an image.
Energy (angular second moment)	$f_2 = \sum_i \sum_j \{P(i,j)\}^2$	A measure of textural uniformity of an image
Correlation	$f_3 = \frac{\sum_i \sum_j (i,j)\, P(i,j) - \mu_i \mu_j}{\sigma_i \sigma_j}$	A measure of grey level linear dependencies in an image
Homogeneity (inverse difference moment)	$f_4 = \sum_{i,j} \frac{P(i,j)}{1+\lvert i-j\rvert}$	A measure of image homogeneity and is the opposite of contrast.

Where: *i*, *j*: neighbouring grey level values; *P* (i, j): i, jth entry in the normalized GLCM; μ mean; σ: standard deviation (Haralick & Shanmugam, 1973).

Principal component analysis

Principal component analysis (PCA) was used to explore differences or similarities between extracted image features measured and samples, and thus reveal natural trends and clustering in the data. PCA is an unsupervised multivariate method that transforms the original measured variables into a set of new orthogonal variables called principal components (PCs) (Abdi & Williams, 2010). The PCs are linear combinations of the original variables, with the first PC lying along the direction of maximum variance in the data set. The second PC is orthogonal to the first and accounts for as much of the remaining variability, in the original variables, as possible. The other remaining PCs are linearly uncorrelated to each other and account for as much of the remaining variability as possible (Jolliffe, 2002).

A PCA model is characterised by two complementary set of attributes; loadings and scores. Loadings give information about the relationship between the original variables and the principal components, while the scores value represents the projection of each sample onto the PCs (Esbensen *et al.*, 2002). When the principal component scores are plotted, they show natural patterns and grouping in the samples. PCA was performed on the data set using PLS_Toolbox from Eigenvector Research in MATLAB (R2017a).

Classification model

A classification model provides a method to predict the membership of a given observation/treatment to a qualitative group, using a supervised approach. Partial least squares discriminant analysis (PLS-DA) was applied to investigate the possibility of discriminating the control from infected kernels. PLS-DA seeks to find a straight line that divides the samples into two groups, and thus decide which of the two groups a sample is most likely to belong to from a set of analytical measurements (Brereton & Lloyd, 2014). PLS-DA was carried out in MATLAB (R2017a) using PLS_Toolbox. Pre-processing was set at autoscale and venetian blinds was used for cross-validation in building the PLS-DA model. The classification accuracy of each class was calculated as given below:

$$\%\ Classification\ accuracy = \frac{number\ of\ positive\ classified\ samples\ per\ class}{total\ number\ of\ sample\ in\ a\ given\ class} \times 100$$

Scanning electron microscopy (SEM)

One control and one infected kernel were cut vertically into halves using a Solingen blade on day 9 post inoculation. This was done to view the interior of the kernels. The sectioned kernels were mounted on aluminium specimen stubs with double sided carbon tape and coated with a thin layer of gold palladium using a 5150A sputter-coater (HHV, Crawley, United Kingdom). This was done to make the sample surface electrically conductive to avoid electron build-up on the sample surface, which can cause electron charge. The SEM micrographs were acquired using the Zeiss MERLIN Field Emission-SEM at the Electron Microbeam Unit of Stellenbosch University's Central Analytical Facility. Beam conditions during imaging were 5 kV accelerating voltage, 250 µA probe current, with a working distance of approximately 4 mm.

Results and discussion

Visual assessment

All infected kernels were visibly infected by the fungus on day 8 post-inoculation, while the controls showed no signs of infection, as shown in Fig. 5.2. (only images of one control and infected kernel are shown). The white/pinkish moulds seen on the surface of the infected kernels is typical evidence of infection by *F. verticillioides* (Afolabi *et al.*, 2007). Viewing the cut kernels, clear differences were observed between the interior of the control and infected. A major portion of the infected kernel's internal structure was powdery/whitish, and this could be attributed to fungal

activity. The control remained intact with the major components (i.e. germ, floury and vitreous endosperm) of the kernel clearly visible.

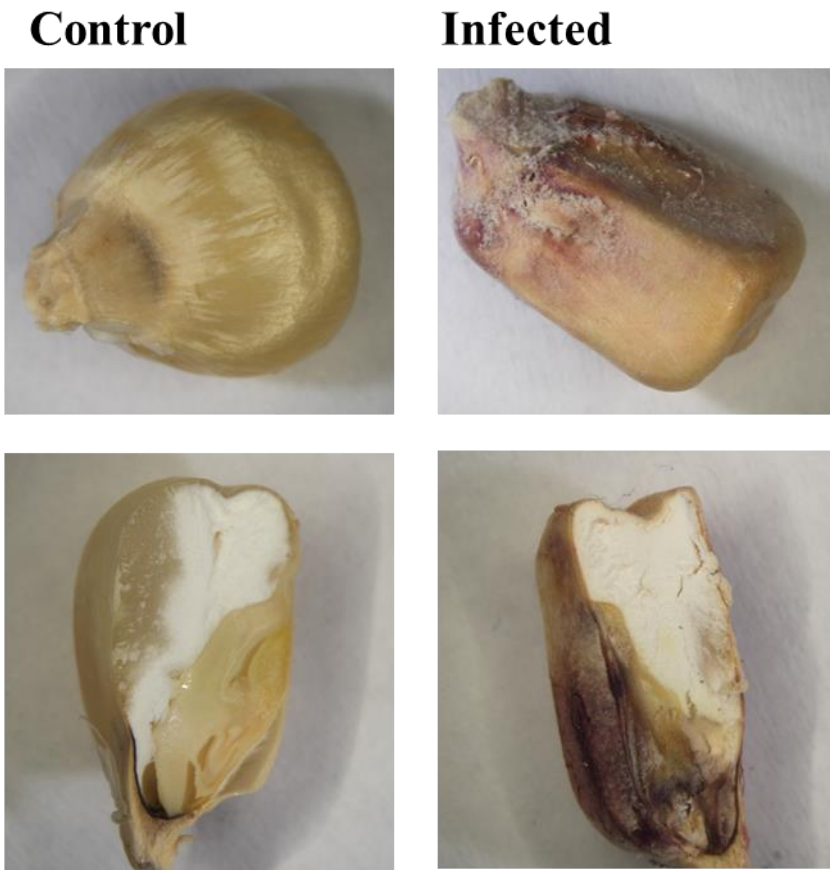

Figure 5.2. Digital images of one control and one infected maize kernel taken on day 9 post inoculation demonstrating the effect of fungal damage on the surface and interior of the kernel.

Qualitative X-ray image analysis

The 2D X-ray images allowed visualisation of the internal structural changes in the kernels over time, as shown in Fig. 5.3. Images of only one control and one infected kernel of the front view are shown, since similar changes were observed over time for the other kernels. The brighter grey regions correspond to denser regions within the kernels and the black/darker regions represents air voids, since they have a lower absorption coefficient with respect to kernel structure. Widening of the existing pores as well as presence of additional ones were observed over time, especially in the germ and floury endosperm regions of the kernels. The infected kernels, on the other hand, became friable and porous over time with the germ region being the most affected. The floury endosperm has more voids compared to the vitreous endosperm over time, especially in the region surrounding the germ, in both the control and infected kernels (Fig. 5.3.). The floury endosperm is known to have more intercellular spaces between the starch granules making the region more susceptible to damage

(Dombrink-Kurtzman & Knutson, 1997). The vitreous endosperm has lesser structural damage, and this is attributed to the region being solid with fewer intercellular pores.

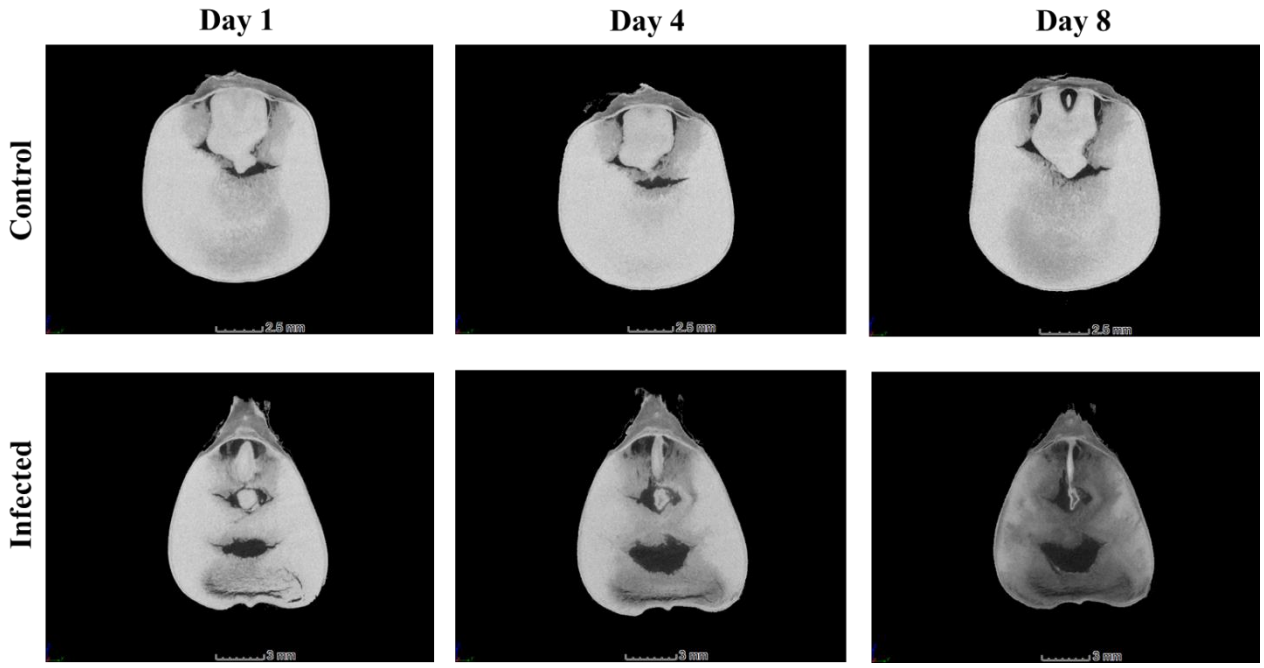

Figure 5.3. Grey scale 2D images of one control and one infected kernel in the frontal view on the three days scanned, illustrating internal structural changes over time.

Microstructural details of the effect of fungal damage on the kernel structure could be clearly observed when scanning was done on one control and one infected kernel at higher resolution (7 µm) on day 9 post inoculation (as shown in Fig. 5.4). The germ region of the control kernel was generally intact, while in the infected kernel this region was quite damaged. Fungal activity in grains has been reported to cause undesirable effects, including utilization of kernel reserves as energy source leading to losses in dry matter, and thus kernel density (Seitz *et al.*, 1982; Magan *et al.*, 2004). The germ and surrounding regions were shown, in previous studies, to be regions preferred by most fungi including *F. verticillioides* used in this study (Bacon *et al.*, 1992; Duncan & Howard, 2010). This was evident as shown in Fig. 5.4. The germ region of maize kernels is nutritious with high lipid content (Evers & Millar, 2002), and the fungus invades this region to produce hydrolytic enzymes for degrading the kernel reserves (Magan *et al.*, 2004).

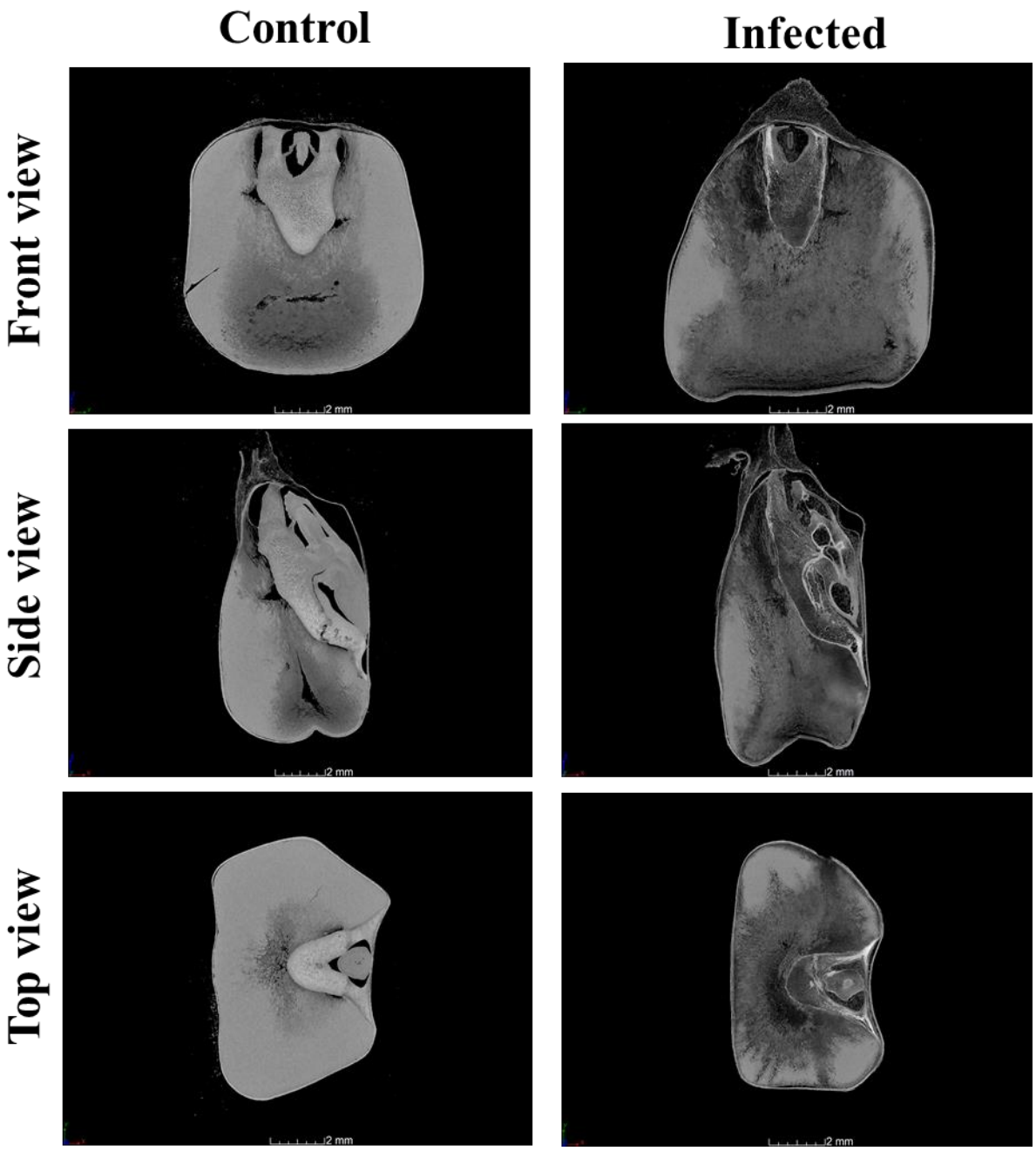

Figure 5.4. High resolution images (7 µm) of one control and one infected kernel taken on day 9 post inoculation in the different views (front, side, top) demonstrating the effect of fungal damage on the internal structure of maize kernels.

It was apparent that fungal activity softens the kernel by creating more voids, especially the germ and floury endosperm regions, and thus influencing the integrity of the internal structure and ultimately the density of the kernel. In the SEM micrographs taken on day 9 post inoculation (Fig. 5.5), more pores and voids could be observed in the starch granules of the infected kernel, while the control kernel was intact (images of only infected and one control kernel are shown). This can be attributed to breakdown of kernel reserves, which results in less kernel material attenuating the X-

rays. It is worth mentioning that uninfected kernels respire resulting in a loss of kernel reserves (Seitz *et al.*, 1982), and this explains the changes observed in the control kernels over time.

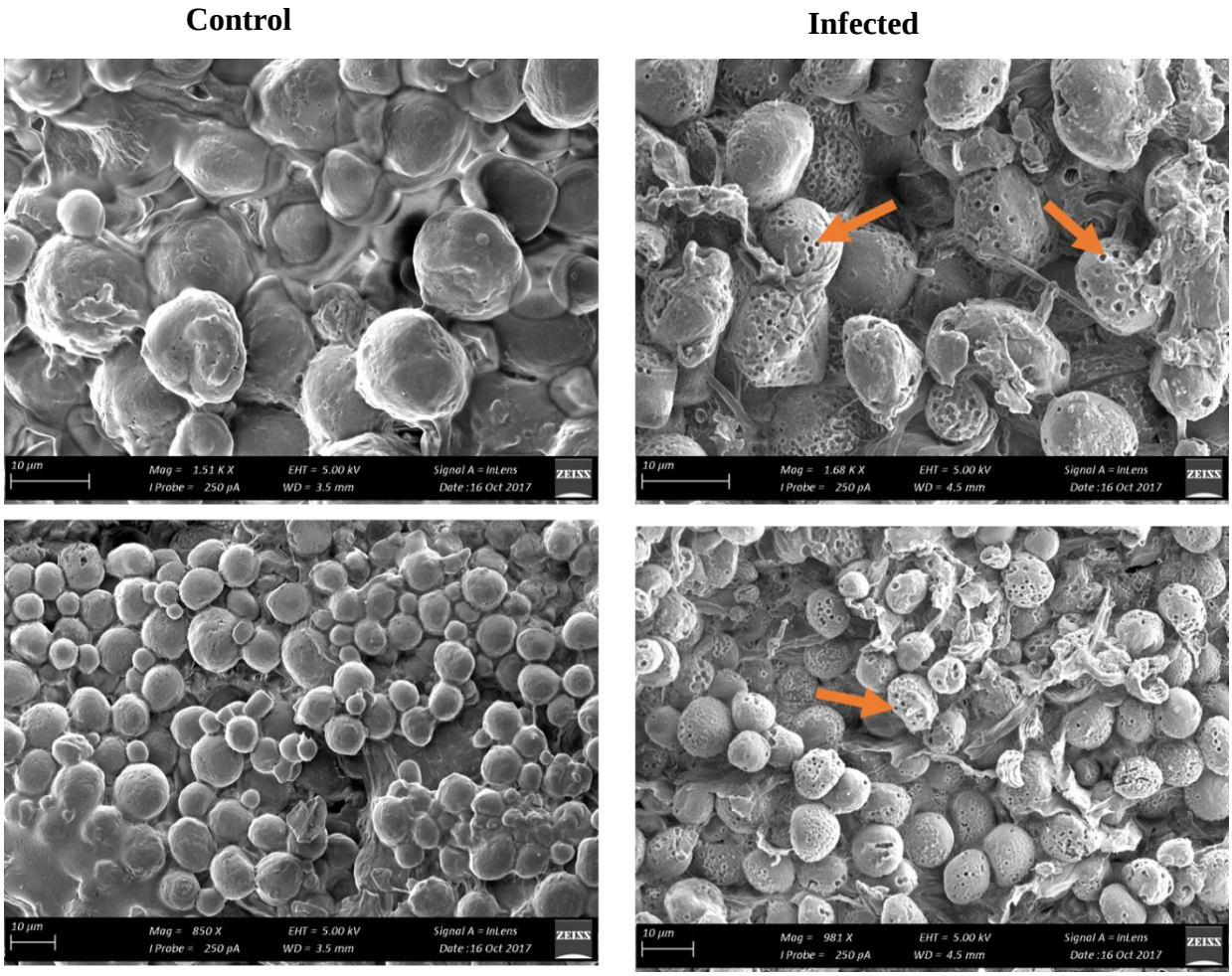

Figure 5.5. SEM micrographs of one control and one infected kernel on day 9 post inoculation, the arrows indicate pores formed on the starch granules of the infected kernels (scale bar = 10 µm).

Texture analysis using first order statistical features

PCA calculated with the first order image features for all the views (i.e. front, side and top) for the three days scanned is shown in Fig. 5.6. This was performed to reveal any trend and grouping within and between the kernels. PC1 explained 66.54% of the total variance in the data set while PC2 explained 16.14%. Clear separation of the control from infected kernels was seen on day 8 (Fig. 5.6a). Majority of the infected kernels on day 8 were grouped on the quadrant where PC1 and PC2 are negative, and thus positively correlated to skewness. Skewness calculates the shift in the distribution of the grey level intensities. This measure is 0 for symmetric histograms, positive for histograms skewed to the right and negative for histograms skewed to the left (Patel *et al.*, 2012). Meaning there was a greater shift to the lower grey level intensities on day 8 of the infected kernels compared to the

rest of the days and kernels. This is attributed to the increase in voids within the infected kernel due to breakdown of kernel reserves.

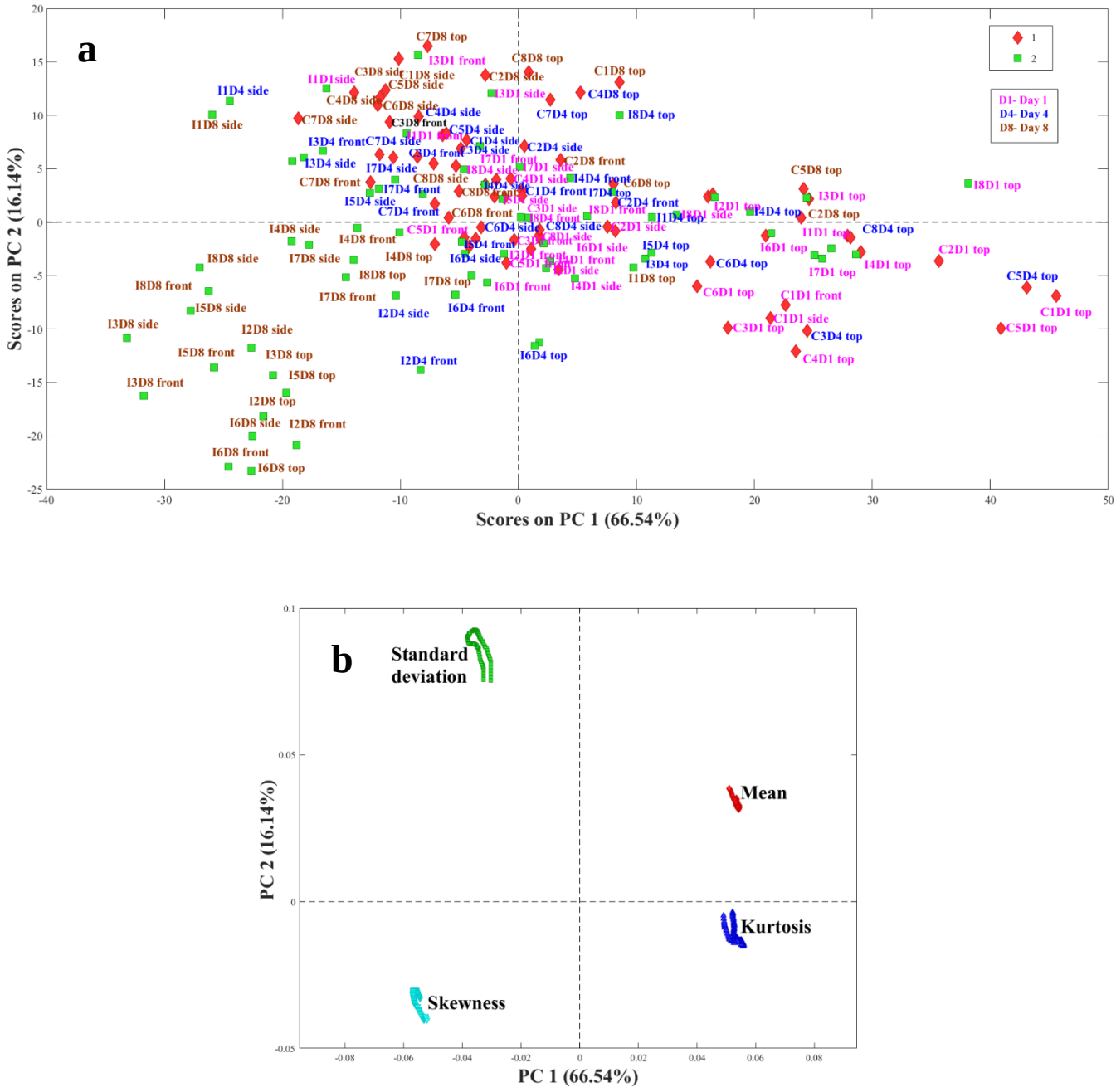

Figure 5.6. PCA (a) score plot of the controls (red diamond shape) and infected (green square shape) maize kernels in the three different views (top, side, front) and (b) loading plot for the four first order statistical image features for the three days scanned.

Several control and infected kernels on day 1 were located on the positive side of PC1, and hence positively correlated to mean and kurtosis and negatively correlated to skewness. Mean measures the total brightness of an image (grey level intensity) (Bountris *et al.*, 2005). A higher mean signifies a dense sample/more material within the kernel, therefore kernels on day 1 were denser

compared to the rest of the days. Furthermore, mean decreased with time implying the kernels were getting less dense over time, thus infected kernels on day 8 had a lower mean value. Kurtosis on the other hand describes the sharpness of the peak of the grey level distribution histogram. Positive kurtosis indicates heavy tails and peakedness relative to the normal distribution, whereas negative kurtosis indicates light tails and flatness (DeCarlo, 1997). Kernels on day 1 had a high kurtosis which decreased over time (Fig. 5.6). Control kernels on day 4, day 8 and some of the infected kernels on day 4 were located on the positive side of PC2; this correlates to high standard deviation. Standard deviation determines the average contrast in the image (Patel *et al.*, 2012), meaning the difference between the highest and lowest grey values on the day was high, and thus the discriminating factor of the kernels on these days.

PLS-DA was used to develop a model to distinguish the control from the infected kernels using the first order statistics image features. Table 5.2 shows the results in the form of a confusion matrix. Two of the controls were misclassified as infected, while 32 infected were misclassified as control, resulting into a classification accuracy of 97.22% and 55.56% respectively. The infected kernels classified as control were mostly kernels on day 1 and 4 as seen in Fig. 5.7. The PLS-DA score plot (Fig. 5.7) revealed how the developed model predicted which class (i.e. either infected or control) each kernel belonged to. This could be explained by minimal structural changes due to infection on day 1 post inoculation. Previous studies have also reported little fungal activity in maize kernels during early stages of infection using near infrared (NIR) hyperspectral imaging (Del Fiore *et al.*, 2010; Williams *et al.*, 2012). Similar changes were observed in both the control and infected kernels in the first four days in this study, affecting the classification accuracy.

Table 5.2. Confusion matrix for first order statistics features

	Actual class		Accuracy
	Control (72)	Infected (72)	
Predicted as control	70	32	97.22%
Predicted as infected	2	40	55.56%

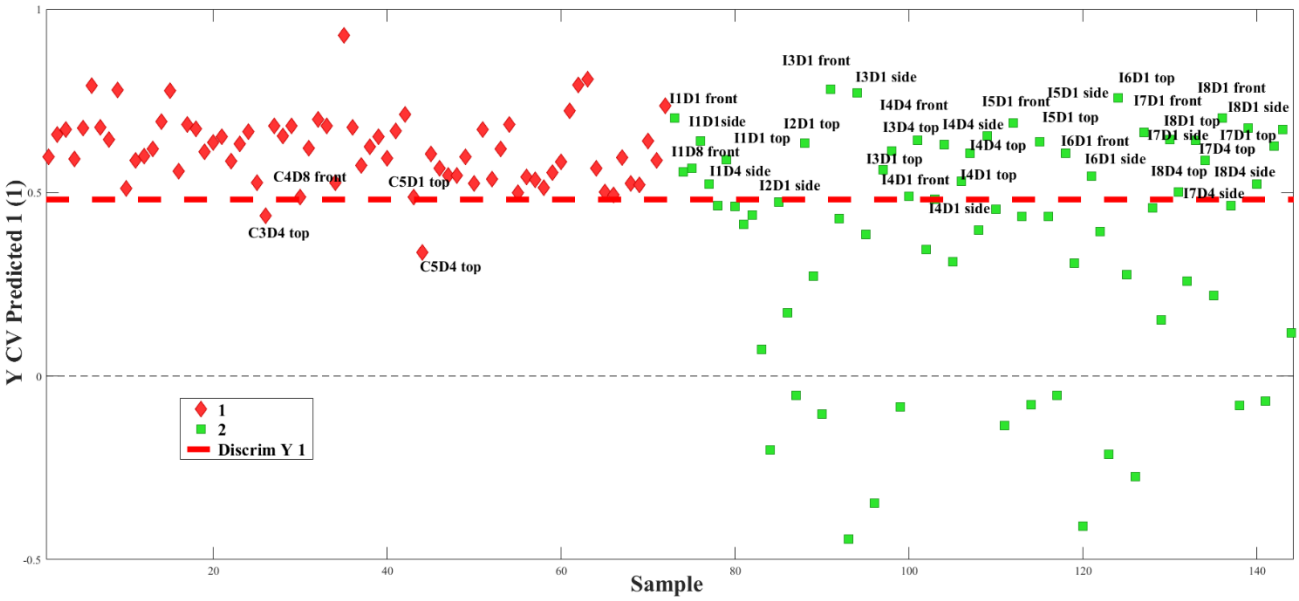

Figure 5.7. PLS-DA score plot illustrating the number of samples predicted as control (1). The red diamond shape are controls while the green square shape are the infected. Samples above the red line are those predicted as controls, while those below this line were predicted as infected. It is evident that numerous infected kernels (on day 1 and 4) were misclassified as control kernels.

Texture analysis using GLCM extracted image features

The outputs of the textural features extracted from the GLCM were used as inputs for PCA. The sample score plots for front and top view are shown in Fig. 5.8a and Fig. 5.9a. No clear separation was observed between the controls and infected kernels for the three days scanned in both views. From the loading plots in Fig. 5.8b and Fig. 5.9b, it could be seen that the correlation textural feature was the variable contributing to the grouping along PC2. Thus, most kernels (both control and infected) had a high correlation on day 4 and 8. This meant there were more consistent grey levels or pixels with similar grey level intensities at these time points in both the control and infected kernels.

It could be visualised that infected kernels had a lower intensity over time in comparison to the uninfected kernels as shown in Fig. 5.3 (images at 14 µm). The GLCM extracted textural features were not able to accurately discriminate the control from infected kernels, possibly due to the high variation within the 100 images chosen from the same kernel, and contrast enhancement of the original X-ray images should be done before extracting the GLCM features. Contrast enhancement is an essential step in image processing done to increase image quality (Wang *et al.*, 1983), and thus easily discern the differences between studied samples.

(a)

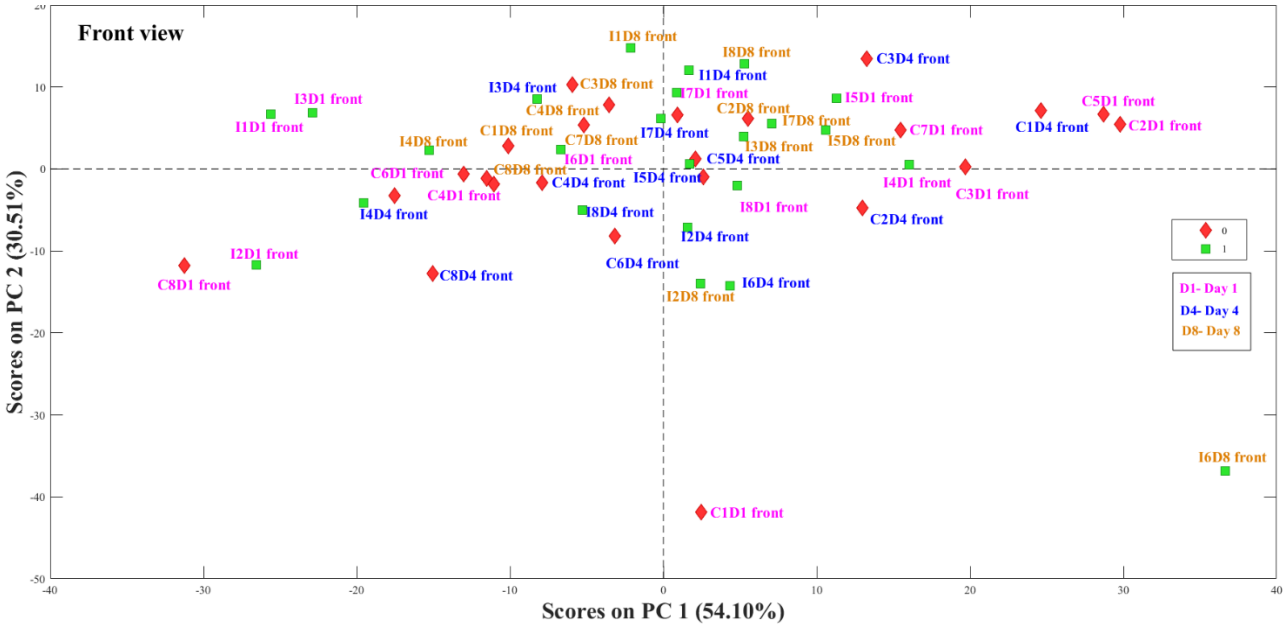

(b)

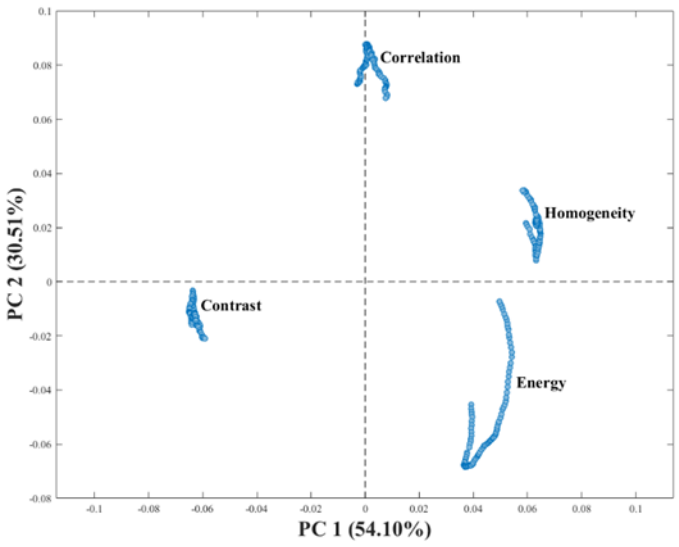

Figure 5.8 PCA (a) score plot for the controls (red diamond shape) and infected (green square shape) maize kernels and (b) loading plot for the GCLM image features in the front view for the three days scanned.

(a)

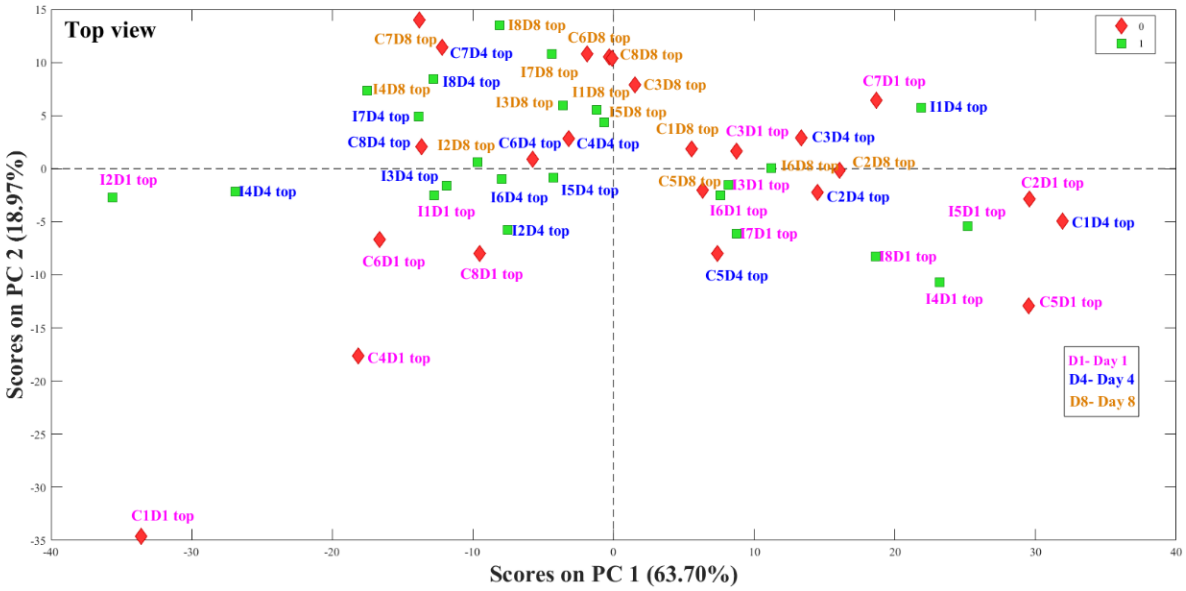

(b)

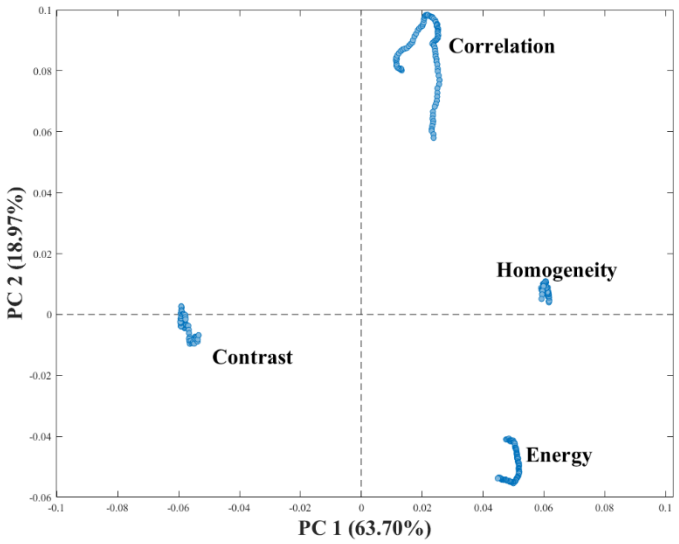

Figure 5.9 PCA **(**a**)** score plots for the controls (red diamond shape) and infected (green square shape) maize kernels and (b) loading plot for the GLCM image features in the top view for the three days scanned.

The PLS-DA model developed using the GLCM extracted features achieved a classification accuracy of 79.17% and 60.41% for infected and control respectively. Although contrast enhancement was not done, the developed model was able to predict less infected kernels as controls. It was noted that 38 infected kernels out of the 48 used were correctly classified (Table 5.3). However, 19 of the control were misclassified as infected, this could be due to a high correlation textural feature

as evident in Fig 5.8. This implied that majority of the kernels had similar grey level intensity hence classified as the same class (both control and infected). The kernels classified as controls in both classes had a high contrast and were mostly kernels on day 1 and 4.

Table 5.3. Confusion matrix for GLCM extracted features

	Actual class		Accuracy
	Control (48)	Infected (48)	
Predicted as control	29	10	60.41%
Predicted as infected	19	38	79.16%

Conclusion

It was possible to visualise the effect of fungal damage on the internal structure of maize kernels non-destructively using high resolution X-ray micro CT. Structural changes in the kernels could be observed in the 2D images, with the infected kernels having more voids over time, especially in the germ and floury endosperm regions. The presence of more voids with time weakened the kernel's ability to attenuate X-rays, and thus resulted into a decrease in grey level intensities over time.

Image texture analysis allowed extraction of image features to aid in distinguishing control from infected kernels. Clear separation of the infected from control kernels was seen on day 8 post inoculation in the PCA score plots using first order statistical features however, no clear separation was observed using the GLCM textural features. The lack of separation using GLCM textural features revealed a need for contrast enhancement of the original X-ray images before extracting these features. First order statistics were used to develop a classification model using PLS-DA. Most infected kernels on day 1 and 4 were classified as control lowering the classification accuracy to 55.67%. The GLCM extracted features gave a better classification of 79.16% for the infected kernels.

High resolution X-ray micro-CT is a powerful non-destructive technique for investigating the microstructural changes in maize kernels infected by fungi, and would be complementary to other conventional microscopic techniques such as light microscopy and SEM.

Reference

Abdi, H. & Williams, L.J. (2010). Principal component analysis. *Wiley Interdisciplinary Reviews: Computational Statistics*, **2**, 433-459.

Afolabi, C., Ojiambo, P., Ekpo, E., Menkir, A. & Bandyopadhyay, R. (2007). Evaluation of maize inbred lines for resistance to *Fusarium* ear rot and fumonisin accumulation in grain in tropical Africa. *Plant Disease*, **91**, 279-286.

Bacon, C., Bennett, R., Hinton, D. & Voss, K. (1992). Scanning electron microscopy of *Fusarium moniliforme* within asymptomatic corn kernels and kernels associated with equine leukoencephalomalacia. *Plant Disease*, **76**, 144-148.

Bharati, M.H., Liu, J.J. & MacGregor, J.F. (2004). Image texture analysis: methods and comparisons. *Chemometrics and Intelligent Laboratory Systems*, **72**, 57-71.

Bountris, P., Farantatos, E. & Apostolou, N. (2005). Advanced image analysis tools development for the early stage bronchial cancer detection. *PWASET*, **9**, 151-156.

Brereton, R.G. & Lloyd, G.R. (2014). Partial least squares discriminant analysis: taking the magic away. *Journal of Chemometrics*, **28**, 213-225.

Cnudde, V. & Boone, M.N. (2013). High-resolution X-ray computed tomography in geosciences: A review of the current technology and applications. *Earth-Science Reviews*, **123**, 1-17.

De Chiffre, L., Carmignato, S., Kruth, J.-P., Schmitt, R. & Weckenmann, A. (2014). Industrial applications of computed tomography. *CIRP Annals-Manufacturing Technology*, **63**, 655-677.

DeCarlo, L.T. (1997). On the meaning and use of kurtosis. *Psychological Methods*, **2**, 292-307.

Del Fiore, A., Reverberi, M., Ricelli, A., Pinzari, F., Serranti, S., Fabbri, A., Bonifazi, G. & Fanelli, C. (2010). Early detection of toxigenic fungi on maize by hyperspectral imaging analysis. *International Journal of Food Microbiology*, **144**, 64-71.

Dombrink-Kurtzman, M. & Knutson, C. (1997). A study of maize endosperm hardness in relation to amylose content and susceptibility to damage. *Cereal Chemistry*, **74**, 776-780.

Donis-González, I.R., Guyer, D.E., Fulbright, D.W. & Pease, A. (2014). Postharvest noninvasive assessment of fresh chestnut (*Castanea* spp.) internal decay using computer tomography images. *Postharvest Biology and Technology*, **94**, 14-25.

Duncan, K.E. & Howard, R.J. (2010). Biology of maize kernel infection by *Fusarium verticillioides*. *Molecular Plant-Microbe Interactions*, **23**, 6-16.

Esbensen, K.H., Guyot, D., Westad, F. & Houmoller, L.P. (2002). Multivariate data analysis: in practice: an introduction to multivariate data analysis and experimental design. Multivariate Data Analysis, 5th edition, CAMO process AS, Oslo, Norway.

Evers, T. & Millar, S. (2002). Cereal grain structure and development: some implications for quality. *Journal of Cereal Science*, **36**, 261-284.

Fandohan, P., Hell, K., Marasas, W. & Wingfield, M. (2003). Infection of maize by *Fusarium* species and contamination with fumonisin in Africa. *African Journal of Biotechnology*, **2**, 570-579.

Gourama, H. & Bullerman, L.B. (1995). Detection of molds in foods and feeds: potential rapid and selective methods. *Journal of Food Protection*, **58**, 1389-1394.

Guelpa, A., du Plessis, A., Kidd, M. & Manley, M. (2015). Non-destructive estimation of maize (*Zea mays* L.) kernel hardness by means of an X-ray micro-computed tomography (µCT) density calibration. *Food and Bioprocess Technology*, **8**, 1419-1429.

Gustin, J.L., Jackson, S., Williams, C., Patel, A., Armstrong, P., Peter, G.F. & Settles, A.M. (2013). Analysis of maize (*Zea mays*) kernel density and volume using microcomputed tomography and single-kernel near-infrared spectroscopy. *Journal of Agricultural and Food Chemistry*, **61**, 10872-10880.

Haralick, R.M. & Shanmugam, K. (1973). Textural features for image classification. *IEEE Transactions on Systems, Man, and Cybernetics*, **3**, 610-621.

Herremans, E., Verboven, P., Bongaers, E., Estrade, P., Verlinden, B.E., Wevers, M., Hertog, M.L. & Nicolai, B.M. (2013). Characterisation of 'Braeburn'browning disorder by means of X-ray micro-CT. *Postharvest Biology and Technology*, **75**, 114-124.

Isaacson, C. (2005). The change of the staple diet of black South Africans from sorghum to maize (corn) is the cause of the epidemic of squamous carcinoma of the oesophagus. *Medical Hypotheses*, **64**, 658-660.

Jolliffe, I.T. (2002). Principal component analysis and factor analysis. In. Principal component analysis, Springer series in statistics. Springer, New York, NY. pp. 150-166.

Kayode, O., Sulyok, M., Fapohunda, S., Ezekiel, C., Krska, R. & Oguntona, C. (2013). Mycotoxins and fungal metabolites in groundnut-and maize-based snacks from Nigeria. *Food Additives & Contaminants: Part B*, **6**, 294-300.

Landis, E.N. & Keane, D.T. (2010). X-ray microtomography. *Materials Characterization*, **61**, 1305-1316.

Léonard, A., Blacher, S., Nimmol, C. & Devahastin, S. (2008). Effect of far-infrared radiation assisted drying on microstructure of banana slices: An illustrative use of X-ray microtomography in microstructural evaluation of a food product. *Journal of Food Engineering*, **85**, 154-162.

Lim, K. & Barigou, M. (2004). X-ray micro-computed tomography of cellular food products. *Food Research International*, **37**, 1001-1012.

Magan, N., Sanchis, V. & Aldred, D. (2004). Role of spoilage fungi in seed deterioration. Fungal biotechnology in agricultural, food and environmental applications, Mycology, volume 21, Marcel Dekker, Inc. New York, NY, pp 311-323.

Manonmani, H., Anand, S., Chandrashekar, A. & Rati, E. (2005). Detection of aflatoxigenic fungi in selected food commodities by PCR. *Process Biochemistry*, **40**, 2859-2864.

Marin, S., Magan, N., Ramos, A.J. & Sanchis, V. (2004). Fumonisin-producing strains of *Fusarium*: a review of their ecophysiology. *Journal of Food Protection*, **67**, 1792-1805.

Mathanker, S.K., Weckler, P.R. & Bowser, T.J. (2013). X-ray applications in food and agriculture: a review. *Transactions of the ASABE*, **56**, 1227-1239.

Mizutani, R. & Suzuki, Y. (2012). X-ray microtomography in biology. *Micron*, **43**, 104-115.

Mohorič, A., Vergeldt, F., Gerkema, E., van Dalen, G., Van den Doel, L., Van Vliet, L., Van As, H. & Van Duynhoven, J. (2009). The effect of rice kernel microstructure on cooking behaviour: A combined μ-CT and MRI study. *Food Chemistry*, **115**, 1491-1499.

Orina, I., Manley, M. & Williams, P.J. (2017). Use of High-Resolution X-Ray Micro-Computed Tomography for the Analysis of Internal Structural Changes in Maize Infected with *Fusarium verticillioides*. *Food Analytical Methods*, **10**, 2919-2933.

Paepens, C., De Saeger, S., Sibanda, L., Barna-Vetro, I., Léglise, I., Van Hove, F. & Van Peteghem, C. (2004). A flow-through enzyme immunoassay for the screening of fumonisins in maize. *Analytica Chimica Acta*, **523**, 229-235.

Patel, K.K., Kar, A., Jha, S. & Khan, M. (2012). Machine vision system: a tool for quality inspection of food and agricultural products. *Journal of Food Science and Technology*, **49**, 123-141.

Popovski, S. & Celar, F.A. (2013). The impact of environmental factors on the infection of cereals with *Fusarium* species and mycotoxin production-a review. *Acta Agriculturae Slovenica*, **101**, 105-116.

Prats-Montalbán, J., De Juan, A. & Ferrer, A. (2011). Multivariate image analysis: a review with applications. *Chemometrics and Intelligent Laboratory Systems*, **107**, 1-23.

Salvo, L., Suéry, M., Marmottant, A., Limodin, N. & Bernard, D. (2010). 3D imaging in material science: Application of X-ray tomography. *Comptes Rendus Physique*, **11**, 641-649.

Schoeman, L., du Plessis, A. & Manley, M. (2016a). Non-destructive characterisation and quantification of the effect of conventional oven and forced convection continuous tumble (FCCT) roasting on the three-dimensional microstructure of whole wheat kernels using X-ray micro-computed tomography (μCT). *Journal of Food Engineering*, **187**, 1-13.

Schoeman, L., du Plessis, A., Verboven, P., Nicolaï, B.M., Cantre, D. & Manley, M. (2017). Effect of oven and forced convection continuous tumble (FCCT) roasting on the microstructure and dry milling properties of white maize. *Innovative Food Science & Emerging Technologies*, **44**, 54-66.

Schoeman, L., Williams, P., du Plessis, A. & Manley, M. (2016b). X-ray micro-computed tomography (μCT) for non-destructive characterisation of food microstructure. *Trends in Food Science & Technology*, **47**, 10-24.

Seitz, L., Sauer, D., Mohr, H. & Aldis, D. (1982). Fungal Growth and Dry Matter Loss During Bin Storage of High-Moisture Corn. *Cereal Chemistry*, **59**, 9-14.

Suleiman, R.A., Rosentrater, K.A. & Bern, C.J. (2013). Effects of deterioration parameters on storage of maize. *Journal of Natural Sciences Research*, **3**, 147-165.

Suresh, A. & Neethirajan, S. (2015). Real-time 3D visualization and quantitative analysis of internal structure of wheat kernels. *Journal of Cereal Science*, **63**, 81-87.

Velu, V., Nagender, A., Prabhakara Rao, P.G. & Rao, D.G. (2006). Dry milling characteristics of microwave dried maize grains (Zea mays L.). *Journal of Food Engineering*, **74**, 30-36.

Wang, D.C.C., Vagnucci, A.H. & Li, C.C. (1983). Digital image enhancement: A survey. *Computer Vision, Graphics, and Image Processing*, **24**, 363-381.

Williams, P.J., Geladi, P., Britz, T.J. & Manley, M. (2012). Investigation of fungal development in maize kernels using NIR hyperspectral imaging and multivariate data analysis. *Journal of Cereal Science*, **55**, 272-278.

Winston, P.W. & Bates, D.H. (1960). Saturated solutions for the control of humidity in biological research. *Ecology*, **41**, 232-237.

Zheng, C., Sun, D.-W. & Zheng, L. (2006). Recent applications of image texture for evaluation of food qualities—a review. *Trends in Food Science & Technology*, **17**, 113-128.

Chapter 6
General discussion and conclusion

Fungal infection of maize kernels is a challenging problem despite decades of extensive research (Munkvold, 2003). The main concern is the production of mycotoxins by fungi, which are harmful to humans and animals. Therefore, early detection and if possible removal of contaminated grains is an essential control measure in ensuring food safety and storage longevity. In this study, the effect of fungal contamination on maize internal structure was evaluated using high resolution X-ray micro-CT as a non-destructive technique combined with image texture analysis and multivariate analysis. X-ray micro-CT is a radiographic imaging techniques that allows visualisation and characterisation of a sample's internal structure at high resolution (Schoeman *et al.*, 2016b). The maize kernels were infected with *Fusarium verticillioides* and scanned over time. *Fusarium verticillioides* is among the most common fungi associated with maize (Popovski & Celar, 2013). The detection of fungal infection in maize kernels using X-ray micro-CT was based on changes in kernel density resulting from loss in dry matter (breakdown of kernel reserves).

The results from this study clearly showed that it was possible to distinguish the major components of a maize kernel, i.e. germ, floury and vitreous endosperm based on their difference in X-ray attenuation. The germ and vitreous endosperm appeared brighter as they were regions of higher attenuation, while the voids within the kernel were dark. Reconstructed 3D volumes obtained from a series of 2D images allowed for visualisation of the kernel at different orientations, i.e. front, side and top view. More voids were observed with time, especially in the germ and floury endosperm regions in both the control and infected kernels. This affected the integrity of the grains resulting in less kernel material attenuating X-rays. The resultant 3D volumes enabled quantitative characterisation of the effect of fungal infection on the maize kernels. Total kernel volume and mean grey value decreased while total volume of voids increased over time in both the control and infected kernels. No significant difference ($P > 0.05$) between the control and infected kernels was reported using these quantitative measurements.

Therefore, it was apparent that respiration of the grain itself and fungi in the grain contribute to loss in dry matter, and hence changes in kernel density. The contribution to loss in dry matter by the fungi was minimal during early stages of infection (first three days post inoculation) and increased at a rate dependent on moisture and temperature of the surrounding environment. Therefore, environment conditions especially temperature (25-30º C) and relative humidity (above 90%) play an important role in growth of fungi in grains (Fandohan *et al.*, 2003), hence should be taken into consideration in studies that seek to monitor the effect of fungal infection on kernel microstructure.

Image texture analysis using first order statistics and grey level co-occurrence matrix (GLCM) was employed to extract image features from the X-ray images to aid in discrimination of control from infected kernels. Under favourable conditions for fungal growth (controlled relative humidity and temperature), minimal structural changes were reported in the first four days of scanning post inoculation. These resulted into similar structural changes in the control and infected kernels, and thus no clear differences observed using extracted image textural features. Variability within the kernels (i.e. response to infection) was a concern given the small sample size (3 kernels per treatment) used initially, a larger sample size would be ideal however due to high cost of acquiring high resolution X-ray images and image analysis, only 8 kernels per treatment would be scanned.

Clear separation of the control from infected kernels was observed on day 8 post inoculation using first order statistical image features in the principal component analysis (PCA) score plots and classification accuracy of 55.56% for infected kernels was achieved with partial least square discriminant analysis (PLS-DA) model. Kernels on day 1 and 4 of both the control and infected grouped together, and this was attributed to minimal structural changes due to fungal infection at these times interval. GLCM extracted features did not reveal a clear separation between the control and infected kernels. This revealed the need for further image pre-processing to enhance image features (e.g. contrast enhancement). However, a better classification accuracy of 76.16% for infected kernels was achieved. Further studies are also recommended using wavelet transform analysis. A wavelet is a mathematical function that can decompose an image with a series of averaging and differencing calculations. Wavelets calculates average intensity properties as well as several detailed contrast levels distributed throughout the image (Semler *et al.*, 2005; Singh *et al.*, 2010). Wavelets are sensitive to spatial distribution of grey level pixels and able to differentiate and preserve details at various scales or resolution (Semler *et al.*, 2005).

High resolution images (voxel size of 7 µm) taken on day 8 post inoculation gave more details of fungal damage on the internal structure of the maize kernels. The infected kernels became friable and porous, with the germ being the most damaged region of the kernels because this is where most of the nutrients are located. Previous studies using scanning electron microscopy (SEM) (Bacon *et al.*, 1992) and transmission electron microscopy (TEM) (Duncan & Howard, 2010b) also reported the germ being the region preferred by *F. verticillioides.* SEM and TEM techniques though effective are destructive in nature and require sectioning of the sample to access regions of interest.

Limited studies have utilized X-ray micro-CT to evaluate the effect of fungal infection on maize kernels. Pearson and Wicklow (2006) and Narvankar *et al.* (2009a) used traditional X-ray imaging to detect fungal infection in maize and wheat respectively. Unlike X-ray micro-CT, traditional X-ray imaging yields only one projection image that displays the X-ray transmission

through the sample. Williams (2013) used X-ray micro-CT to evaluate the effect of fungal contamination on the internal structure of maize kernel over time. This study however used only one infected kernel, and no control kernel was scanned for comparison. The current study overcame this drawback by scanning more kernels (3-8) of both the control and infected over time.

Although changes in density due to fungal infection are minimal during early stages of infection, the effectiveness of this technique, like other non-destructive techniques, in detection of fungal infection largely depends on the virulence of the fungus and the extent of damage it has caused. X-ray micro-CT would serve as very valuable research tool for visualisation of the effect of fungal infection on internal structure of maize and other cereal grains non-destructively. It has an added advantage of viewing the kernel from different angles as enabled by the resultant 3D volume. Since the main concern with fungal infection is mycotoxins, it is therefore important to investigate further the correlation between microstructural changes or loss in kernel density and toxins production within the kernel. X-ray micro CT could be complementary to destructive techniques such as SEM, and useful to plant pathologists and breeders seeking to study individual grains.

Unfortunately, X-ray micro-CT is a time-consuming and costly technique. To acquire a high-resolution image (voxel size of 7 µm) takes approximately two hours, this results to high costs and limits use of large sample size. Large data volumes (up to 50 gigabytes) obtained during scanning require huge computer resources with considerable storage capacity for visualisation and analysis. Segmenting kernels to remove unwanted regions (e.g. plastic pipette tip and surrounding area) is tedious and time-consuming leading to high cost of image analysis. Accessibility to X-ray micro-CT is limited by the availability of facilities. However, it is anticipated with the advancements in high-performance computing systems, new detection technologies which offer real-time imaging, high performance X-ray tubes, reduction in equipment costs and reduction in reconstruction time, X-ray micro CT will become more applicable in the future (Hanke *et al.*, 2008).

The outcomes from this study can be summarized as follows:

- internal structure of maize kernels could be imaged non-destructively, and yielded 2D and 3D images at relatively high resolution;
- monitoring of internal structural changes could be done based on the changes in grey level intensity over time;
- environment conditions especially relative humidity and temperature influences the growth of fungi within the kernel, and should be taken into consideration during experimental setups;

- image textural features extracted from the resulting digital image data coupled with multivariate analysis could aid in discrimination of control from infected kernels.

Finally, even though it was not possible to differentiate control from infected kernels in the early stages of infection, X-ray micro-CT offers the ability to visualise, in fine detail, the effect of fungal infection on the internal structure of maize kernels. This work has the potential to be extended to visualising small volumes within the maize kernel, e.g. the germ in higher detail, and hence provide new scientific insights especially on the mode of entry, the spread and survival of the fungus within maize kernels. Combining X-ray micro-CT with other imaging techniques such scanning electron microscopy (SEM) and near infrared hyperspectral imaging can give more comprehensive evaluation of the effect of fungal infection on maize kernels and other cereal grains.

References

Bacon, C., Bennett, R., Hinton, D. & Voss, K. (1992). Scanning electron microscopy of *Fusarium moniliforme* within asymptomatic corn kernels and kernels associated with equine leukoencephalomalacia. *Plant Disease*, **76**, 144-148.

Duncan, K.E. & Howard, R.J. (2010). Biology of maize kernel infection by *Fusarium verticillioides*. *Molecular Plant-Microbe Interactions*, **23**, 6-16.

Fandohan, P., Hell, K., Marasas, W. & Wingfield, M. (2003). Infection of maize by *Fusarium* species and contamination with fumonisin in Africa. *African Journal of Biotechnology*, **2**, 570-579.

Hanke, R., Fuchs, T. & Uhlmann, N. (2008). X-ray based methods for non-destructive testing and material characterization. *Nuclear Instruments and Methods in Physics Research Section A: Accelerators, Spectrometers, Detectors and Associated Equipment*, **591**, 14-18.

Munkvold, G.P. (2003). Cultural and genetic approaches to managing mycotoxins in maize. *Annual Review of Phytopathology*, **41**, 99-116.

Narvankar, D., Singh, C., Jayas, D. & White, N. (2009). Assessment of soft X-ray imaging for detection of fungal infection in wheat. *Biosystems Engineering*, **103**, 49-56.

Pearson, T. & Wicklow, D. (2006). Detection of corn kernels infected by fungi. *Transactions of the ASABE*, **49**, 1235-1245.

Popovski, S. & Celar, F.A. (2013). The impact of environmental factors on the infection of cereals with *Fusarium* species and mycotoxin production-a review. *Acta Agriculturae Slovenica*, **101**, 105-116.

Schoeman, L., Williams, P., du Plessis, A. & Manley, M. (2016). X-ray micro-computed tomography (μCT) for non-destructive characterisation of food microstructure. *Trends in Food Science & Technology*, **47**, 10-24.

Semler, L., Dettori, L. & Furst, J. (2005). Wavelet-based texture classification of tissues in computed tomography. In: Computer-Based Medical Systems. Proceedings. 18th IEEE Symposium on computer based medical systems (CBMS'05) . pp. 265-270.

Singh, C.B., Choudhary, R., Jayas, D.S. & Paliwal, J. (2010). Wavelet analysis of signals in agriculture and food quality inspection. *Food and Bioprocess Technology*, **3**, 2-12.

Williams, P.J. (2013). Near infrared (NIR) hyperspectral imaging and X-ray computed tomography combined with statistical and multivariate data analysis to study *Fusarium* infection in maize. PhD thesis.Stellenbosch University.